

PB95192183



REPORT NO.
UCB/EERC-93/08
DECEMBER 1993

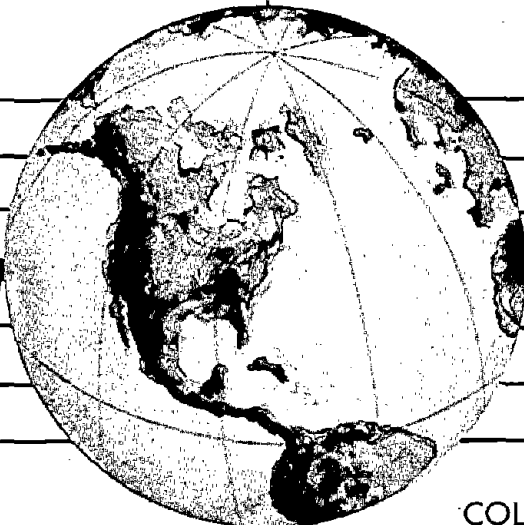
EARTHQUAKE ENGINEERING RESEARCH CENTER

MODEL FOR ANCHORED REINFORCING BARS UNDER SEISMIC EXCITATIONS

by

GIORGIO MONTI
ENRICO SPACONE
FILIP C. FILIPPOU

Report to the National Science Foundation



COLLEGE OF ENGINEERING

UNIVERSITY OF CALIFORNIA AT BERKELEY

REPRODUCED BY: **NTIS**
U.S. Department of Commerce
National Technical Information Service
Springfield, Virginia 22161

For sale by the National Technical Information
Service, U.S. Department of Commerce, Spring-
field, Virginia 22161

See back of report for up to date listing of EERC
reports.

DISCLAIMER

Any opinions, findings, and conclusions or
recommendations expressed in this publication
are those of the authors and do not necessarily
reflect the views of the National Science
Foundation or the Earthquake Engineering
Research Center, University of California at
Berkeley.



**MODEL FOR ANCHORED REINFORCING BARS
UNDER SEISMIC EXCITATIONS**

by

Giorgio Monti

Visiting Scholar

Dipartimento di Ingegneria Strutturale e Geotecnica
University of Rome, Italy

Enrico Spacone

Doctoral Student

and

Filip C. Filippou

Associate Professor

Department of Civil Engineering

A Report on Research Conducted
under Grant ECE-8657525
from the National Science Foundation

Report No. UCB/EERC-93/08
Earthquake Engineering Research Center
College of Engineering
University of California, Berkeley

December 1993



ABSTRACT

This study presents a finite element model for reinforcing bars anchored in concrete and subjected to severe cyclic excitations. The solution to the problem of stress transfer between reinforcing steel and concrete is based on the flexibility method. In this case the governing differential equations are solved by force interpolation functions that strictly satisfy equilibrium along the anchored reinforcing bar. This solution method results in a very robust and stable nonlinear algorithm, particularly, for systems that exhibit severe stiffness and strength deterioration, as is the case for anchored reinforcing bars.

In the systematic derivation of the proposed solution method the model is viewed as a simple mechanical system that is made up of two components in parallel. The first component is the reinforcing bar and the second is the interface between reinforcing steel and surrounding concrete. The nonlinear hysteretic behavior of the model derives entirely from the nonlinear constitutive behavior of these two components. The hysteretic behavior of the reinforcing bar is described by a cyclic steel stress-strain relation, while the hysteretic behavior of the interface derives from a cyclic bond stress-slip relation that includes a damage parameter for representing the progressive deterioration of bond.

In formulating the finite element solution of the governing differential equations of the stress transfer problem, two different methods are discussed and compared. In the first method the governing differential equations are solved by approximating the displacement field with interpolation functions. The selection of appropriate displacement shape functions that are compatible with the node displacements is straightforward. In the second method the governing differential equations are solved by approximating the stress field with interpolation functions. In this case the selection of appropriate interpolation functions is not straightforward. In a parallel system the total stress field results from the superposition of the component stress fields. In this case the force interpolation functions in the components of the proposed model must satisfy the requirement that the steel force distribution be in strict equilibrium with the bond force distribution along the element. The proposed model is based on the second method, since this offers significant numerical advantages over the first.

The integration of the flexibility based finite element model in a conventional stiffness based finite element program faces several challenges that are addressed in this study with a new iterative algorithm. This algorithm is characterized by robust and stable

numerical behavior even under conditions of significant strength and stiffness loss of the anchored reinforcing bar.

The study concludes with correlation studies between analytical and experimental results and several parametric studies. The former are intended to establish the validity of the proposed model, while the latter serve the purpose of identifying the significance of key parameters on the local and global response of anchored reinforcing bars and for providing some guidance for their design in regions of high seismic risk.

ACKNOWLEDGMENTS

This study was supported by Grant No. ECE-8657525 from the National Science Foundation with Drs. A.J. Eggenberger, H. Lagorio and V.P. Singh as program directors. The opinions expressed in this report are those of the authors and do not reflect the views of the sponsoring agency.

The first author would like to thank Professors Paolo E. Pinto and Camillo Nuti of the University of Rome, La Sapienza for their support and encouragement during the course of this study.

TABLE OF CONTENTS

ABSTRACT	i
ACKNOWLEDGMENTS	iii
TABLE OF CONTENTS	v
LIST OF FIGURES	vii
LIST OF TABLES	ix
CHAPTER 1 INTRODUCTION	1
1.1 General.....	1
1.2 Review of Previous Studies	2
1.3 Objectives and Scope.....	4
CHAPTER 2 FINITE ELEMENT FORMULATION	5
2.1 General.....	5
2.2 Governing Differential Equations of the Problem.....	7
2.3 Finite Element Approximation	9
2.4 Stiffness Formulation.....	11
2.5 Flexibility Formulation.....	14
2.5.1 Approximation of Stress Field.....	15
2.5.2 Element State Determination	18
2.5.3 Determination of Element Stiffness Matrix.....	19
2.5.4 Determination of Residual Displacements	21
2.5.5 Selection of Interpolation Functions and Explicit Forms of Element Stiffness Matrix and Displacement Residuals	22
2.6 Numerical Integration	23
2.7 Summary of Element State Determination Algorithm.....	24
CHAPTER 3 ANALYTICAL STUDIES UNDER MONOTONIC LOADING	29
3.1 General.....	29

3.2	Correlation Studies with Experimental Results	29
3.3	Assessment of Model Accuracy and Convergence Characteristics	32
3.4	Parametric Studies	36
3.4.1	Effect of Steel Hardening on Spread of Yielding	36
3.4.2	Effect of Yield Strength, Anchorage Length and Hardening Ratio Under Monotonic Pull-Out	40
3.4.3	Effect of Yield Strength, Anchorage Length and Hardening Ratio Under Monotonic Push-Pull	44
CHAPTER 4	ANALYTICAL STUDIES UNDER CYCLIC LOADING	49
4.1	General	49
4.2	Correlation Studies	49
4.2.1	Bar Specimen B85 of Lin and Hawkins (1982)	50
4.2.2	Straight Anchored Bar of Viathanatepa et al. (1979)	56
4.3	Parameter Studies under Cyclic Push-Pull Loading Conditions	59
4.3.1	Reinforcing Bar with Anchorage Length of 15 Bar Diameters	60
4.3.2	Reinforcing Bar with Anchorage Length of 25 Bar Diameters	60
4.3.3	Reinforcing Bar with Anchorage Length of 35 Bar Diameters	65
4.3.4	Bond Damage Distribution Along Anchorage	65
CHAPTER 5	CONCLUSIONS	69
	REFERENCES	71
APPENDIX A	MATERIAL MODELS	73
A.1	Steel Stress-Strain Relation	73
A.2	Bond Stress-Slip Model	76
A.2.1	General Model Description	77
A.2.2	Bond Stress-Slip Relation in Confined Concrete	80
A.2.3	Bond Stress-Slip Relation in Hook Anchorages	81

LIST OF FIGURES

FIGURE	TITLE	PAGE
FIGURE 2.1	INFINITESIMAL SEGMENT OF ANCHORED REINFORCING BAR	6
FIGURE 2.2	RELATION AMONG THE FOUR FIELDS	8
FIGURE 2.3	BAR ELEMENT WITH END FORCES, DISPLACEMENTS AND BOND STRESSES.....	10
FIGURE 3.1	MATERIAL PARAMETERS FOR STEEL AND BOND MODEL.....	30
FIGURE 3.2	ANCHORED BAR SPECIMEN FROM VIWATHANATEPA ET AL. (1979): MONOTONIC PULL-OUT TEST CASE A: $q_1 = 13.5$ MPa AND $q_3 = 6$ MPa CASE B: $q_1 = 14.85$ MPa AND $q_3 = 6.6$ MPa.....	31
FIGURE 3.3	ANCHORED BAR SPECIMEN FROM VIWATHANATEPA ET AL. (1979): MONOTONIC PUSH-PULL TEST CASE A: $q_1 = 13.5$ MPa AND $q_3 = 6$ MPa CASE B: $q_1 = 14.85$ MPa AND $q_3 = 6.6$ MPa.....	32
FIGURE 3.4	MONOTONIC LOADING OF A SINGLE ELEMENT WITH VARIABLE NUMBER OF INTEGRATION POINTS.....	33
FIGURE 3.5	MONOTONIC LOADING OF ANCHORED REINFORCING BAR WITH VARIABLE NUMBER OF ELEMENTS AND INTEGRATION POINTS	35
FIGURE 3.6	YIELD PENETRATION FOR A STRAIN HARDENING RATIO VALUE OF 1.4% A: STEEL STRESS VERSUS SLIP AT PULL-OUT END B: SLIP AT ALL NODES VERSUS SLIP AT PULL-OUT END	37
FIGURE 3.7	YIELD PENETRATION FOR A STRAIN HARDENING RATIO VALUE OF 7% A: STEEL STRESS VERSUS SLIP AT PULL-OUT END B: SLIP AT ALL NODES VERSUS SLIP AT PULL-OUT END	38
FIGURE 3.8	YIELD PENETRATION FOR A STRAIN HARDENING RATIO VALUE OF 14% A: STEEL STRESS VERSUS SLIP AT PULL-OUT END B: SLIP AT ALL NODES VERSUS SLIP AT PULL-OUT END	39
FIGURE 3.9	EFFECT OF YIELD STRENGTH ON ANCHORED BAR WITH 1.4% HARDENING A: STEEL STRESS = 380 MPa B: STEEL STRESS = 550 MPa.....	41
FIGURE 3.10	EFFECT OF YIELD STRENGTH ON ANCHORED BAR WITH 3.5% HARDENING A: STEEL STRESS = 380 MPa B: STEEL STRESS = 550 MPa.....	42
FIGURE 3.11	EFFECT OF YIELD STRENGTH ON ANCHORED BAR WITH 7% HARDENING A: STEEL STRESS = 380 MPa B: STEEL STRESS = 550 MPa.....	43
FIGURE 3.12	EFFECT OF YIELD STRENGTH ON ANCHORED BAR WITH 1.4% HARDENING A: STEEL STRESS = 380 MPa B: STEEL STRESS = 550 MPa.....	45
FIGURE 3.13	EFFECT OF YIELD STRENGTH ON ANCHORED BAR WITH 3.5% HARDENING A: STEEL STRESS = 380 MPa B: STEEL STRESS = 550 MPa.....	46

FIGURE 3.14	EFFECT OF YIELD STRENGTH ON ANCHORED BAR WITH 7% HARDENING A: STEEL STRESS = 380 MPA B: STEEL STRESS = 550 MPA	47
FIGURE 4.1	SPECIMEN B85 OF LIN, HAWKINS (1982): GEOMETRY AND FINITE ELEMENT MODEL	50
FIGURE 4.2	CYCLIC LOADING HISTORY FOR SPECIMEN B85 OF LIN AND HAWKINS (1982).....	51
FIGURE 4.3	STEEL STRESS-STRAIN RELATION: MONOTONIC ENVELOPE.....	51
FIGURE 4.4	BOND FORCE-SLIP MODEL: MONOTONIC ENVELOPES	52
FIGURE 4.5	COMPARISON BETWEEN EXPERIMENTAL AND ANALYTICAL RESULTS: STEEL STRESS- BAR PULL OUT RELATION	53
FIGURE 4.6	STEEL STRESS DISTRIBUTION ALONG REINFORCING BAR UNDER PULL-OUT (LEFT) AND PUSH-IN (RIGHT) CONDITIONS	54
FIGURE 4.7	RELATIVE SLIP DISTRIBUTION ALONG REINFORCING BAR UNDER PULL-OUT (LEFT) AND PUSH-IN (RIGHT) CONDITIONS	54
FIGURE 4.8	BOND STRESS DISTRIBUTION ALONG REINFORCING BAR UNDER PULL-OUT (LEFT) AND PUSH-IN (RIGHT) CONDITIONS	54
FIGURE 4.9	BOND STRESS- BAR PULL OUT RELATION AT NODES 2 THROUGH 7	55
FIGURE 4.10	STRESS-SLIP RESPONSE OF ANCHORED REINFORCING BAR UNDER CYCLIC PUSH-PULL: ANALYTICAL RESULTS.....	57
FIGURE 4.11	STRESS-SLIP RESPONSE OF ANCHORED REINFORCING BAR UNDER CYCLIC PUSH-PULL: EXPERIMENTAL RESULTS.....	58
FIGURE 4.12	CYCLIC PUSH-PULL ON BAR WITH ANCHORAGE LENGTH OF 15 BAR DIAMETERS	60
FIGURE 4.13	EFFECT OF YIELD STRENGTH ON CYCLIC PUSH-PULL OF ANCHORED BAR. ANCHORAGE LENGTH = $25 d_b$; STRAIN HARDENING RATIO = 1.4%	61
FIGURE 4.14	EFFECT OF YIELD STRENGTH ON CYCLIC PUSH-PULL OF ANCHORED BAR. ANCHORAGE LENGTH = $25 d_b$; STRAIN HARDENING RATIO = 3.5%	62
FIGURE 4.15	EFFECT OF YIELD STRENGTH ON CYCLIC PUSH-PULL OF ANCHORED BAR. ANCHORAGE LENGTH = $35 d_b$; STRAIN HARDENING RATIO = 1.4%	63
FIGURE 4.16	EFFECT OF YIELD STRENGTH ON CYCLIC PUSH-PULL OF ANCHORED BAR. ANCHORAGE LENGTH = $35 d_b$; STRAIN HARDENING RATIO = 3.5%	64
FIGURE 4.17	BOND DAMAGE DISTRIBUTION FOR REINFORCING BARS WITH ANCHORAGE LENGTH OF 15 AND 25 BAR DIAMETERS	66
FIGURE 4.18	BOND DAMAGE DISTRIBUTION FOR REINFORCING BARS WITH ANCHORAGE LENGTH OF 35 BAR DIAMETERS.....	67
FIGURE 4.19	BOND DAMAGE DISTRIBUTION FOR A BAR MODEL WITH 8 ELEMENTS.....	68
FIGURE A.1	MENEGOTTO-PINTO REINFORCING STEEL MODEL	73
FIGURE A.2	DEFINITION OF CURVATURE PARAMETER R IN MENEGOTTO-PINTO STEEL MODEL	74
FIGURE A.3	BOND STRESS-SLIP RELATION	77

LIST OF TABLES

TABLE	TITLE	PAGE
TABLE 2.1	INTEGRATION POINTS AND WEIGHTS FOR GAUSS-LOBATTO SCHEME.....	24
TABLE 4.1	SELECTED PARAMETER VALUES	59
TABLE A.1	CHARACTERISTIC VALUES OF MONOTONIC ENVELOPE OF BOND STRESS-SLIP RELATION FOR DEFORMED STRAIGHT BARS EMBEDDED IN CONFINED CONCRETE	80
TABLE A.2	CHARACTERISTIC VALUES OF MONOTONIC ENVELOPE OF BOND STRESS-SLIP RELATION FOR HOOKED BARS EMBEDDED IN CONFINED CONCRETE	81

CHAPTER 1

INTRODUCTION

1.1 General

The hysteretic behavior of reinforced concrete (RC) structures under severe seismic excitations depends on the hysteretic behavior of the constituent materials and on several factors related to the interaction between reinforcing steel and concrete under cyclic load reversals. A manifestation of this interaction is the relative slip between steel and concrete in the form of pull-out of reinforcement from footings and exterior beam-column joints. It also manifests itself in the form of large cracks at the interface between beam and column in interior beam-column joints.

A number of experimental studies on reinforced concrete frame subassemblages in the last twenty years (e.g. Bertero and Popov 1977) have shown that the deformations due to relative slip of reinforcement account for a significant portion of the global displacement of the subassemblage. Most importantly, this contribution increases with the number of load reversals, as bond between reinforcing steel and concrete deteriorates. In spite of the importance of the subject, very little analytical work has been conducted to date and efforts to account for the effect of pull-out on the seismic response of entire structures are very few.

In the last years the Finite Element Method (FEM) has gained acceptance in practice, as a powerful and reliable tool for the evaluation of existing structures and the design of complex new structures. This interest has led to increased attention to the modeling of bond on the part of researchers. Even though accurate constitutive relations for bond have been established experimentally under general cyclic excitations (Eligehausen et al. 1983), no analytical model has yet been proposed that can be used in conjunction with a general purpose finite element program and is, at the same time, capable of describing the complex hysteretic behavior of anchored reinforcing bars under cyclic excitations. An anchored reinforcing bar that is subjected to a tensile force at one end, transfers this force to the surrounding concrete by the interaction of two mechanisms acting in parallel: the uniaxial stress and associated strain in the reinforcing bar and the slip of the bar relative to the

surrounding concrete, which produces a bond-stress field over the bar surface. A brief summary of past analytical efforts is presented in the next section.

1.2 Review of Previous Studies

The first model for bond-slip of reinforcing bars was proposed by Ngo and Scordelis (1967) who developed a linear elastic FE model of a simply supported beam that consisted of constant strain triangular elements for concrete and steel. In the study concentrated (lumped) bond link elements were introduced at the nodes where concrete and steel elements were connected. The linkage element had no physical dimensions and could be visualized as two orthogonal springs. The same approach was followed by Nilson (1972) who introduced nonlinear constitutive relations for steel and concrete and a nonlinear bond-slip relation. A bond-zone element of finite thickness with distributed bond action was developed by deGroot et al. (1981) and by Keuser and Mehlhorn (1987) who showed that concentrated bond link elements are capable of representing correctly only uniform slip distributions and who, therefore, introduced a contact element which provides a continuous interaction between steel and concrete. In the latter studies the behavior of concrete was modified in the vicinity of the contact surface between reinforcing steel and concrete to account for the properties of the bond zone. None of these studies, however, addressed directly the numerical solution of an anchored reinforcing bar under cyclic excitations.

A more rational approach was followed by Filippou et al. (1983). In this study the weighted residual method is used to solve the differential equations of equilibrium and compatibility of an anchored reinforcing bar. This approach gave rise to a mixed finite element with independent approximations of the displacement and stress field in the bar. Unfortunately, the formulation was not carried through to permit implementation in a general purpose finite element program.

Yankelevsky (1985) proposed a finite element with displacement interpolation functions. The study is, however, limited to linear elastic reinforcing bars under monotonic pull-out conditions with rather small maximum pull-out values of 0.3 mm. This does not permit an assessment of the performance of this type of element in the presence of bond softening under cyclic excitations.

The reinforcing bar elements are typically arranged along the sides of concrete finite elements and this feature leads to the double node concept that results in an appreciable

increase of the total number of nodes in the finite element representation of the structure. Implementations of these elements under cyclic load conditions are very rare. To alleviate the double node problem Kwak and Filippou (1990) proposed an embedded reinforcing bar element for finite element analysis that still interacts with concrete elements via concentrated bond links at the two end nodes. Their studies encompass reinforcing bar anchorages under monotonic and cyclic load conditions, as well as reinforced concrete beams, slabs and beam-column joints under monotonic loads.

In summary, the solutions proposed so far are hampered by the following limitations: (a) bond is typically lumped at the nodes of the FE model, where concentrated springs with appropriate constitutive relationships connect the reinforcing bar with the surrounding concrete; (b) the models are limited to linear elastic behavior in either steel or bond behavior, rarely include the nonlinear behavior of both and are not capable of simulating cyclic behavior and bond deterioration; (c) most existing models are based on the displacement (stiffness) method of analysis and, thus, center on the assumption of a displacement interpolation function for the relative slip. The presence of very steep slip gradients along the yielding portion of reinforcing bars demands a large number of elements for good accuracy. Even so, displacement based models are plagued by numerical problems in the presence of bond softening, as few studies to date have shown (Viwathanatepa et al. 1979); (d) models proposed to date lack a clear implementation in a general purpose finite element program.

Recent studies (Filippou 1986, Zulfqar and Filippou 1990) have shown that, on account of the smooth character of stress distributions, it is numerically advantageous to approximate the bond or steel stress distribution rather than the relative slip along the anchored reinforcing bar.

The desire to base the element formulation on the approximation of the steel or bond stress distribution along the anchored reinforcing bar leads to a force (flexibility) based element formulation. Such an approach has not received much attention in finite element models to date, because of the difficulty of implementing a flexibility based nonlinear element in a general purpose finite element program that centers on the displacement (stiffness) method. Ciampi and Carlesimo (1986) were the first to propose a consistent implementation of a flexibility based element in a program that is based on the displacement method of analysis. Their method was refined and extended by Taucer et al. (1991) within the general purpose finite element program FEAP documented in Zienkiewicz and Taylor (1989 and 1991).

1.3 Objectives and Scope

This study presents the development and the numerical implementation of a finite element for anchored reinforcing bars. The objective of the study is the development of a robust and efficient model within the framework of classical finite element methodology, so that the model can be later implemented in the analysis of reinforced concrete members, such as beam-column joints, where the interaction between reinforcing steel and concrete through bond plays an essential role in the characterization of the hysteretic behavior.

The development of the proposed model is based on the flexibility method of analysis. In this case force interpolation functions are used to approximate the force fields in the governing differential equations of the problem. For the problem of stress transfer between reinforcing steel and concrete through bond the force fields are the steel stress in the reinforcement and the bond stress acting on the circumference of the anchored bar. Since these two fields are, however, related by the equilibrium equation of the problem, only one can be selected independently. The development of the flexibility based model is motivated by the fact that anchored reinforcing bars that are subjected to large deformation reversals exhibit a smooth distribution of steel stress, while the strain and relative displacement between reinforcing steel and surrounding concrete are characterized by steep gradients in the inelastic portion of the anchored bar.

In Chapter 2 the theoretical formulation of the flexibility-based finite element is presented along with a comparison between the stiffness and flexibility method and some important considerations regarding the selection of shape functions. The chapter concludes with the implementation of the proposed element in general purpose finite element analysis program and the summary of the state determination algorithm. Chapters 3 and 4 contain several correlation studies of the model with experimental results from anchored reinforcing bars. Chapter 3 is concerned with monotonic loads and Chapter 4 with cyclic. A series of parameters studies are also included in these chapters for the purpose of assessing the influence of key material parameters on the hysteretic behavior of anchored reinforcing bars. Conclusions of the study are offered in Chapter 5.

CHAPTER 2

FINITE ELEMENT FORMULATION

2.1 General

This chapter presents the development of a finite element model for a reinforcing bar anchored in concrete with continuous bond. In the systematic derivation of the proposed solution method the model is viewed as a simple mechanical system that is made up of two components in parallel. The first component is the reinforcing bar and the second is the interface between reinforcing steel and surrounding concrete (Fig. 2.1). The nonlinear hysteretic behavior of the model derives entirely from the nonlinear constitutive behavior of these two components. The hysteretic behavior of the reinforcing bar is described by a cyclic steel stress-strain relation, while the hysteretic behavior of the interface derives from a cyclic bond stress-slip relation that includes a damage parameter for representing the progressive deterioration of bond. These material models are discussed in Appendix A. A fundamental difficulty of this model arises from the fact that the constitutive behavior of one component is of the *stress-strain* type, while the constitutive behavior of the other is of the *stress-displacement* type. In a strict sense, the latter cannot be considered a pure constitutive law and is typically called a “local” constitutive relation.

The analytical models proposed to date fall into two categories. The first group is made up of models that are developed for implementation in finite element analysis programs. These include the effect of bond by means of concentrated bond-link elements that connect the reinforcing steel nodes to the corresponding concrete nodes. The bond link element is extremely limited in its ability to represent the actual continuous bond conditions along anchored reinforcing bars, as pointed out in a study by Keuser and Mehlhorn (1987), who overcame these limitations with a continuous bond element. Most importantly, existing finite element models for reinforcing bars with bond-slip are based on displacement interpolation functions and the stiffness method of analysis. In order to simulate the steep displacement gradients associated with the spread of yielding in anchored reinforcing bars, analysts resort to a fine finite element mesh with significant increase in computational cost.

In spite of this, stiffness based elements have been plagued by numerical instabilities and lack of convergence in the post-peak, softening range of the force-displacement relation.

In the second group of anchored reinforcing bar models fall special purpose models of a single reinforcing bar. These devote great attention to representing the continuous nature of bond along the reinforcing bar and devising special solution strategies for bypassing the numerical difficulties of displacement based models. While several such models have been successfully used in the simulation of the hysteretic behavior of anchored reinforcing bars, their implementation in a finite element analysis program is, at best, unclear, if not impossible. Another limitation of these models is their lack of a clear theoretical underpinning of the proposed solution algorithm.

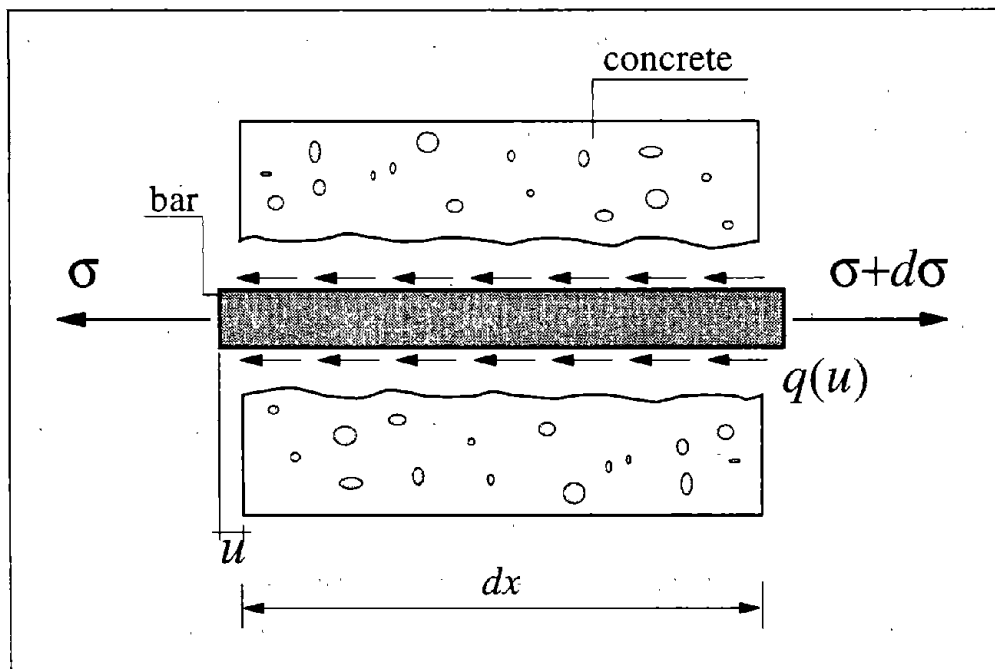


FIGURE 2.1 INFINITESIMAL SEGMENT OF ANCHORED REINFORCING BAR

The proposed anchored reinforcing bar model overcomes these limitations. It is based on the flexibility method of analysis so that force instead of displacement interpolation functions form the starting point of the formulation. With this approach the inclusion of continuous bond is rather straightforward by means of an interpolation function. The steel force interpolation function is selected so as to satisfy equilibrium with the bond forces pointwise along the element. Since bond and reinforcing steel forces change smoothly along

the anchored reinforcing bar, a small number of elements suffices to yield accurate results. Most importantly, the method is characterized by robust and stable numerical behavior even in the post-peak, softening range of response.

After the derivation of the governing differential equations for an anchored reinforcing bar the consistent formulation of the stiffness and flexibility method are juxtaposed in this chapter in the interest of gaining insight in the similarities and differences of these two approaches. The chapter then concludes with the numerical implementation of the proposed flexibility-based model for an anchored reinforcing bar.

2.2 Governing Differential Equations of the Problem

The boundary value problem of a reinforcing bar anchored in concrete (Fig. 2.1) involves four unknown fields: the stress $\sigma = \sigma(x)$ in the reinforcing bar, the bond stress $q = q(x)$ at the interface between bar and concrete, the strain $\varepsilon = \varepsilon(x)$ in the reinforcing bar and the slip $u = u(x)$ of the reinforcing bar relative to the surrounding concrete. The relative slip $u = u(x)$ is the difference between steel and concrete displacements at location x . In the present study the concrete deformations are neglected, so that $\varepsilon_c(x) \equiv 0$. Consequently, $u(x)$ is simply the displacement field of the steel bar. All unknown fields are defined in the one-dimensional $\{x\}$ domain Ω of the embedded length L of the bar.

The four fields are related by the governing equations of the stress transfer problem. These relations are schematically illustrated in Fig. 2.2:

$$\frac{d\sigma}{dx} = \rho q \quad \text{in } \Omega = (0, L) \quad (\text{equilibrium}) \quad (2.1)$$

$$\frac{du}{dx} = \varepsilon - \varepsilon_c = \varepsilon \quad \text{in } \Omega = (0, L) \quad (\text{compatibility}) \quad (2.2)$$

$$\sigma = \sigma(\varepsilon) \quad (\text{steel constitutive relation}) \quad (2.3)$$

$$q = q(u) \quad (\text{bond constitutive relation}) \quad (2.4)$$

where d is the reinforcing bar diameter and $\rho = (\pi d)/(\pi d^2/4) = 4/d$ is the ratio of bar circumference to bar area per unit of length.

The boundary conditions on the domain boundary Γ can be either of the essential type

$$\begin{aligned} u &= u_0 & \text{on } \Gamma_u &= \{0\} \\ u &= u_L & \text{on } \Gamma_u &= \{L\} \end{aligned} \quad (2.5)$$

or of the natural type

$$\begin{aligned} \sigma &= \sigma_0 & \text{on } \Gamma_\sigma &= \{0\} \\ \sigma &= \sigma_L & \text{on } \Gamma_\sigma &= \{L\} \end{aligned} \quad (2.6)$$

depending on the problem at hand.

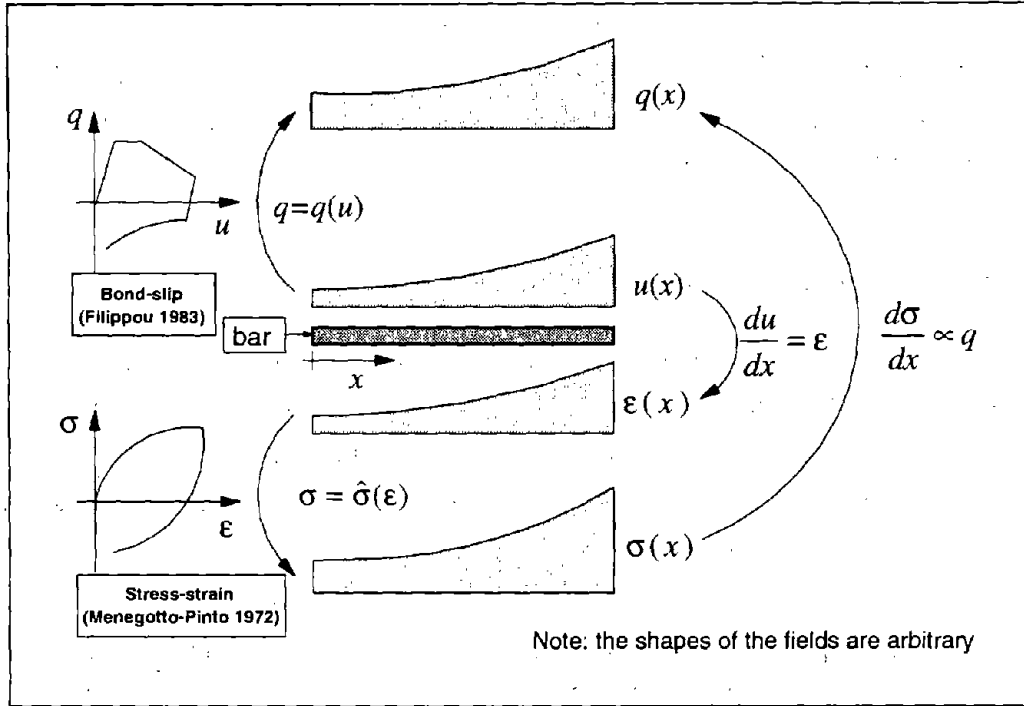


FIGURE 2.2 RELATION AMONG THE FOUR FIELDS

In order to deal with the nonlinear character of the governing equations a linearization is performed. The four fields are expressed in incremental form ($\Delta\sigma$, Δq , Δu , $\Delta\epsilon$) and the strong form of the problem is written in incremental terms:

$$\frac{d}{dx} \Delta\sigma(x) = \rho \Delta q(x) \quad (2.7)$$

$$\frac{d}{dx} \Delta u(x) = \Delta\epsilon(x) \quad (2.8)$$

$$\Delta\sigma(x) = E_\sigma(x) \cdot \Delta\epsilon(x) \quad (2.9)$$

$$\Delta q(x) = E_q(x) \cdot \Delta u(x) \quad (2.10)$$

where E_σ is the tangent stiffness of the steel stress-strain relation, E_q is the tangent stiffness of the bond stress-slip relation and Δ denotes the variation of the corresponding field. The essential boundary conditions become

$$\begin{aligned} \Delta u &= \Delta u_0 & \text{on } \Gamma_u &= \{0\} \\ \Delta u &= \Delta u_L & \text{on } \Gamma_u &= \{L\} \end{aligned} \quad (2.11)$$

and the natural boundary conditions are

$$\begin{aligned} \Delta \sigma &= \Delta \sigma_0 & \text{on } \Gamma_\sigma &= \{0\} \\ \Delta \sigma &= \Delta \sigma_L & \text{on } \Gamma_\sigma &= \{L\} \end{aligned} \quad (2.12)$$

2.3 Finite Element Approximation

In passing from the governing differential equations in Eqs. (2.7)-(2.10) to the finite element approximation the following steps are undertaken (Reddy 1993):

- (1) The domain Ω is subdivided into a set of finite elements $\Omega^e = (x_I, x_J)$ where I and J denote the element boundaries;
- (2) The weak form of the problem is constructed within a single element;
- (3) One or more unknown fields are approximated by a polynomial within the element;
- (4) The governing equations of the finite element approximation result from the substitution of the field approximations into the weak form of step 2.

The integration of the weak form is performed numerically for the *master element* $\hat{\Omega}$ in the local coordinate system $\{\xi\}$ defined by: $\hat{\Omega} \equiv \{-1 < \xi < 1\} = (-1, 1)$. The bar master element is illustrated in Fig. 2.3. The element end forces, end displacements and bond forces are shown in the positive direction. For the sake of compact notation these are grouped in the following vectors:

$$\mathbf{S} = \{S_I, S_J\}^T \quad \text{element end forces} \quad (2.13)$$

$$\mathbf{u} = \{u_I, u_J\}^T \quad \text{element end displacements} \quad (2.14)$$

$$\mathbf{q} = \{q_I, q_J\}^T \quad \text{element bond forces} \quad (2.15)$$

The local coordinate systems $\{x\}$ and $\{\xi\}$ are shown in Fig. 2.3. The transformation between these two systems is such that:

$$dx = J_e \cdot d\xi \quad \text{or} \quad \frac{dx}{d\xi} = J_e \quad \text{or} \quad \frac{d\xi}{dx} = J_e^{-1} \quad (2.16)$$

where J_e is the Jacobian of the transformation, which for straight elements is

$$J_e = \frac{L}{2} \quad (2.17)$$

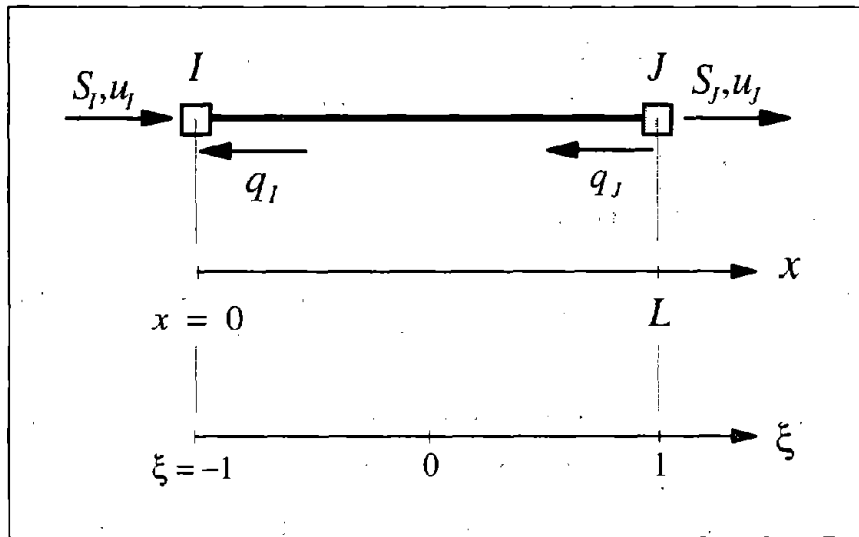


FIGURE 2.3 BAR ELEMENT WITH END FORCES, DISPLACEMENTS AND BOND STRESSES

The polynomial approximation of generic field n is defined in the $\{\xi\}$ -coordinate system by

$$\Delta n(\xi) \approx \mathbf{N}(\xi) \cdot \Delta \mathbf{n} \quad (2.18)$$

where $\Delta \mathbf{n}$ is the vector of node value increments of field $n(\xi)$ and $\mathbf{N}(\xi)$ is the row vector of element interpolation functions. The selection of the field that is to be approximated by the element interpolation functions $\mathbf{N}(\xi)$ determines the form of the finite element equations in Step 2 above and the type of method. The approximation of the displacement field gives rise to the classical stiffness method, whereas the approximation of the stress field leads to the flexibility approach.

In the following the differences between these two methods will be highlighted. The commonly used stiffness method is dealt with by adhering to common practice: a compatible displacement field approximation is selected and substituted into the weak form that is derived with the virtual displacement principle. This process transforms the set of differential equations into a set of algebraic equations. Special emphasis is placed on the flexibility method, which is much less common in finite element analysis, since this forms the basis of the proposed model. Particular attention is paid to establishing criteria for the selection of force interpolation functions for the proposed model.

2.4 Stiffness Formulation

In the stiffness approach the differential equations are recast in terms of the displacement field $\Delta u(x)$ as the only unknown. Upon substitution of Eqs. (2.9) and (2.10) into Eq. (2.7) and using Eq. (2.8) the following relation results

$$\frac{d}{dx} \left(E_\sigma \cdot \frac{d}{dx} \Delta u \right) = \rho \cdot E_q \cdot \Delta u \quad \text{in } \Omega = (0, L) \quad (2.19)$$

This governing equation is supplemented by the boundary conditions in Eq. (2.11) or Eq. (2.12).

The weak form is obtained as follows:

- (1) Each term is transferred to the left side of the equation which is then pre-multiplied by an arbitrary weight function $w(x)$ and integrated over the element domain Ω^e

$$\int_{\Omega^e} w(x) \cdot \left[\frac{d}{dx} \left(E_\sigma \cdot \frac{d}{dx} \Delta u \right) - \rho \cdot E_q \cdot \Delta u \right] dx = 0 \quad (2.20)$$

- (2) Differentiation is traded from Δu to w using integration by parts

$$\left(w \cdot E_\sigma \cdot \frac{d}{dx} \Delta u \right) \Big|_{\Gamma^e} - \int_{\Omega^e} \frac{dw}{dx} \cdot E_\sigma \cdot \frac{d}{dx} \Delta u \cdot dx - \rho \cdot \int_{\Omega^e} w \cdot E_q \cdot \Delta u \cdot dx = 0 \quad (2.21)$$

where the first term represents the natural boundary conditions

$$\left(w \cdot E_\sigma \cdot \frac{d}{dx} \Delta u \right) \Big|_{\Gamma^e} = (w \cdot E_\sigma \cdot \Delta \epsilon) \Big|_{\Gamma^e} = (w \cdot \Delta \sigma) \Big|_{\Gamma^e} \quad (2.22)$$

With the commonly adopted sign convention that stresses are positive in traction

$$\begin{aligned} \Delta \sigma(x_i) &= -\Delta S_i \\ \Delta \sigma(x_j) &= \Delta S_j \end{aligned} \quad (2.23)$$

the boundary terms become

$$\begin{aligned} w(x_i) \cdot \Delta \sigma(x_i) &= w_i \cdot (-\Delta S_i) \\ w(x_j) \cdot \Delta \sigma(x_j) &= w_j \cdot \Delta S_j \end{aligned} \quad (2.24)$$

The variational statement assumes the following incremental form

$$\int_{\Omega^e} \frac{dw}{dx} \cdot E_\sigma \cdot \frac{d}{dx} \Delta u \cdot dx + \rho \cdot \int_{\Omega^e} w \cdot E_q \cdot \Delta u \cdot dx - w_i \cdot \Delta S_i - w_j \cdot \Delta S_j = 0 \quad (2.25)$$

that represents the weak form of the problem.

The next step is to assume a polynomial approximation for the unknown displacement

field over the domain $\hat{\Omega}$ as follows:

$$\Delta u(\xi) \approx \mathbf{N}(\xi) \cdot \Delta \mathbf{u} \quad (2.26)$$

where $\Delta \mathbf{u}$ is the vector of node displacement increments and $\mathbf{N}(\xi)$ is the row vector of element displacement interpolation functions. In order to guarantee convergence of $\mathbf{N}(\xi) \cdot \Delta \mathbf{u}$ to the actual solution $\Delta u(\xi)$ with increasing number of elements, the shape functions $\mathbf{N}(\xi)$ should be:

1. *smooth* as required by the weak form,
2. *complete* in the sense that the polynomial should include all lower-order terms up to the highest order, and
3. *continuous* across the nodes of the finite element. This requirement implies that
$$\sum_{j=1}^n N_j(\xi) = 1.$$

Conditions 1 and 3 are often referred to as compatibility conditions.

The selection of the displacement field as basic unknown results in the approximation of the strain field according to Eqs. (2.8) and (2.16)

$$\Delta \varepsilon(\xi) = \frac{d}{dx} \Delta u(\xi) = \frac{d}{d\xi} \Delta u(\xi) \cdot \frac{d\xi}{dx} \approx \frac{d}{d\xi} \mathbf{N}(\xi) \cdot \Delta \mathbf{u} \cdot J_e^{-1} = \mathbf{B}(\xi) \cdot \Delta \mathbf{u} \cdot J_e^{-1} \quad (2.27)$$

where

$$\mathbf{B}(\xi) = \frac{d}{d\xi} \mathbf{N}(\xi) \quad (2.28)$$

is the row vector of shape function derivatives. Note that, in order for the compatibility equation (Eq. 2.8) to be satisfied, $\mathbf{B}(\xi)$ must include at least a non-zero constant strain field thus leading to at least a linear function approximation of the displacement field.

In the next step the approximation of the displacement field in Eq. (2.26) is substituted in the weak form of Eq. (2.25) and a Bubnov-Galerkin approximation is selected for the weight function

$$w(\xi) \approx \mathbf{N}(\xi) \cdot \mathbf{w} \quad (2.29)$$

yielding

$$\frac{d}{dx} w(\xi) = \frac{d}{d\xi} w(\xi) \cdot \frac{d\xi}{dx} \approx \frac{d}{d\xi} \mathbf{N}(\xi) \cdot \mathbf{w} \cdot J_e^{-1} = \mathbf{B}(\xi) \cdot \mathbf{w} \cdot J_e^{-1} \quad (2.30)$$

and

$$\mathbf{w}^T \left\{ \left[\int_{-1}^1 \mathbf{B}^T E_\sigma \mathbf{B} \cdot J_e^{-1} d\xi \right] \Delta \mathbf{u} + \rho \left[\int_{-1}^1 \mathbf{N}^T E_q \mathbf{N} \cdot J_e d\xi \right] \Delta \mathbf{u} - \mathbf{N}_I^T \Delta S_I - \mathbf{N}_J^T \Delta S_J \right\} = 0 \quad (2.31)$$

where $\mathbf{N}_I = \mathbf{N}|_{\xi=-1}$ and $\mathbf{N}_J = \mathbf{N}|_{\xi=1}$. Finally, from the fact that \mathbf{w} is arbitrary, and, by definition, $\mathbf{N}_I = [1 \ 0]$ and $\mathbf{N}_J = [0 \ 1]$, the following matrix equation results

$$[\mathbf{K}_\sigma + \mathbf{K}_q] \cdot \Delta \mathbf{u} = \Delta \mathbf{S} \quad (2.32)$$

where \mathbf{K}_σ is the element stiffness matrix

$$\mathbf{K}_\sigma = \int_{-1}^1 \mathbf{B}^T(\xi) \cdot E_\sigma(\xi) \cdot \mathbf{B}(\xi) \cdot J_e^{-1} d\xi \quad (2.33)$$

and \mathbf{K}_q is the geometric stiffness matrix

$$\mathbf{K}_q = \rho \int_{-1}^1 \mathbf{N}^T(\xi) \cdot E_q(\xi) \cdot \mathbf{N}(\xi) \cdot J_e d\xi \quad (2.34)$$

The shape functions $\mathbf{N}(\xi)$ must be selected so that the continuity requirements in Eq.(2.31) are satisfied, which means that the first derivative of $\mathbf{N}(\xi)$ should be square-integrable. Experimental results reveal, however, that very steep displacement gradients occur at the two ends of the solution domain Ω . Consequently, a finer mesh becomes necessary near the ends of the bar resulting in considerable increase of computational effort. Alternatively, higher order elements might be developed with the addition of internal nodes that are subsequently condensed out, but the computational cost still increases appreciably. Most importantly, the displacement interpolation functions cannot follow the dramatic changes that take place at the ends of reinforcing bar anchorages due to loss of bond. Stiffness based elements have, thus, been plagued by numerical instabilities and lack of convergence in the post-peak, softening range of the force-displacement relation.

Studies by Ciampi and Carlesimo (1986), Zeris and Mahin (1988) and Taucer et al. (1991) among others have shown that flexibility based elements exhibit excellent numerical characteristics in the post-peak, softening range of the force-displacement relation by virtue of the fact that the force interpolation functions remain exact in the nonlinear range of response. Such a flexibility based element is proposed in the following for reinforcing bar anchorages under seismic excitations.

2.5 Flexibility Formulation

Studies by Filippou et al. (1983), Filippou (1986) and Zulfiqar and Filippou (1990) have shown that the approximation of the bond stress distribution in an anchored reinforcing bar leads to a simpler, and more stable and economical solution of the problem than the approximation of the relative slip distribution. These studies failed, however, to develop a consistent theoretical basis for the implementation of this approach in a finite element analysis program. This is the objective of the following discussion which starts with the theoretical formulation of a flexibility based element for an anchored reinforcing bar and concludes with its implementation in a finite element analysis program.

In the flexibility method the governing differential equations are recast in terms of the stress field $\Delta\sigma(x)$ as the only unknown field. To this end the constitutive relations for steel and bond in Eqs. (2.9) and (2.10), respectively, need to be inverted and become

$$\Delta\varepsilon(x) = E_{\sigma}^{-1}(x) \cdot \Delta\sigma(x) = F_{\sigma}(x) \cdot \Delta\sigma(x) \quad (2.35)$$

$$\Delta u(x) = E_{\eta}^{-1}(x) \cdot \Delta q(x) = F_{\eta}(x) \cdot \Delta q(x) \quad (2.36)$$

where F_{σ} is the steel flexibility and F_{η} is the bond flexibility. Substituting Eqs. (2.35) and (2.36) into Eq. (2.8) and making use of Eq. (2.7) results in the following differential equation

$$\gamma \cdot \frac{d}{dx} \left(F_{\eta} \cdot \frac{d}{dx} \Delta\sigma \right) = F_{\sigma} \cdot \Delta\sigma \quad \text{in } \Omega = (0, L) \quad (2.37)$$

where d is the bar diameter and $\gamma = \rho^{-1} = d/4$. This governing equation is supplemented by the boundary conditions in Eq. (2.11) or Eq. (2.12).

The weak form is obtained with the following process:

- 1) Each term in Eq. (2.37) is transferred to the left side of the equation, which is then pre-multiplied by an arbitrary weight function $w(x)$ and integrated over the element domain Ω^e

$$\int_{\Omega^e} w(x) \cdot \left[\gamma \cdot \frac{d}{dx} \left(F_{\eta} \cdot \frac{d}{dx} \Delta\sigma \right) - F_{\sigma} \cdot \Delta\sigma \right] dx = 0 \quad (2.38)$$

- 2) Differentiation is traded from $\Delta\sigma$ to w using integration by parts

$$\left(w \cdot F_{\eta} \cdot \gamma \cdot \frac{d}{dx} \Delta\sigma \right) \Big|_{\Gamma^e} - \gamma \cdot \int_{\Omega^e} \frac{dw}{dx} \cdot F_{\eta} \cdot \frac{d}{dx} \Delta\sigma \cdot dx - \int_{\Omega^e} w \cdot F_{\sigma} \cdot \Delta\sigma \cdot dx = 0 \quad (2.39)$$

where the first term represents the essential boundary conditions

$$\left(w \cdot F_q \cdot \gamma \cdot \frac{d}{dx} \Delta \sigma \right) \Big|_{\Gamma_n^e} = \left(w \cdot F_q \cdot \Delta q \right) \Big|_{\Gamma_n^e} = \left(w \cdot \Delta u \right) \Big|_{\Gamma_n^e} \quad (2.40)$$

After setting

$$\begin{aligned} w(x_i) \cdot \Delta u(x_i) &= w_i \cdot \Delta u_i \\ w(x_j) \cdot \Delta u(x_j) &= w_j \cdot \Delta u_j \end{aligned} \quad (2.41)$$

the variational statement assumes the following incremental form

$$\gamma \cdot \int_{\Omega^e} \frac{dw}{dx} \cdot F_q \cdot \frac{d}{dx} \Delta \sigma \cdot dx + \int_{\Omega^e} w \cdot F_\sigma \cdot \Delta \sigma \cdot dx + w_i \cdot \Delta u_i - w_j \cdot \Delta u_j = 0 \quad (2.42)$$

Eq. (2.42) represents the weak form of the problem.

2.5.1 Approximation of Stress Field

The proposed reinforcing bar model can be viewed as a simple system that is made up of two components in parallel: the reinforcing bar and the interface between reinforcing bar and surrounding concrete. Since the model formulation is based on the flexibility method, the selection of force interpolation functions is guided by the requirement that these satisfy equilibrium within the element in a strict sense. For the system at hand this implies that the selected force interpolation functions should satisfy Eq. (2.7) pointwise. According to Eq. (2.7) the bond force is the derivative of the force in the reinforcing steel. A clear relation, thus, exists between the interpolation functions of the corresponding force fields so that only one can be selected independently. Using the bond force field for the purpose the approximation is written in the form

$$\Delta q(\xi) \approx \mathbf{B}_q(\xi) \cdot \Delta \mathbf{q} \quad (2.43)$$

where $\mathbf{B}_q(\xi)$ is the row vector of bond interpolation functions. With the inclusion of internal element nodes a higher order polynomial approximation of the bond distribution is possible. In such case the degree of the selected interpolation polynomial is $n - 1$ for an element with n nodes and vectors $\mathbf{B}_q(\xi)$ and $\Delta \mathbf{q}$ have dimensions $(1 \times n)$ and $(n \times 1)$, respectively. Substitution of Eq. (2.43) in Eq. (2.7) yields

$$\frac{d}{d\xi} \Delta \sigma(\xi) \approx J_e \rho \cdot \mathbf{B}_q(\xi) \cdot \Delta \mathbf{q} \quad (2.44)$$

Eq. (2.44) expresses the dependence of the steel stress field approximation on the selected

bond interpolation functions $\mathbf{B}_q(\xi)$ and on the bond stress increments at the nodes $\Delta\mathbf{q}$. The integration of Eq. (2.44) yields

$$\Delta\sigma(\xi) \approx \rho \cdot \int_{-1}^{\xi} \mathbf{B}_q(\zeta) J_e d\zeta \cdot \Delta\mathbf{q} + c \quad (2.45)$$

The integration constant c is determined from the boundary conditions

$$\begin{aligned} \Delta\sigma|_{\xi=-1} = -\Delta S_I &= \rho \cdot \int_{-1}^{-1} \mathbf{B}_q(\xi) J_e d\xi \cdot \Delta\mathbf{q} + c = c \\ \Delta\sigma|_{\xi=1} = \Delta S_J &= \rho \cdot \int_{-1}^1 \mathbf{B}_q(\xi) J_e d\xi \cdot \Delta\mathbf{q} + c \end{aligned} \quad (2.46)$$

With the introduction of the notation

$$\mathbf{1} = [1 \quad 1] \quad (2.47)$$

the above two equations can be combined to a single equation

$$\Delta S_J + \Delta S_I = \mathbf{1} \cdot \Delta\mathbf{S} = J_e \rho \int_{-1}^1 \mathbf{B}_q(\xi) d\xi \cdot \Delta\mathbf{q} \quad (2.48)$$

which represents the statement of element equilibrium. Given the steel stress increment at one end of the element ΔS_I and the bond stress increments at the nodes $\Delta\mathbf{q}$, Eq. (2.48) serves to uniquely determine the steel stress increment at the other end of the element ΔS_J , so that element equilibrium is satisfied.

While it is possible to use either one equation in (2.46) to solve for integration constant c , such an approach would result in a undesirable breakdown of symmetry of the solution relative to the two stresses ΔS_I and ΔS_J at the ends of the element. In order to include both boundary conditions in the expression for integration constant c , these are added up in Eq. (2.46) and the resulting expression is solved for c yielding

$$c = \frac{1}{2} \left(-\Delta S_I + \Delta S_J - J_e \rho \int_{-1}^1 \mathbf{B}_q(\xi) d\xi \cdot \Delta\mathbf{q} \right) \quad (2.49)$$

The substitution of c from Eq. (2.49) in Eq. (2.45) yields the stress field approximation in terms of the steel stress and bond stress values at the nodes of the element

$$\Delta\sigma(\xi) \approx J_e \rho \mathbf{N}_q(\xi) \cdot \Delta\mathbf{q} + \mathbf{N}_s \cdot \Delta\mathbf{S} \quad (2.50)$$

where

$$\mathbf{N}_q(\xi) = \int_{-1}^{\xi} \mathbf{B}_q(\zeta) d\zeta - \frac{1}{2} \int_{-1}^1 \mathbf{B}_q(\xi) d\xi \quad (2.51)$$

and

$$\mathbf{N}_s = \left[-\frac{1}{2} \quad \frac{1}{2} \right] \quad (2.52)$$

The expression $\mathbf{N}_s \cdot \Delta\mathbf{S}$ in Eq. (2.50) represents the average value of the steel stress increments at the element ends.

The evaluation of Eq. (2.50) at the two element ends yields the following matrix relation

$$\Delta\mathbf{S} = J_e \rho \begin{bmatrix} -\mathbf{N}_{qI} \\ \mathbf{N}_{qJ} \end{bmatrix} \cdot \Delta\mathbf{q} + \begin{bmatrix} -\mathbf{N}_s \\ \mathbf{N}_s \end{bmatrix} \cdot \Delta\mathbf{S} = J_e \rho \begin{bmatrix} -\mathbf{N}_{qI} \\ \mathbf{N}_{qJ} \end{bmatrix} \cdot \Delta\mathbf{q} + \mathbf{m}^T \cdot \mathbf{N}_s \cdot \Delta\mathbf{S} \quad (2.53)$$

where $\mathbf{N}_{qI} = \mathbf{N}_q|_{\xi=-1}$ and $\mathbf{N}_{qJ} = \mathbf{N}_q|_{\xi=1}$ are the values of the row vector of interpolation functions at nodes I and J , respectively, and

$$\mathbf{m} = [-1 \quad 1] \quad (2.54)$$

The sign convention in Eq. (2.53) adheres to the definition in Eq. (2.23).

The proposed anchored reinforcing bar element is formulated with the stress field approximations $\Delta q(\xi)$ and $\Delta\sigma(\xi)$ in Eqs. (2.43) and (2.50), respectively. These stress field approximations satisfy the equilibrium conditions along the element pointwise. In the implementation of the element in a finite element analysis program node compatibility is also maintained by keeping the displacement increments at the nodes fixed during the element state determination phase of the algorithm. Since the bond force and stiffness only depend on the node displacements $\Delta\mathbf{u}$, these also remain constant during the element state determination. Thus, the iterative algorithm only adjusts the steel strain field $\Delta\epsilon(\xi)$ in the element until it agrees with the imposed node displacements. The proposed element state determination procedure is discussed in detail in the following section.

2.5.2 Element State Determination

The state determination procedure is a fundamental step in the implementation of a nonlinear element in a finite element analysis program. Finite element analysis programs are

almost exclusively based on the direct stiffness method. In this case the displacement increments at the nodes of the structure are determined in each load step from the applied load increments and the current structure stiffness matrix. The element state determination phase of the algorithm encompasses the set of operations for determining the element stiffness matrix and the element resisting forces that correspond to the current node displacements. In a stiffness-based element these operations are rather straightforward, because the element stiffness matrix and the element resisting forces are the weighted integrals of the corresponding section quantities with the displacement shape functions serving as weights. In a flexibility-based element the state determination requires particular attention, because there is no direct way to determine the element resisting forces from the section forces and the available force interpolation functions.

The element state determination phase of the algorithm in a finite element analysis program starts from the current displacements \mathbf{u} at the nodes of the structure. The corresponding element end displacements are extracted from the structure displacement vector \mathbf{u} by compatibility considerations. In the proposed anchored reinforcing bar element it is possible to immediately calculate the bond stress and corresponding stiffness at the nodes of the element using the element end displacements \mathbf{u} and the bond constitutive relation

$$\mathbf{q} = \mathbf{q}(\mathbf{u}) \quad (2.55)$$

$$\mathbf{E}_q = \mathbf{E}_q(\mathbf{u}) \quad (2.56)$$

This completes the state determination of the bond component of the proposed element. For the state determination of the reinforcing steel bar this is treated as a simple truss element with imposed nodal displacements \mathbf{u} and with a distributed load \mathbf{q} due to bond. The reinforcing bar state determination follows the algorithm of Taucer et al. (1991) for flexibility-based elements. In the interest of brevity the theoretical background of the state determination algorithm is not discussed here. It suffices to recall that the iterations are based on successive corrections of the element deformations, until these satisfy compatibility with the imposed element end displacements. Of particular interest is the determination of the element stiffness matrix and of the residual end displacements which are discussed in the following sections. The summary of the element state determination algorithm is presented in Section 2.7.

2.5.3 Determination of Element Stiffness Matrix

The determination of the element stiffness matrix depends on the selection of the weight function in Eq. 2.42. The choice of a Bubnov-Galerkin approximation for the weight function yields

$$w(\xi) \approx J_e \rho \cdot \mathbf{N}_q(\xi) \cdot \mathbf{v} + \mathbf{N}_s \cdot \mathbf{w} \quad (2.57)$$

\mathbf{v} and \mathbf{w} can be interpreted as virtual variations of the corresponding nodal quantities and the weight function can be regarded as a virtual variation of the stress field along the bar. It is important to note that \mathbf{v} and \mathbf{w} must be such that $w(\xi)$ represents a virtual variation of the stress field in equilibrium. On account of the arbitrariness of the virtual stress field and in the interest of simplifying the element state determination it is assumed that $\mathbf{v} = \mathbf{0}$, so that

$$w(\xi) \approx \mathbf{N}_s \cdot \mathbf{w} \quad (2.58)$$

This selection results in a uniform weight function along the reinforcing bar.

The approximate form of the stress field $\Delta\sigma(\xi)$ in Eq. (2.50) and the weight function $w(\xi)$ in Eq. (2.58) are substituted in the weak form of Eq. (2.42). Noting that $dw(\xi)/dx = 0$ the first term vanishes and, after elimination of \mathbf{w}^T with the standard argument of the arbitrariness of the weight function, the following relation results

$$\left[J_e \rho \int_{-1}^1 \mathbf{N}_s^T F_\sigma \mathbf{N}_q J_e d\xi \right] \Delta\mathbf{q} + \left[\int_{-1}^1 \mathbf{N}_s^T F_\sigma \mathbf{N}_s \cdot J_e d\xi \right] \Delta\mathbf{S} - \mathbf{N}_s^T (\Delta u_j - \Delta u_l) = \mathbf{0} \quad (2.59)$$

With the linearization introduced in Section 2.2 the values of bond stress increments at the nodes are expressed in terms of the displacement increments

$$\Delta\mathbf{q} = \mathbf{E}_q \cdot \Delta\mathbf{u} \quad (2.60)$$

where \mathbf{E}_q is the bond stiffness matrix

$$\mathbf{E}_q = \begin{bmatrix} E_{qj} & 0 \\ 0 & E_{ql} \end{bmatrix} \quad (2.61)$$

With the use of vector \mathbf{m} from Eq. (2.54)

$$\Delta u_j - \Delta u_l = \mathbf{m} \cdot \Delta\mathbf{u} \quad (2.62)$$

Eq. (2.59) becomes

$$\left[\int_{-1}^1 \mathbf{N}_s^T F_\sigma \mathbf{N}_s \cdot J_e d\xi \right] \Delta\mathbf{S} = \left\{ \mathbf{N}_s^T \cdot \mathbf{m} - J_e \rho \int_{-1}^1 \mathbf{N}_s^T F_\sigma \mathbf{N}_q J_e d\xi \cdot \mathbf{E}_q \right\} \cdot \Delta\mathbf{u} \quad (2.63)$$

Since \mathbf{N}_s^T does not depend on ξ , it can be factored out of the integral and canceled out. After simplifying and rearranging Eq. (2.63) the following expression results

$$\mathbf{N}_s \cdot \Delta \mathbf{S} = \left[\int_{-1}^1 F_\sigma J_e d\xi \right]^{-1} \left\{ \mathbf{m} - J_e \rho \int_{-1}^1 F_\sigma \mathbf{N}_q J_e d\xi \cdot \mathbf{E}_q \right\} \cdot \Delta \mathbf{u} \quad (2.64)$$

After substitution of Eqs. (2.60) and (2.64) in Eq. (2.53) it becomes

$$\Delta \mathbf{S} = J_e \rho \begin{bmatrix} \mathbf{N}_{qi} \\ \mathbf{N}_{qj} \end{bmatrix} \cdot \mathbf{E}_q \Delta \mathbf{u} + \left[\int_{-1}^1 F_\sigma J_e d\xi \right]^{-1} \mathbf{m}^T \cdot \left\{ \mathbf{m} - J_e \rho \int_{-1}^1 F_\sigma \mathbf{N}_q J_e d\xi \cdot \mathbf{E}_q \right\} \cdot \Delta \mathbf{u} \quad (2.65)$$

where $\mathbf{N}_{qi} = \mathbf{N}_q|_{\xi=-1}$ and $\mathbf{N}_{qj} = \mathbf{N}_q|_{\xi=1}$ are the values of the row vector of interpolation function at nodes I and J . Finally, after regrouping terms and introducing the notation

$$k_1 = \left[\int_{-1}^1 F_\sigma(\xi) J_e d\xi \right]^{-1} \quad (2.66)$$

$$\mathbf{N}_q = \int_{-1}^1 F_\sigma(\xi) \mathbf{N}_q(\xi) J_e d\xi \quad (2.67)$$

Eq. (2.65) becomes

$$\Delta \mathbf{S} = [\mathbf{K}_s + \mathbf{K}_q] \cdot \Delta \mathbf{u} = \mathbf{K} \cdot \Delta \mathbf{u} \quad (2.68)$$

where \mathbf{K} is the element stiffness matrix defined by

$$\mathbf{K} = \mathbf{K}_s + \mathbf{K}_q \quad (2.69)$$

The first stiffness contribution in Eq. (2.69), namely

$$\mathbf{K}_s = k_1 \mathbf{m}^T \cdot \mathbf{m} = k_1 \begin{bmatrix} 1 & -1 \\ -1 & 1 \end{bmatrix} \quad (2.70)$$

is the stiffness matrix of the simple truss element. Note that it is determined by inversion of the element flexibility according to Eq. (2.66), which is a scalar in this case. The second contribution

$$\mathbf{K}_q = J_e \rho \left\{ \begin{bmatrix} -\mathbf{N}_{qi} \\ \mathbf{N}_{qj} \end{bmatrix} - k_1 \mathbf{m}^T \cdot \mathbf{N}_q \right\} \cdot \mathbf{E}_q \quad (2.71)$$

is the geometric stiffness matrix of the element. The latter arises from the action of the

distributed bond forces along the reinforcing bar.

It is interesting to note that the combined element stiffness matrix in Eq. (2.69) is invertible. The rigid body modes in the truss element stiffness matrix are eliminated by the action of bond forces along the reinforcing bar, and, consequently, an assembly of such elements does not need to be restrained.

2.5.4 Determination of Residual Displacements

The determination of element resisting forces follows the nonlinear algorithm of Taucer et al. (1991). The algorithm centers around the determination of residual strains at the integration points of the element and the subsequent determination of the corresponding residual displacements at the element ends by integration. According to the procedure in Taucer et al. (1991) the residual steel strains $\epsilon_r(\xi)$ at the section are determined with the following procedure:

1. With the known steel stress increment $\Delta\sigma(\xi)$ and the current flexibility of the steel stress-strain relation determine the steel strain increment $\Delta\epsilon(\xi)$ and update the steel strain field $\epsilon(\xi)$

$$\Delta\epsilon(\xi) = F_\sigma(\xi) \Delta\sigma(\xi) \quad (2.72)$$

$$\epsilon(\xi) = \epsilon(\xi) + \Delta\epsilon(\xi) \quad (2.73)$$

2. Determine the resisting stress $\sigma_R(\xi)$ and the tangent flexibility of the steel stress-strain relation that corresponds to the new total steel strain $\epsilon(\xi)$

$$\sigma_R(\xi) = \sigma_R[\epsilon(\xi)] \quad \text{and} \quad F_\sigma(\xi) = F_\sigma[\epsilon(\xi)] \quad (2.74)$$

3. Determine the difference between applied stress $\sigma(\xi)$ and resisting stress $\sigma_R(\xi)$

$$\sigma_U(\xi) = \sigma(\xi) - \sigma_R(\xi) \quad (2.75)$$

4. Determine the residual strain $\epsilon_r(\xi)$ that is associated with the unbalanced stress $\sigma_U(\xi)$

$$\epsilon_r(\xi) = F_\sigma(\xi) \sigma_U(\xi) \quad (2.76)$$

The residual strain field $\epsilon_r(\xi)$ along the element gives rise to residual displacements u_r at the element ends. These are determined by selecting a virtual stress field $\delta\sigma(\xi)$ in equilibrium and applying the virtual force principle

$$\delta \mathbf{S}^T \cdot \mathbf{u}_r = \int_{-1}^1 \delta \sigma(\xi) \varepsilon_r(\xi) J_e d\xi \quad (2.77)$$

where the virtual nodal forces $\delta \mathbf{S}$ are in equilibrium with the virtual stress field $\delta \sigma(\xi)$. The expression under the integral is the complementary work of the virtual stress field variation on the actual strain field. The most general form of the virtual stress field is

$$\delta \sigma(\xi) \approx J_e \rho \mathbf{N}_q(\xi) \cdot \delta \mathbf{q} + \mathbf{N}_s \cdot \delta \mathbf{S} \quad (2.78)$$

Similar to the simplification in Section 2.5.2.1, $\delta \mathbf{q}$ is assumed to be zero, so that

$$\delta \sigma(\xi) \approx \mathbf{N}_s \cdot \delta \mathbf{S} \quad (2.79)$$

Substitution of Eq. (2.73) in Eq. (2.71) and cancellation of $\delta \mathbf{S}^T$ with the standard argument of the arbitrariness of the virtual stress field yields

$$\mathbf{u}_r = \int_{-1}^1 \mathbf{N}_s^T \varepsilon_r(\xi) J_e d\xi \quad (2.80)$$

The role of the residual strains and corresponding end displacements in the nonlinear algorithm of element state determination is presented in Section 2.7.

2.5.5 Selection of Interpolation Functions and Explicit Forms of Element Stiffness Matrix and Displacement Residuals

From Eqs. (2.43) and (2.51) it is clear that the force interpolation functions depend on the selected approximation of the bond stress field along the reinforcing bar. For the proposed two-node element the simplest choice is the following linear approximation of the bond stress field, which is used in this study:

$$\mathbf{B}_q(\xi) = \frac{1}{2} [(1-\xi) \quad (1+\xi)] \quad (2.81)$$

According to Eq. (2.51) the steel stress interpolation functions $\mathbf{N}_q(\xi)$ in Eq. (2.50) become

$$\mathbf{N}_q(\xi) = \left[\left(-\frac{1}{4}(1-\xi)^2 + \frac{1}{2} \right) \quad \left(\frac{1}{4}(1+\xi)^2 - \frac{1}{2} \right) \right] \quad (2.82)$$

With this selection of interpolation functions the element stiffness matrix becomes

$$\mathbf{K} = k_1 \begin{bmatrix} 1 & -1 \\ -1 & 1 \end{bmatrix} + J_e \rho \left\{ \frac{1}{2} \mathbf{1}^T \cdot \mathbf{1} - k_1 \mathbf{m}^T \cdot \mathbf{N}_q \right\} \cdot \mathbf{E}_q \quad (2.83)$$

where k_1 and \mathbf{N}_ϱ are given by Eqs. (2.66) and (2.67), respectively and $\mathbf{1} = [1 \ 1]$. It is interesting to note that the element stiffness matrix is symmetric for the linear elastic case

$$\mathbf{K} = k_1 \begin{bmatrix} 1 & -1 \\ -1 & 1 \end{bmatrix} + \frac{1}{6} J_e \rho \begin{bmatrix} 5E_{qI} & E_{qJ} \\ E_{qI} & 5E_{qJ} \end{bmatrix} \quad (2.84)$$

since $E_{qI} = E_{qJ}$ in this case. \mathbf{K} , however, becomes nonsymmetric as soon as the bond slip value at either end enters the nonlinear range.

Finally, the substitution of Eq. (2.52) in Eq. (2.80) yields the following expression for the residual displacements at the element ends

$$\mathbf{u}_r = \int_{-1}^1 \begin{bmatrix} -\frac{1}{2} \\ \frac{1}{2} \end{bmatrix} \varepsilon_r(\xi) J_e d\xi \quad (2.85)$$

2.6 Numerical Integration

The integrals that appear in the equations of the element state determination are evaluated numerically with the Gauss-Lobatto integration scheme. This is based on the expression

$$I = \int_{-1}^1 g(\xi) \cdot d\xi = W_1 \cdot g(-1) + \sum_{h=2}^{m-1} W_h \cdot g(\xi_h) + W_m \cdot g(1) \quad (2.86)$$

where h denotes the monitored section and W_h is the corresponding weight factor (Stroud and Secrest 1966). The Gauss-Lobatto scheme with m integration points permits the exact integration of polynomials of degree up to $(2m-3)$. This procedure is superior to the classical Gauss integration method when it is important to include in the numerical evaluation of the integrals the end points of the element. Table 1 lists the values of ξ_h and W_h for different values m of the number of integration points.

With the Gauss-Lobatto integration scheme the element integrals become

$$k_1 = \left[\sum_{h=1}^m F_\sigma(\xi_h) J_e W_h \right]^{-1} \quad (2.87)$$

$$\mathbf{N}_\varrho = \sum_{h=1}^m F_\sigma(\xi_h) \mathbf{N}_\varrho(\xi_h) J_e W_h \quad (2.88)$$

$$\mathbf{u}_r = \sum_{h=1}^m \begin{bmatrix} -\frac{1}{2} \\ \frac{1}{2} \end{bmatrix} \epsilon_r(\xi_h) J_e W_h \quad (2.89)$$

m	ξ_{h_i}	W_h
2	± 1.0000000000	1.0000000000
3	± 1.0000000000	0.3333333333
	0.0000000000	1.3333333333
4	± 1.0000000000	0.1666666666
	± 0.4472135955	0.8333333333
5	± 1.0000000000	0.1000000000
	± 0.6546536707	0.5444444444
	0.0000000000	0.7111111111

TABLE 2.1 INTEGRATION POINTS AND WEIGHTS FOR GAUSS-LOBATTO SCHEME

The minimum number of integration points that yield sufficient accuracy for anchored reinforcing bar elements was four (4). This selection is discussed in some detail in the following chapter. The choice of four integration points implies that the numerical scheme integrates exactly a fifth degree polynomial. Since function N_q is quadratic, any variation of the steel flexibility $F_o(\xi)$ up to a cubic polynomial is integrated exactly.

2.7 Summary of Element State Determination Algorithm

The proposed anchored reinforcing bar element was implemented in program FEAP (Finite Element Analysis Program) that is well documented by Zienkiewicz and Taylor (1989 and 1991). In program FEAP the element subroutines handle all element specific operations such as the determination of the stiffness matrix and the resisting forces, while the main program performs the assembly of the element stiffness matrices and the resisting forces into the global stiffness matrix and resisting force vector of the structure. The main program is also responsible for the solution of the global equations of equilibrium and returns to the element subroutine the displacement increments for a given load increment. From this clear division between element and structure it is apparent that the nonlinear solution strategy is independent from the element state determination algorithm.

Program FEAP offers several alternative strategies for the solution of the nonlinear global equilibrium equations. In this study the classical Newton-Raphson algorithm is used. In this case the main program expects from the element subroutine the current tangent stiffness matrix. This is determined according to Eq. (2.84) from the bond stiffness E_{qt} and E_{qf} at the two end nodes of the element and the reinforcing bar stiffness k_1 . The latter is determined according to (2.87) by inverting the reinforcing bar flexibility, which is the integral of the flexibilities $F_{\sigma}(\xi_h)$ at the control sections. The bond stiffness and section flexibilities depend on the material laws for bond stress-slip and steel stress-strain which are discussed in Appendix A. Different global solution strategies could be readily implemented by revising the type of stiffness that the element returns to the main program. With the material laws in Appendix A it is possible to also use initial stiffness, initial secant and incremental secant stiffness methods without any complications.

In the following summary of the element state determination no mention is made of the global solution strategy. The element state determination is based on the current displacement increments $\Delta \mathbf{u}$ and the total displacements \mathbf{u} at the ends of the element which the main program passes to the element subroutine at the start of a new iteration of the global solution strategy. A detailed discussion of the relation between global solution strategy and element state determination in the context of a flexibility-based element is presented by Taucer et al. (1991).

The element state determination algorithm consists of the following steps:

- (1) *Start of element state determination.*

Set $j=1$.

- (2) *Bond state determination.*

Determine the bond stress and corresponding stiffness from the displacements \mathbf{u} at the element ends

$$\mathbf{q} = \mathbf{q}(\mathbf{u})$$

$$\mathbf{E}_q = \mathbf{E}_q(\mathbf{u})$$

From the current and last value of bond stress determine the bond stress increments $\Delta \mathbf{q}$.

- (3) *Determine the steel force increments.*
-

With the current reinforcing bar stiffness \mathbf{K}_s and the displacement increments $\Delta \mathbf{u}$ at the element ends determine the corresponding steel stress increments $\Delta \mathbf{S}_s$ and update the steel stress vector \mathbf{S}_s

$$\Delta \mathbf{S}_s = \mathbf{K}_s \cdot \Delta \mathbf{u}$$

$$\mathbf{S}_s = \mathbf{S}_s + \Delta \mathbf{S}_s$$

- (4) *Determine the steel force increments at each control section.*

Using the bond and steel force increments at the element ends the force interpolation functions yield the steel stress increment at each control section. With these the corresponding stress is updated to the current value

$$\Delta \sigma(\xi_h) = \rho J_e \mathbf{N}_q(\xi_h) \cdot \Delta \mathbf{q} + \mathbf{N}_s \cdot \Delta \mathbf{S}_s$$

$$\sigma(\xi_h) = \sigma(\xi_h) + \Delta \sigma(\xi_h)$$

Noting that the element end displacements do not change in subsequent iterations and, thus, $\Delta \mathbf{u} \equiv 0$ for $j > 1$, so is also $\Delta \mathbf{q} \equiv 0$.

- (5) *Determine the steel strain increments at each control section.*

The steel strain increments at each control section are derived the current stress increment $\Delta \sigma$ and the last value of residual strain ε_r . The total strain at the section is updated to the current value.

$$\Delta \varepsilon(\xi_h) = \varepsilon_r(\xi_h) + F_\sigma(\xi_h) \Delta \sigma(\xi_h)$$

$$\varepsilon(\xi_h) = \varepsilon(\xi_h) + \Delta \varepsilon(\xi_h)$$

- (6) *Reinforcing bar state determination.*

With the current strain value $\varepsilon(\xi_h)$ at each control section the steel stress-strain relation yields the resisting stress $\sigma_R(\xi_h)$ and tangent flexibility $F_\sigma(\xi_h)$ at the section.

$$\sigma_R(\xi_h) = \sigma_R[\varepsilon(\xi_h)]$$

$$F_\sigma(\xi_h) = F_\sigma[\varepsilon(\xi_h)]$$

- (7) *Calculate the steel stress unbalance and residual strain at each control section.*

The difference between applied and resisting steel stress yield the steel stress unbalance at each control section. The product of the steel stress unbalance with the current value of section flexibility yields the residual strain at each control section

$$\sigma_U(\xi_h) = \sigma(\xi_h) - \sigma_R(\xi_h)$$

$$\varepsilon_r(\xi_h) = F_\sigma(\xi_h) \cdot \sigma_U(\xi_h)$$

- (8) Determine the reinforcing bar stiffness matrix.

The reinforcing bar stiffness matrix is the sum of section flexibilities at the m monitored sections

$$\mathbf{K}_S = k_1 \begin{bmatrix} 1 & -1 \\ -1 & 1 \end{bmatrix} = J_e \left[\sum_{h=1}^m F_\sigma(\xi_h) W_h \right]^{-1} \begin{bmatrix} 1 & -1 \\ -1 & 1 \end{bmatrix}$$

- (9) Check for element convergence.

The criterion for element convergence is identical to that used by Taucer et al. (1991).

- (a) If the convergence criterion is satisfied, the element stiffness matrix \mathbf{K} and the element resisting forces \mathbf{S} are determined from

$$\mathbf{K} = k_1 \begin{bmatrix} 1 & -1 \\ -1 & 1 \end{bmatrix} + J_e \rho \left\{ \begin{bmatrix} -N_{qj} \\ N_{qj} \end{bmatrix} - k_1 \begin{bmatrix} -\mathbf{N}_\rho \\ \mathbf{N}_\rho \end{bmatrix} \right\} \cdot \mathbf{E}_q$$

$$\mathbf{S} = \mathbf{m}^T \cdot \mathbf{S}_S + J_e \begin{bmatrix} -N_{qj} \\ N_{qj} \end{bmatrix} \mathbf{q}$$

The element stiffness matrix \mathbf{K} and the element resisting forces \mathbf{S} are returned to the main program which assembles the global stiffness matrix and the structure resisting force vector.

- (b) If the convergence criterion is not satisfied, the residual end displacements are determined from the residual strains at the control sections according to

$$\mathbf{u}_r = J_e \begin{bmatrix} -\frac{1}{2} \\ \frac{1}{2} \end{bmatrix} \sum_{h=1}^m \varepsilon_r(\xi_h) W_h$$

whereupon iteration index j is increased by one to $j+1$ and steps (3) through (9) are repeated with $\Delta \mathbf{u} = -\mathbf{u}_r$, until convergence is achieved.

CHAPTER 3

ANALYTICAL STUDIES UNDER MONOTONIC LOADING

3.1 General

The validity of the proposed model is established in this chapter by correlation studies with experimental results of anchored reinforcing bars under monotonic loading conditions. Similar correlation studies under cyclic loading conditions are deferred to the following chapter. Since the hysteretic behavior of anchored reinforcing bars is very sensitive to key material parameters, the material parameters for these correlation studies are provided in tables and graphs either in Chapters 3 and 4 or in Appendix A, which discusses the material models for the steel stress-strain and bond stress-slip relation.

The present chapter is divided in three parts. The first part encompasses the correlation studies with experimental results of two anchored straight reinforcing bars under different monotonic loading conditions: one anchorage is subjected to monotonic pull-out at one end only, while the second is subjected to monotonic pull-out at one end and simultaneous push-in at the other. These studies intend to establish the validity and accuracy of the proposed model. The second part is devoted to parametric studies of the numerical characteristics of the proposed model, such as the effect of the number of elements and the number of integration points on the accuracy and stability of the results. Finally, the last part deals with parametric studies of the influence of key model parameters on monotonic response.

3.2 Correlation Studies with Experimental Results

Several specimens were tested by Viwathanatepa et al. (1979) under conditions simulating the effect of seismic excitations on anchored reinforcing bars in interior beam-column joints. From these tests two are selected in the following to study the accuracy of the proposed finite element model. Both tests were conducted on a straight #8 (24.5 mm diameter) reinforcing bar that was embedded in a well confined concrete block of 612.5 mm

width. The anchorage length, thus, amounts to 25 bar diameters. In the first test the specimen was subjected to a monotonic pull-out under displacement control at one end only, while in the second test it was subjected to monotonic pull-out at one end and simultaneous push-in at the other. The imposed relative bar displacements and resulting forces were measured at the loaded ends of the anchored reinforcing bars. Both specimens were the subject of previous analytical correlation studies in Viathanatepa et al. (1979), Ciampi et al. (1982), Yankelevsky (1985) and Filippou (1986). In the original tests two elastic cycles were performed prior to imposing the final monotonic loading to failure. These initial cycles are neglected in this study, since they have negligible effect on the nonlinear monotonic response. The material parameters of the reinforcing steel stress-strain relation and the bond stress-slip relation are the same as those used in the study by Filippou (1986) and are summarized in Fig. 3.1.

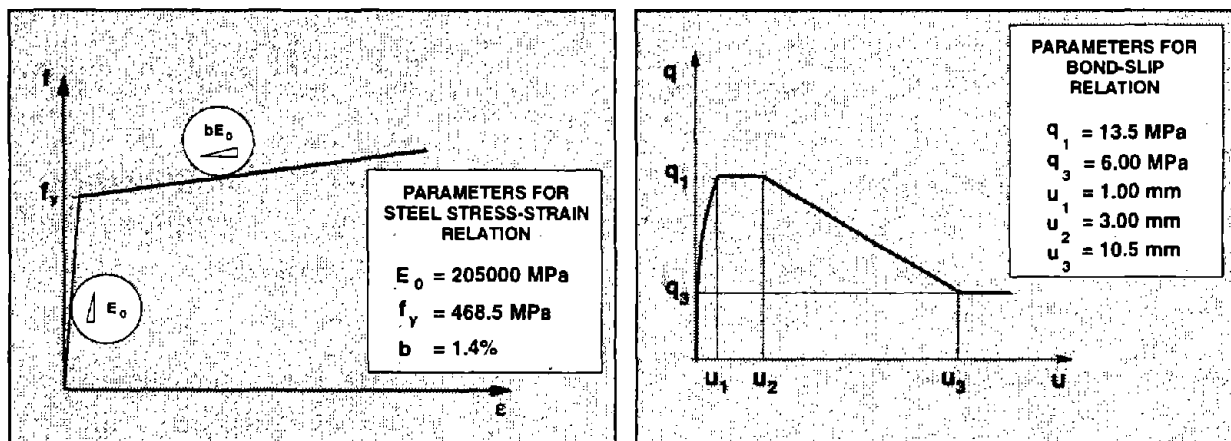


FIGURE 3.1 MATERIAL PARAMETERS FOR STEEL AND BOND MODEL

The anchored reinforcing bars are represented with 5 finite elements having 4 Gauss-Lobatto integration points each. A great advantage of the proposed model lies in the element size, which is significantly larger than in displacement based models (Ciampi et al. 1982) and need not vary along the anchored reinforcing bar. Another significant advantage concerns the bond stress-slip relation along the anchored reinforcing bar. It is well established that bond conditions are inferior in the unconfined cover portion of interior beam-column joints where a pull-out cone forms under large pull-out values. If small size elements are used in this zone, it becomes necessary to assign a bond stress-slip relation to the end nodes of these elements. No experimental data are presently available for the bond behavior in unconfined and partially confined zones under cyclic loading conditions. Moreover, assigning different bond

slip relations along the anchored reinforcing bar results in appreciable increase of the complexity and cost of the model. With the large size elements permitted by the flexibility method this problem is bypassed, since one element now spans the entire unconfined zone. The bond slip relation at the end of the element that coincides with the end of the anchored bar is damaged very rapidly and has little effect on the response. The other end is far enough, so that the bond slip relation for confined concrete is sufficiently accurate. The linear bond stress distribution within the element is a good approximation of the gradual penetration of bond damage and is very similar to the idea of the simplified model proposed by Filippou (1986) and later extended by Zulfiqar and Filippou (1990). Thus, the correlation studies in this and the following chapter use a single bond stress-slip relation along the anchored reinforcing bar.

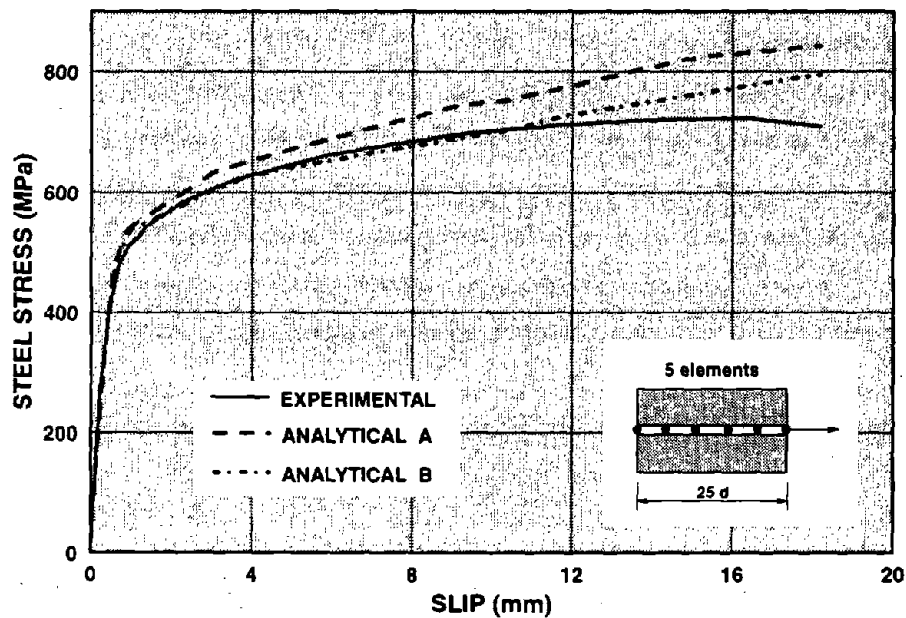


FIGURE 3.2 ANCHORED BAR SPECIMEN FROM VIWATHANATEPA ET AL. (1979):
 MONOTONIC PULL-OUT TEST
 CASE A: $q_1 = 13.5$ MPa AND $q_3 = 6$ MPa
 CASE B: $q_1 = 14.85$ MPa AND $q_3 = 6.6$ MPa

The agreement between analytical and experimental results in Figs. 3.2 and 3.3. is very satisfactory. The observed discrepancy in the last portion of the monotonic pull-out test in Fig. 3.2 is caused by the limitation of the reinforcing steel model, which assumes a constant strain hardening ratio in the post-yield range. Actual reinforcing steel behavior is

characterized by nonlinear strain hardening that becomes smaller with increasing strain until necking occurs. In the push-pull test in Fig. 3.3 there is a notable discrepancy between analysis and experiment regarding the onset of softening. The analytical results for case A correspond to the material parameters for the bond-slip relation in Fig. 3.1. Experimental observations, however, by Eligehausen et al. (1983) show that the bond strength scatters as much as 15% from the average value. Consequently, a second analysis was conducted with bond strength values q_1 and q_3 10% higher than the values in Fig. 3.1, in agreement with a similar conclusion by Ciampi et al. (1982). The analytical results for case B are also shown in Fig. 3.3 where the agreement with the experimental values is remarkable.

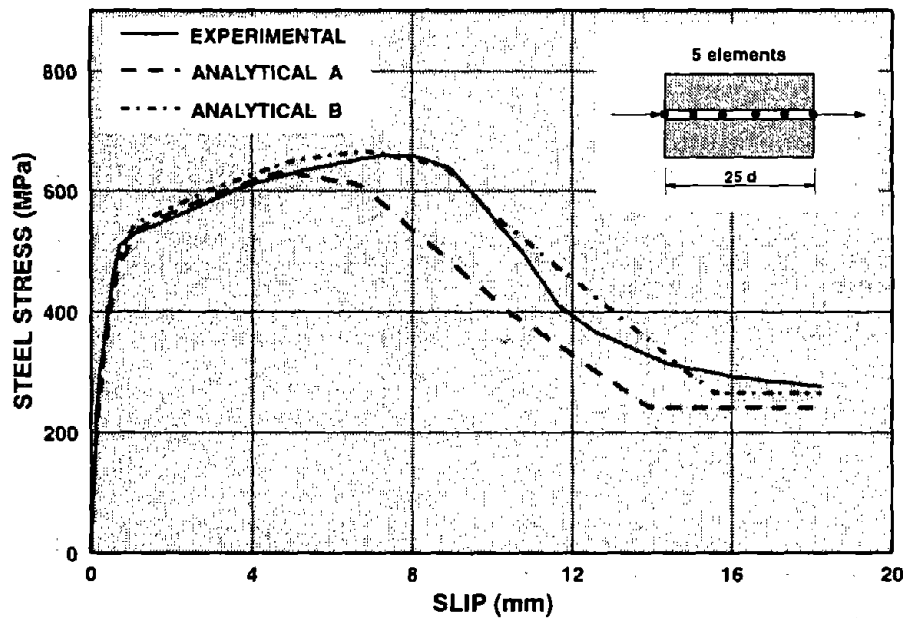


FIGURE 3.3 ANCHORED BAR SPECIMEN FROM VIWATHANATEPA ET AL. (1979):
 MONOTONIC PUSH-PULL TEST
 CASE A: $q_1 = 13.5$ MPa AND $q_3 = 6$ MPa
 CASE B: $q_1 = 14.85$ MPa AND $q_3 = 6.6$ MPa

3.3 Assessment of Model Accuracy and Convergence Characteristics

A series of tests were conducted with the objective to assess the accuracy and convergence characteristics of the model. The tests involve an anchored reinforcing bar that is subjected to monotonic pull-out at one end. The parametric studies focus on the effect of the number of elements and integration points in the finite element model on the response of

the anchored reinforcing bar. The bond properties are the same as those used in the correlation study of the previous section.

At first, a single element is used to model a short anchored reinforcing bar for studying the effect of the number of integration points on the response. The length of the anchorage is 10 bar diameters and was selected based on the following considerations: a shorter anchorage length does not suffice to induce yielding of the reinforcing bar, so that the number of integration points does not have any effect on the response; a long anchorage, on the other hand, cannot be represented with a single element, because the resulting bond stress distribution is grossly inaccurate, if it is only based on the values at the element ends, as is the case in the proposed model.

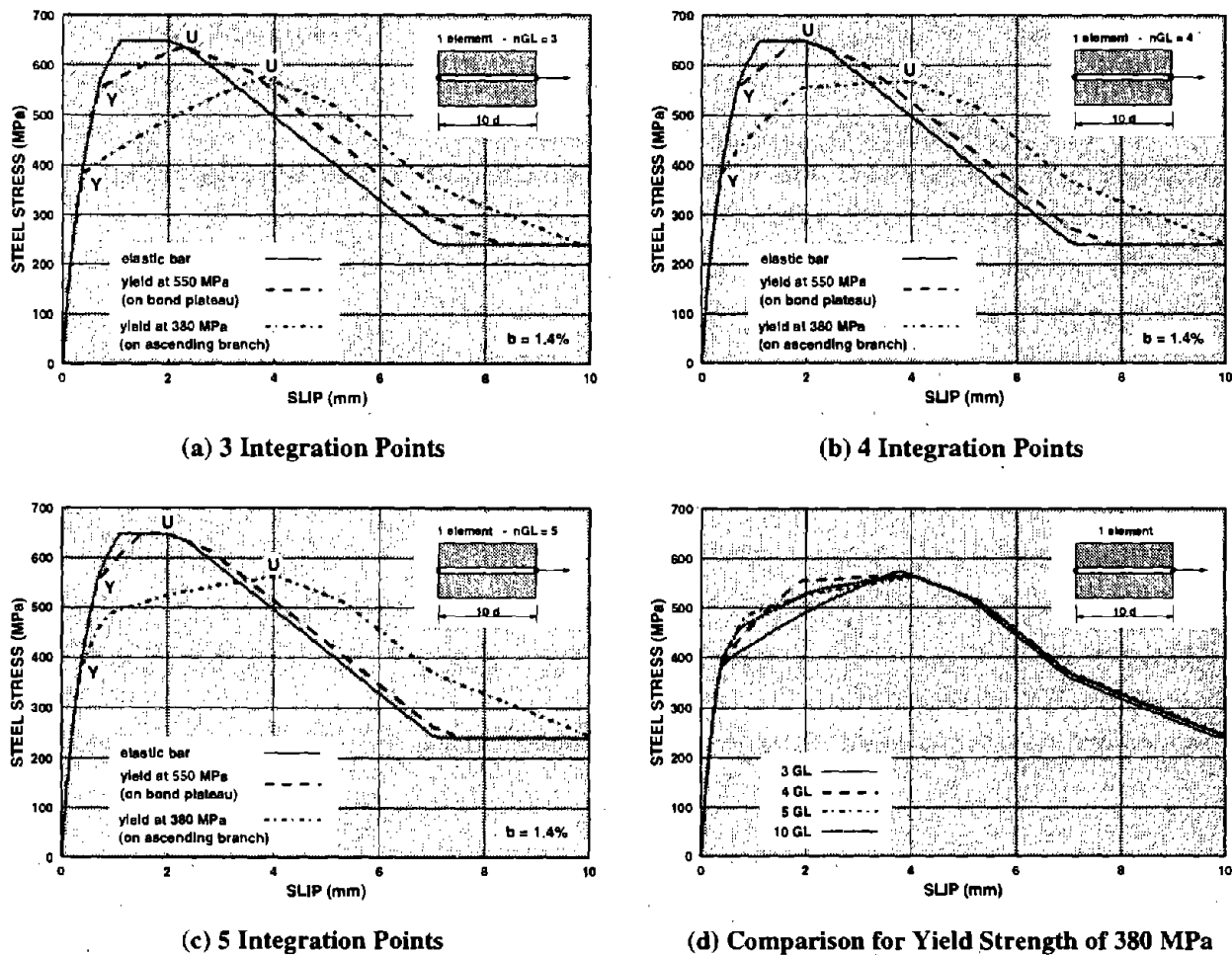
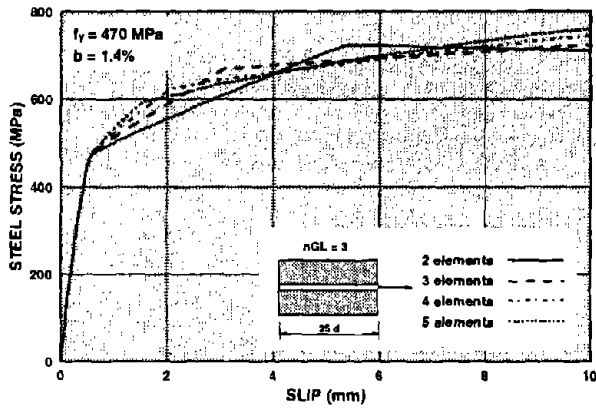


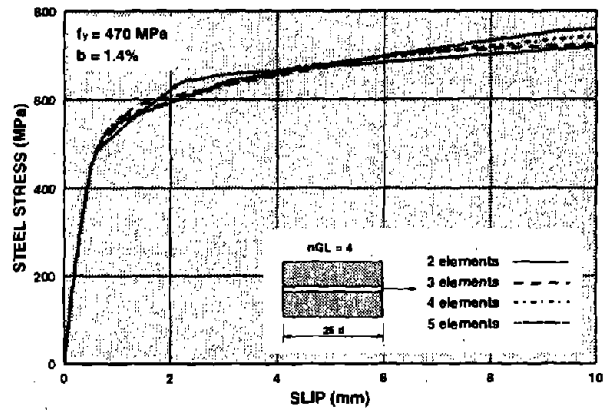
FIGURE 3.4 MONOTONIC LOADING OF A SINGLE ELEMENT WITH VARIABLE NUMBER OF INTEGRATION POINTS

The response of the single element under monotonic pull-out at one end is compared in Fig. 3.4 for variable number of integration points in the model. The penetration of yielding into the anchorage is controlled by the yield strength of steel. In this respect three cases are shown in Fig. 3.4: (a) an elastic reinforcing bar, (b) a reinforcing bar with a yield strength of 550 MPa, and (c) a reinforcing bar with a yield strength of 380 MPa. In the first case no yielding takes place in the reinforcing bar and the response is not affected by the variation in the number of integration points n_{GL} in the model, as is apparent in Figs. 3.4a, b and c. In the second case the spread of yielding is limited, since significant bond damage along the anchored bar precedes the onset of yielding that is denoted by Y in the figures. There is some change in the response in Figs. 3.4a, b and c by increasing the number of integration points from three to four and little additional change when going from four to five integration points. The most interesting case of the effect of the number of integration points on the response is the third case. In this case the yield strength of the reinforcing bar is sufficiently low, that yielding spreads over an extensive portion of the bar before bond is completely damaged and the bar pulls out at point U of the stress-slip relation. Consequently, the number of integration points plays an important role in the determination of the stiffness and resisting force of the reinforcing steel component of the model. To facilitate the comparison four cases are singled out for presentation in Fig. 3.4d. It is remarkable to note the relative insensitivity of the model to the number of integration points. With as few as three integration points the element yields very satisfactory results, even though clearly, the smaller the number of integration points, the more sudden is the stiffness change of the anchored reinforcing bar. It is also interesting to note that the numerical stability of the model is not affected by the number of integration points.

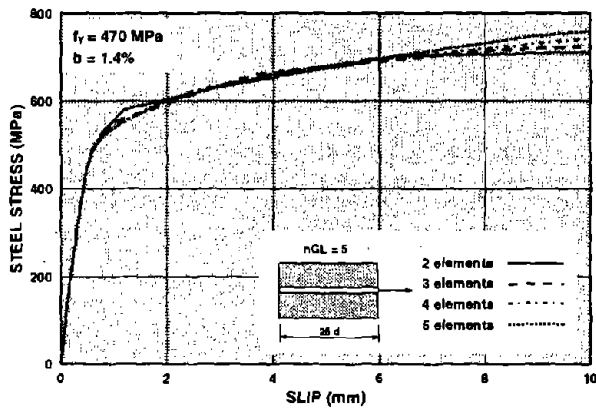
To further explore the issue of accuracy and stability of the model under variable number of integration points a second series of parametric studies is conducted on longer anchorages with variable number of elements in the analytical model of the anchored bar. In these studies the reinforcing steel properties are also kept constant. These correspond very closely to the values of the specimen that was used in the correlation studies of the previous section, so that a comparison with experimental data is also possible. The anchorage length of the reinforcing bar is equal to 25 bar diameters. Figs. 3.5a-d depict the analytical response of the anchored reinforcing bar for a total of sixteen cases. The number of integration points varies from figure to figure and covers the cases of three, four, five and ten integration points. For each case the response is compared for two, three, four and five elements.



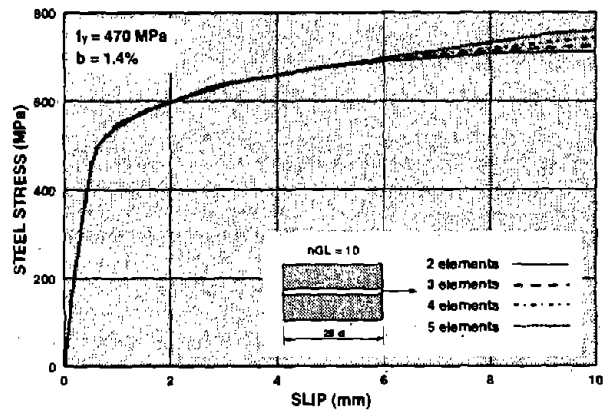
(a) 3 Integration Points



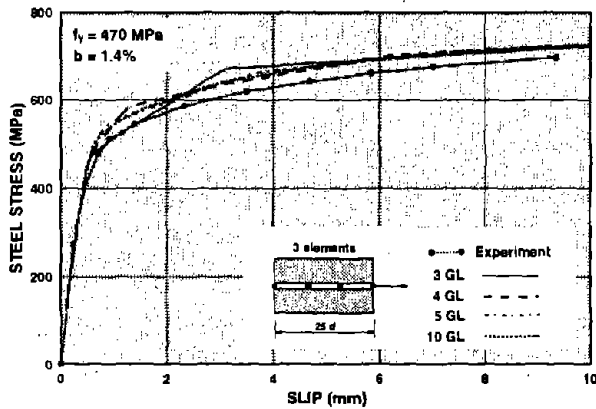
(b) 4 Integration Points



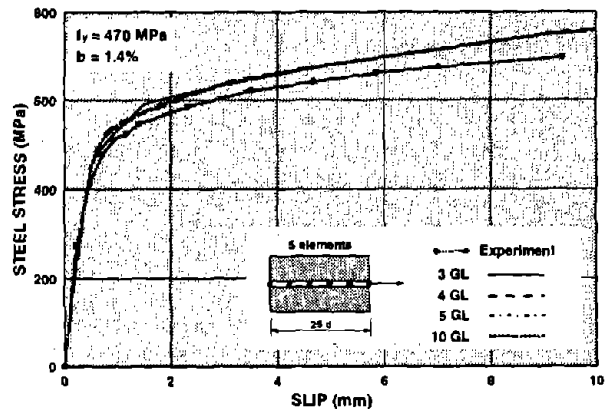
(c) 5 Integration Points



(d) 10 Integration Points



(e) 3 Elements



(f) 5 Elements

FIGURE 3.5 MONOTONIC LOADING OF ANCHORED REINFORCING BAR WITH VARIABLE NUMBER OF ELEMENTS AND INTEGRATION POINTS

Figs. 3.5e and f depict the response of the anchored reinforcing bar for three and five elements, respectively, and different number of integration points. The experimental results are also included in Fig. 3.5e and f for reference, even though the yield strength of reinforcing steel in the parametric studies ($f_y = 470$ MPa) does not exactly match the yield strength of the anchored bar in the specimen ($f_y = 468.5$ MPa).

The following observations result from the study of Fig. 3.5:

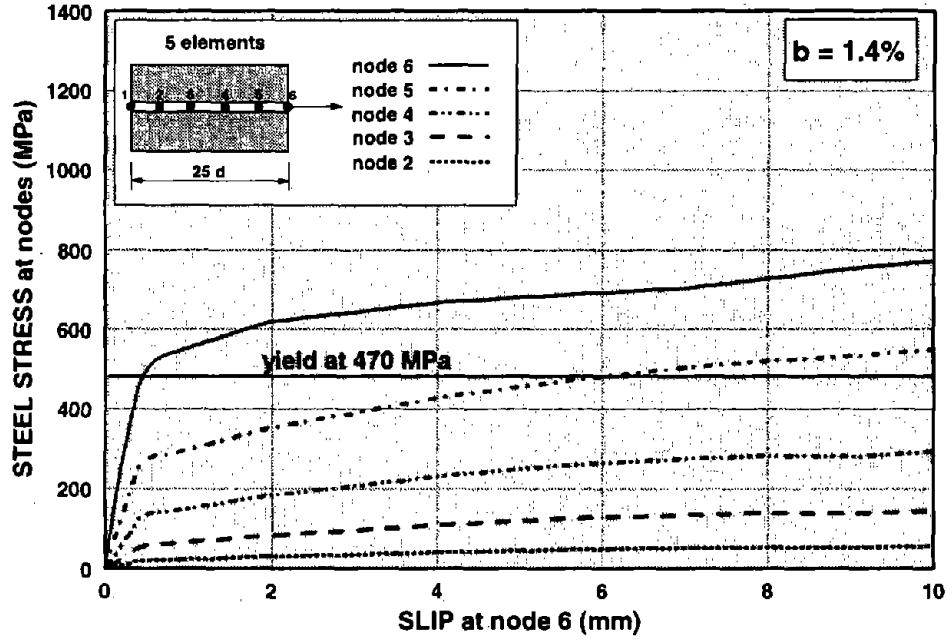
- The model shows excellent consistency and convergence characteristics. As the number of either the integration points or the elements is increased, the results converge to the analytical solution of the problem, which agrees quite well with the experimental results in Figs. 3.5e and f.
- The response of the model with two (2) elements and three (3) integration points in Fig. 3.5a is characterized by abrupt stiffness changes and an unsatisfactory softening trend under large pull-out values. Clearly, the accurate evaluation of the stiffness and resisting force integrals in Chapter 2 requires at least 4 integration points. With this number of integration points even two (2) elements result in very satisfactory results in Fig. 3.5b. On the other hand it is surprising to see that even three (3) integration points yield excellent results in Fig. 3.5a, as long as more than three (3) elements are used in the anchored reinforcing bar model.
- The conclusion from the parametric studies in Fig. 3.5 is that, while the proposed model shows impressive accuracy and convergence characteristics, at least four (4) integration points should be used in each element. While the accuracy of the results improves with the number of the elements, this improvement is so small that it does not justify the associated increase in computational cost. The distinction of the proposed model lies in its impressive accuracy and convergence characteristics, even for a small number of elements.

3.4 Parameter Studies

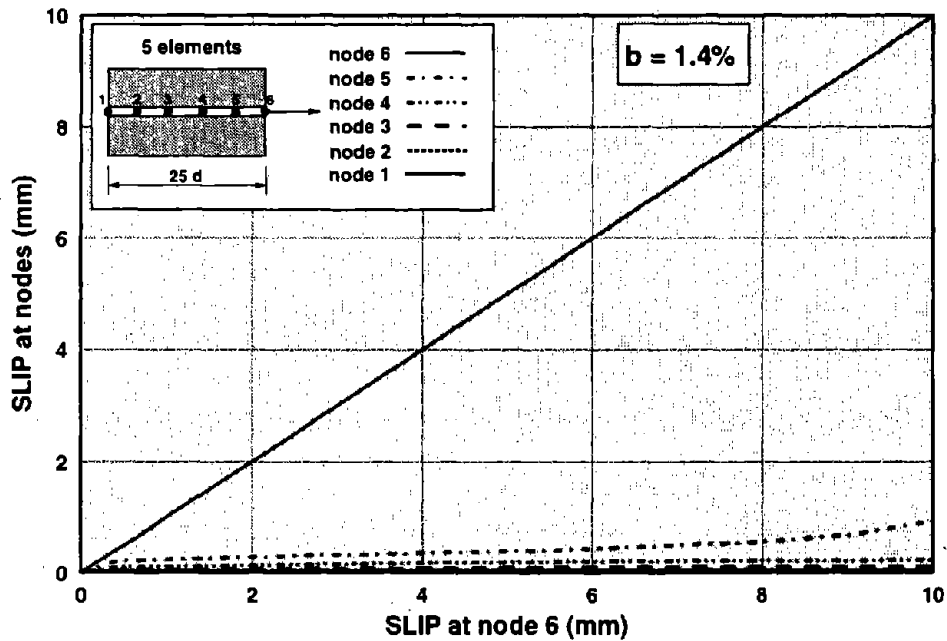
3.4.1 Effect of Steel Hardening on Spread of Yielding

The following parametric studies are conducted on a anchored reinforcing bar with an anchorage length of 25 bar diameters. The bar is modeled by 5 elements with 5 integration

points each and the objective of the study is to investigate the spread of yielding into the bar as a function of the steel strain hardening ratio.

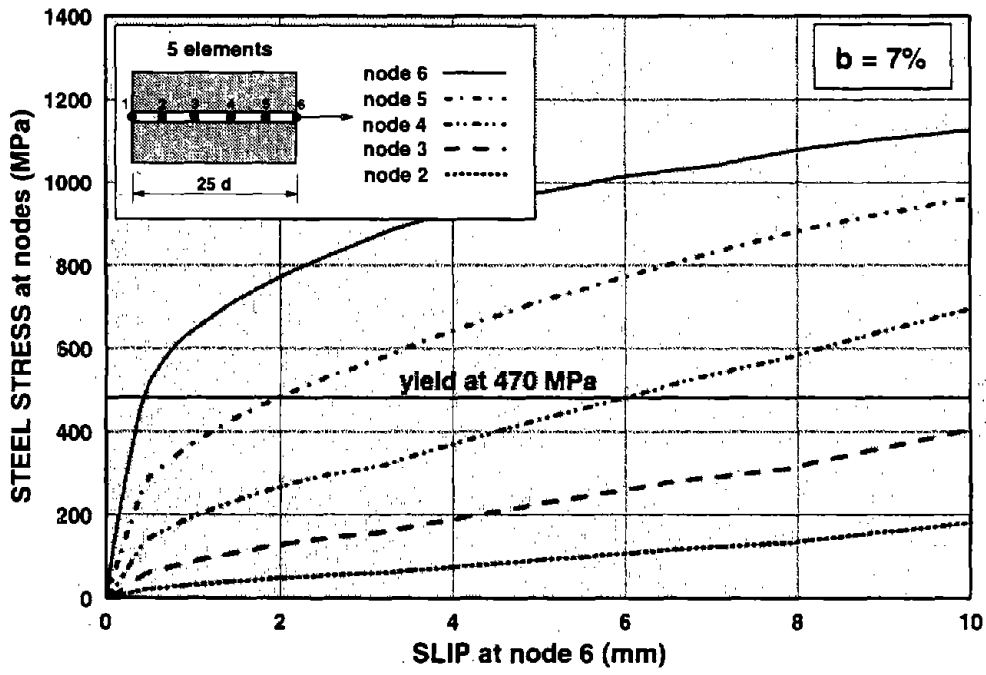


A: STEEL STRESS VERSUS SLIP AT PULL-OUT END

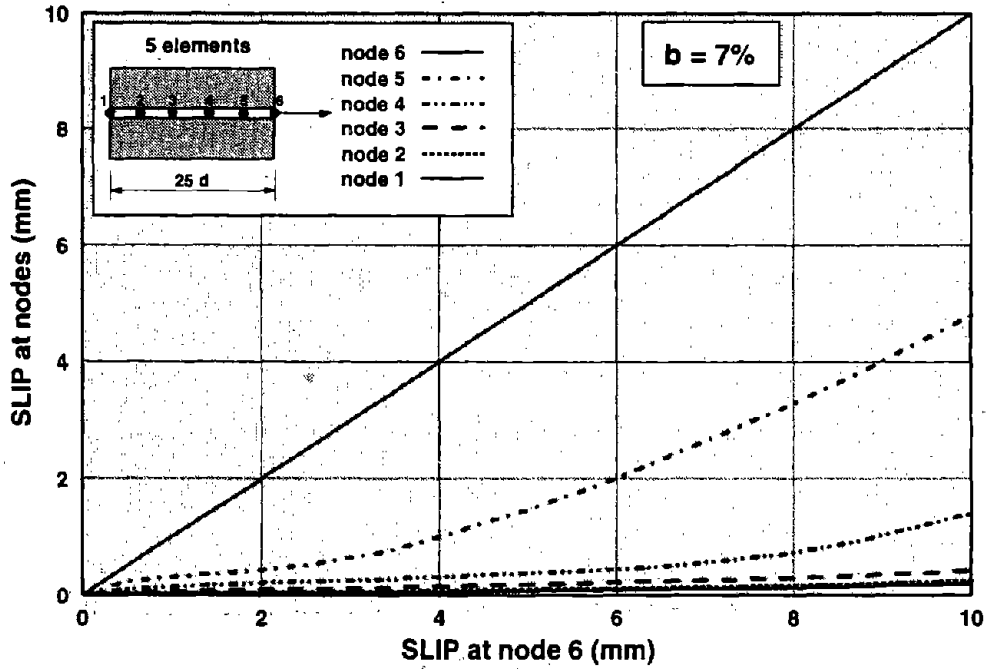


B: SLIP AT ALL NODES VERSUS SLIP AT PULL-OUT END

FIGURE 3.6 YIELD PENETRATION FOR A STRAIN HARDENING RATIO VALUE OF 1.4%

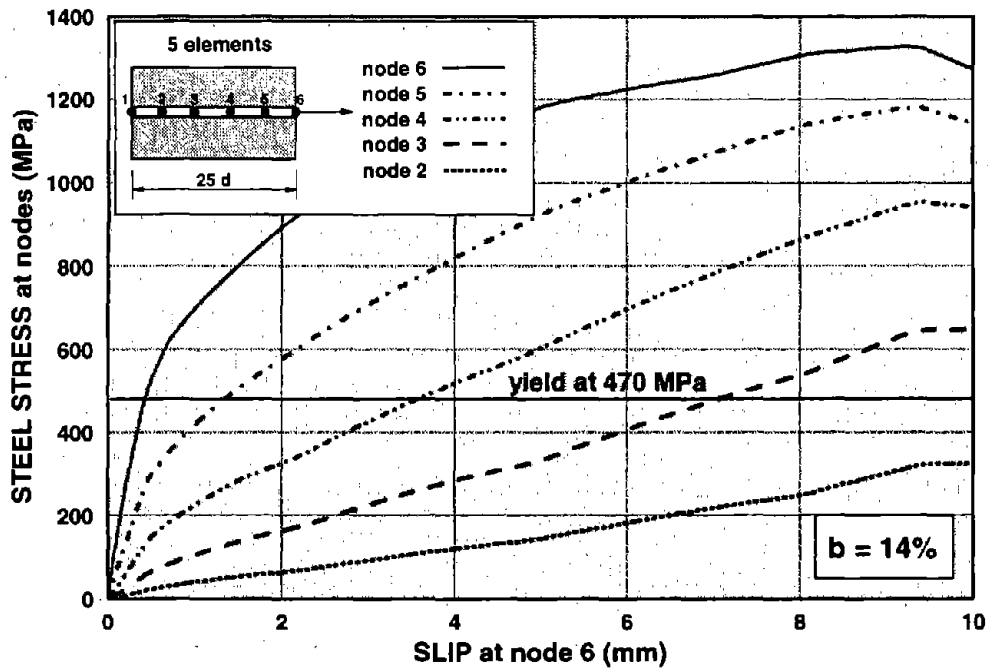


A: STEEL STRESS VERSUS SLIP AT PULL-OUT END

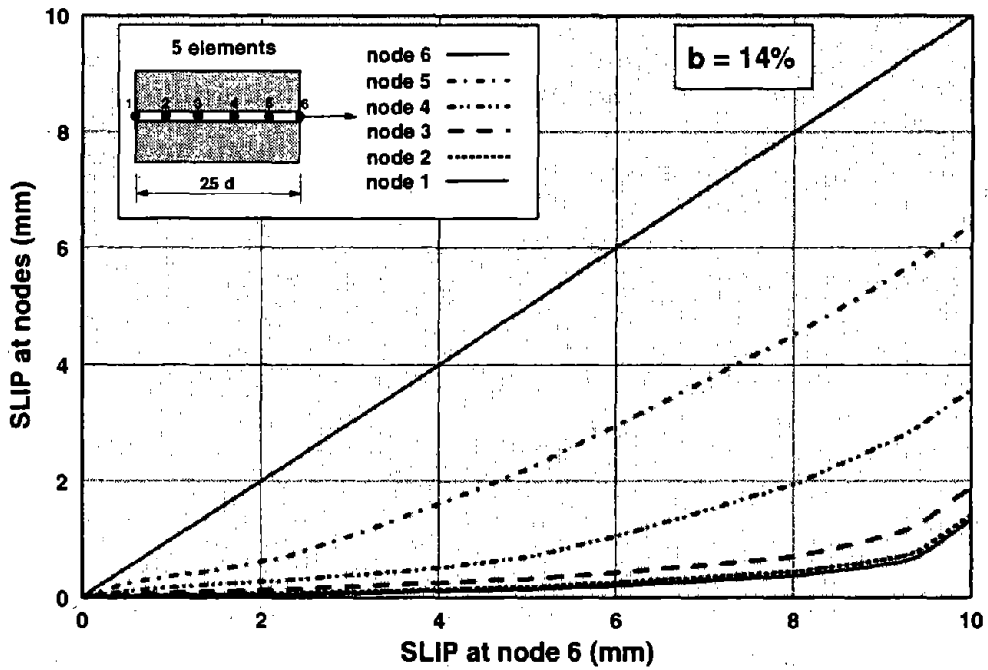


B: SLIP AT ALL NODES VERSUS SLIP AT PULL-OUT END

FIGURE 3.7 YIELD PENETRATION FOR A STRAIN HARDENING RATIO VALUE OF 7%



A: STEEL STRESS VERSUS SLIP AT PULL-OUT END



B: SLIP AT ALL NODES VERSUS SLIP AT PULL-OUT END

FIGURE 3.8 YIELD PENETRATION FOR A STRAIN HARDENING RATIO VALUE OF 14%

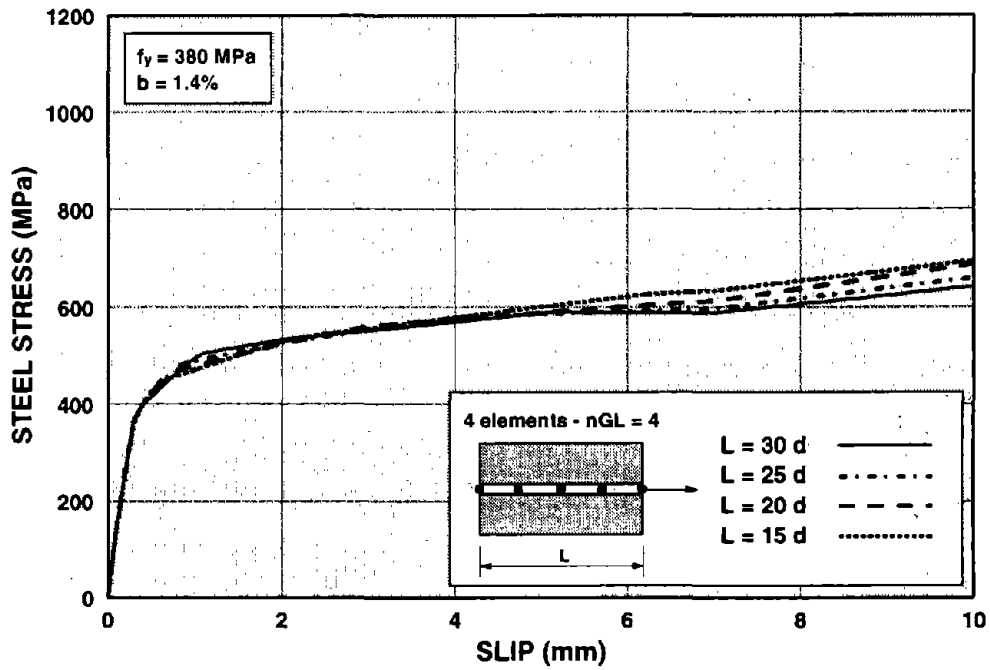
The analyses in Figs. 3.6-3.8 were conducted with three values of strain hardening ratio b for the reinforcing steel: these were equal to 1.4%, 7%, and 14% (see Fig. 3.1). The first two values are characteristic of the hardening ratio of mild and cold-formed construction steel, respectively. Figs. 3.6-3.8 show the response to an imposed monotonic pull-out displacement at node 6. Each figure is divided in two parts: part A shows the steel stress at each node against the slip at the pull-out end of the bar, while part B shows the relative slip at each node against the slip at the pull-out end of the bar. For $b=1.4\%$ and $b=7\%$ the yield penetration is more pronounced as the hardening ratio increases. For the strain hardening ratio of $b=1.4\%$ in Fig. 3.6 node 5 experiences yielding only when the relative slip at node 6 reaches the value of 6 mm. At the final pull-out stage slip is essentially concentrated at the pull-out node and the difference in the relative slip value between node 6 and node 5 is about 9 mm, implying that about 90% of the pull-out displacement stems from the extension of the first 5 diameter segment of the bar. For the strain hardening ratio of $b=7\%$ in Fig. 3.7 node 5 experiences yielding when the pull-out at node 6 reaches the value of only 2 mm. Node 4 experiences yielding when the pull-out at node 6 reaches the value of 6 mm. At the final pull-out slip is distributed in the first half of the bar and the difference in the relative slip value between nodes 6 and 5 is about 5 mm, and that between nodes 5 and 4 is about 4 mm, indicating that about 90% of the pull-out displacement stems from the extension of the first 10 diameter segment of the bar.

The third case with a strain hardening value of $b=14\%$ in Fig. 3.8 was selected for the purpose of studying the behavior of the model under an extreme case. In fact, when the relative slip value at node 6 reaches about 9 mm the displacement gradient is the same for all six nodes indicating that the bond-stress slip relation has reached the friction plateau at all nodes. Even though the anchored bar can still resist a certain force, it slips through the concrete block as a rigid body, since the bond stiffness is equal to zero at all nodes.

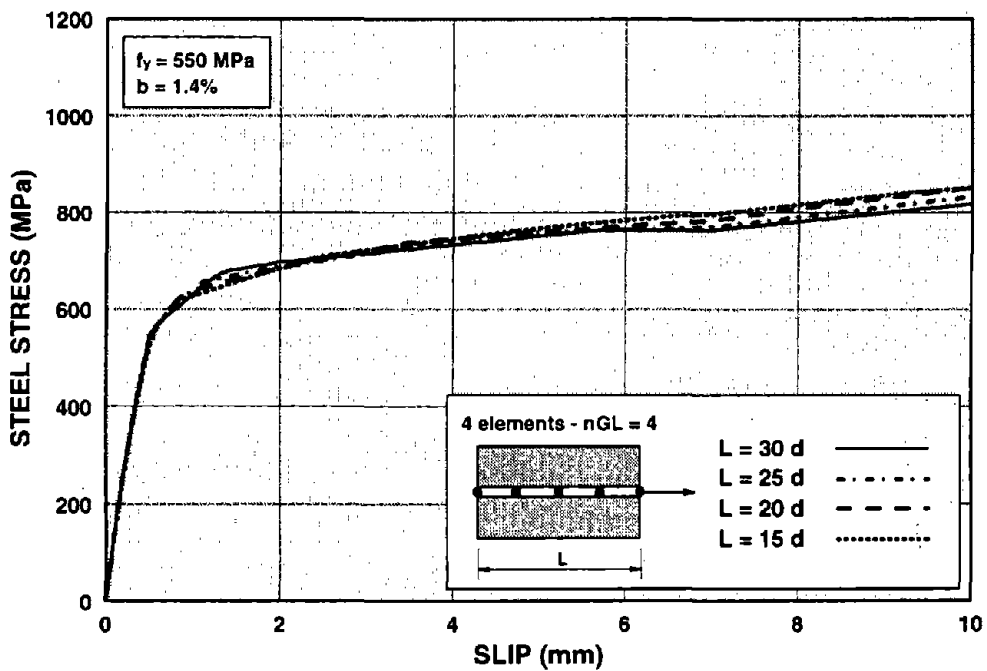
3.4.2 Effect of Yield Strength, Anchorage Length and Hardening Ratio Under Monotonic Pull-Out

Figs. 3.9 through 3.11 illustrate the results of parametric studies on anchored reinforcing bars of different anchorage length, yield strength and strain hardening ratio of reinforcing steel under monotonic pull-out. The following values are used in the parametric studies:

- (a) the anchorage length is equal to 15, 20, 25 and 30 bar diameters;
-

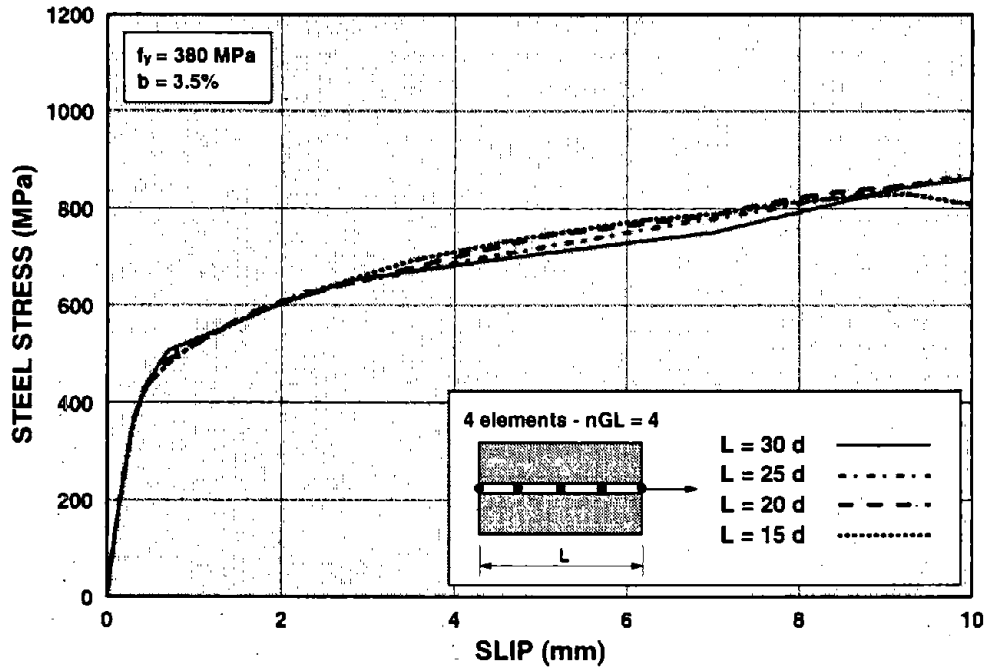


A: STEEL STRESS = 380 MPa

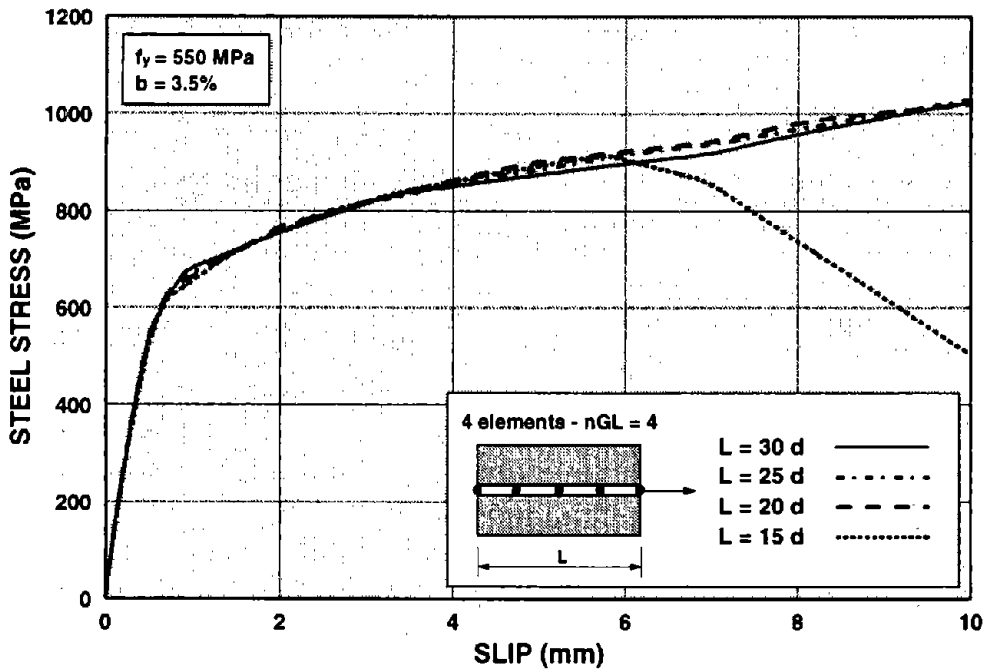


B: STEEL STRESS = 550 MPa

FIGURE 3.9 EFFECT OF YIELD STRENGTH ON ANCHORED BAR WITH 1.4% HARDENING

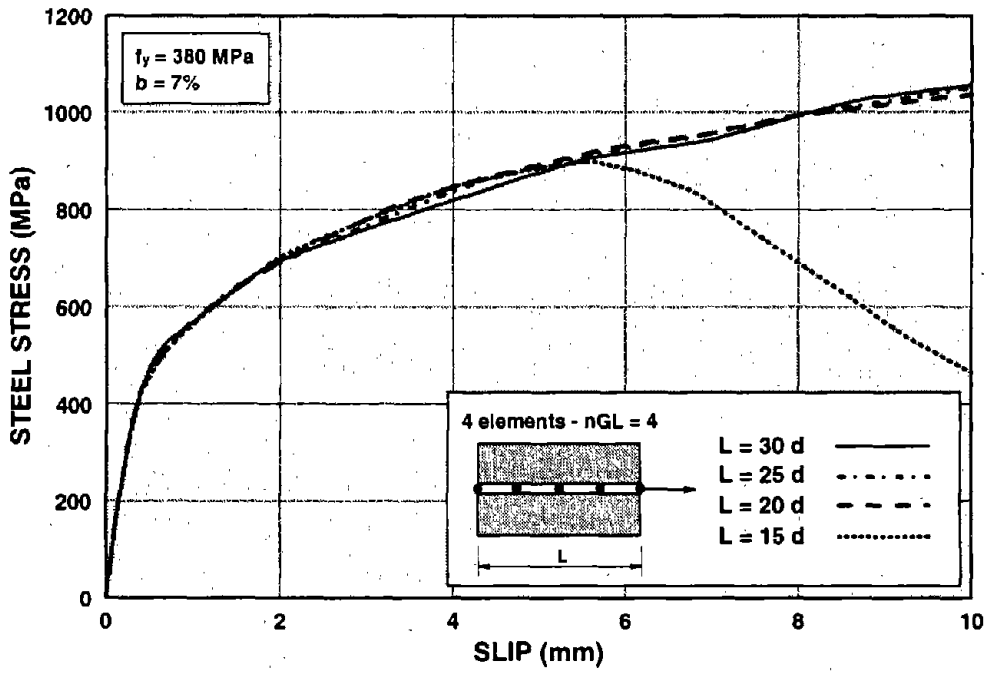


A: STEEL STRESS = 380 MPa

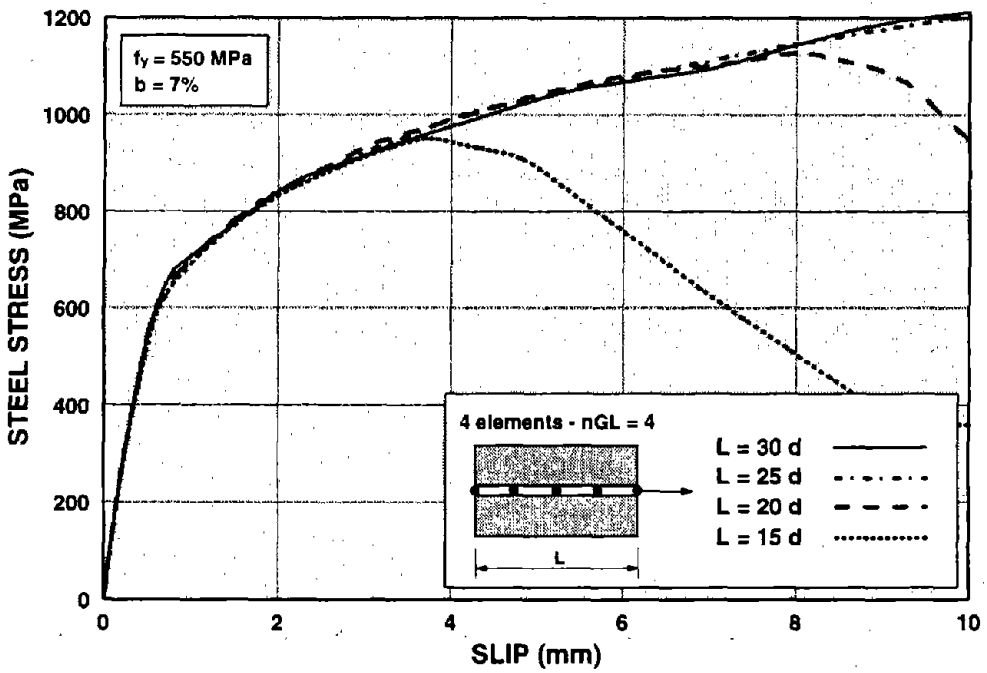


B: STEEL STRESS = 550 MPa

FIGURE 3.10 EFFECT OF YIELD STRENGTH ON ANCHORED BAR WITH 3.5% HARDENING



A: STEEL STRESS = 380 MPa



B: STEEL STRESS = 550 MPa

FIGURE 3.11 EFFECT OF YIELD STRENGTH ON ANCHORED BAR WITH 7% HARDENING

- (b) the steel strain hardening ratio assumes values of 1.4%, 3.5% and 7% ;
- (c) the yield strength assumes values of 380 MPa and 550 MPa.

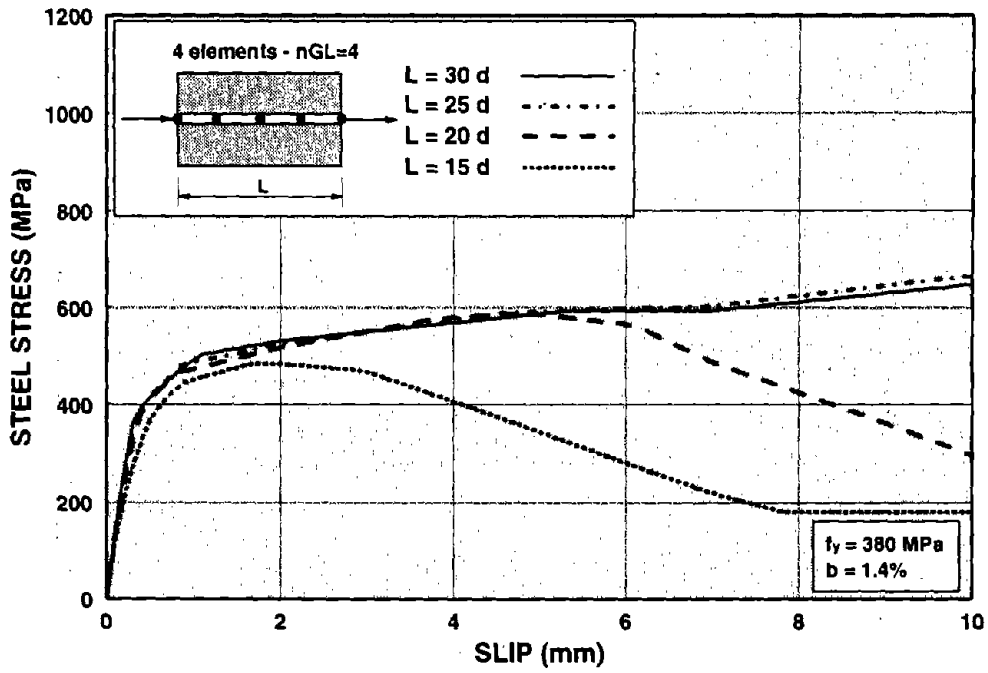
For strain hardening ratio values of $b=1.4\%$ and $b=3.5\%$ the reinforcing bars show stable behavior for all four anchorage lengths, i.e. no pull-out takes place, as is evident by the absence of any strength loss in the stress-slip relations in Figs. 3.9 and 3.10. The only exception is the shortest bar with an anchorage length of 15 bar diameters, a strain hardening ratio of 3.5% and a yield strength of 550 MPa, which pulls-out of the anchorage block at a pull-out value of about 6 mm in Fig. 3.10b.

For a strain hardening ratio value of $b=7\%$ there are more cases of loss of strength and pull-out in Fig. 3.11. For a low yield strength value of 380 MPa for which the anchored bar yields while the bond stress-slip relation is on the ascending branch, only the bar with an anchorage length of 15 bar diameters shows signs of pull-out at a pull-out value of about 6 mm. For the higher yield strength value of 550 MPa for which the anchored bar yields while the bond stress-slip relation is on the horizontal plateau, the bar with an anchorage length of 20 bar diameters also shows signs of pull-out at a pull-out value of about 8 mm, while the shorter bar pulls-out at a pull-out value of a little less than 4 mm. In both yield strength cases the reinforcing bars with anchorage lengths of 25 and 30 bar diameters do not pull-out.

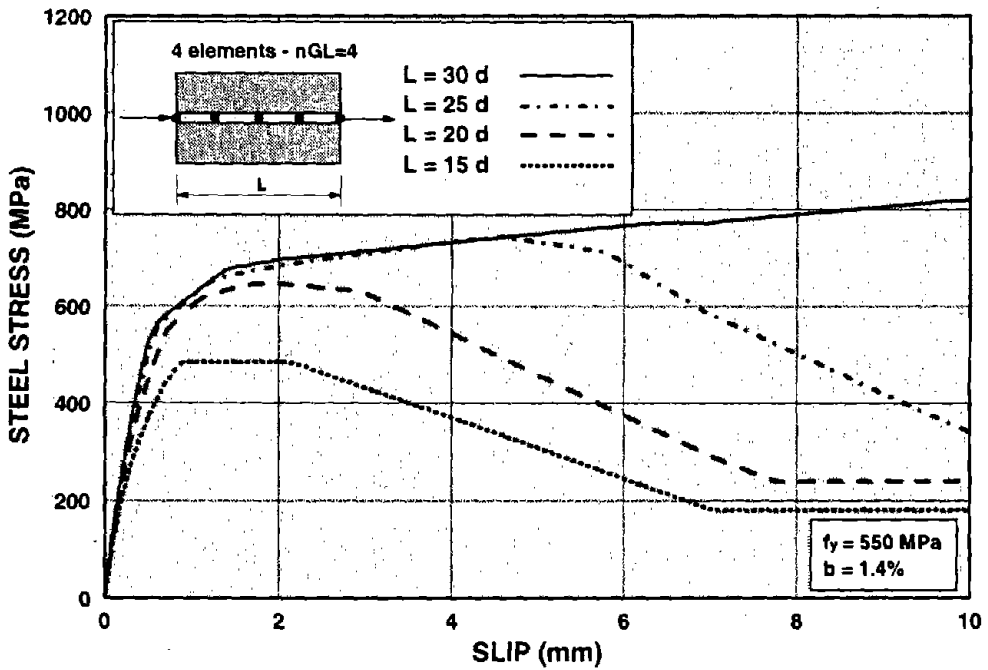
These parametric studies confirm the observations of earlier studies (Ciampi et al. 1982), that not only the yield strength, but also the strain hardening ratio of the reinforcing steel are key parameters that affect the anchorage length.

3.4.3 Effect of Yield Strength, Anchorage Length and Hardening Ratio Under Monotonic Push-Pull

The behavior of anchored reinforcing bars is even more profoundly affected by the yield strength, the strain hardening ratio and the anchorage length under loading conditions that induce a pull-out at one end and a push-in at the other end of the anchored bar. The parametric studies in Figs. 3.12 through 3.14 are conducted for the same parameter values are in the previous section, namely, the strain hardening ratio assumes values of 1.4%, 3.5% and 7%, the yield strength takes on the values of $f_y=380$ MPa and 550 MPa and the anchorage length is equal to 15, 20, 25 and 30 bar diameters.

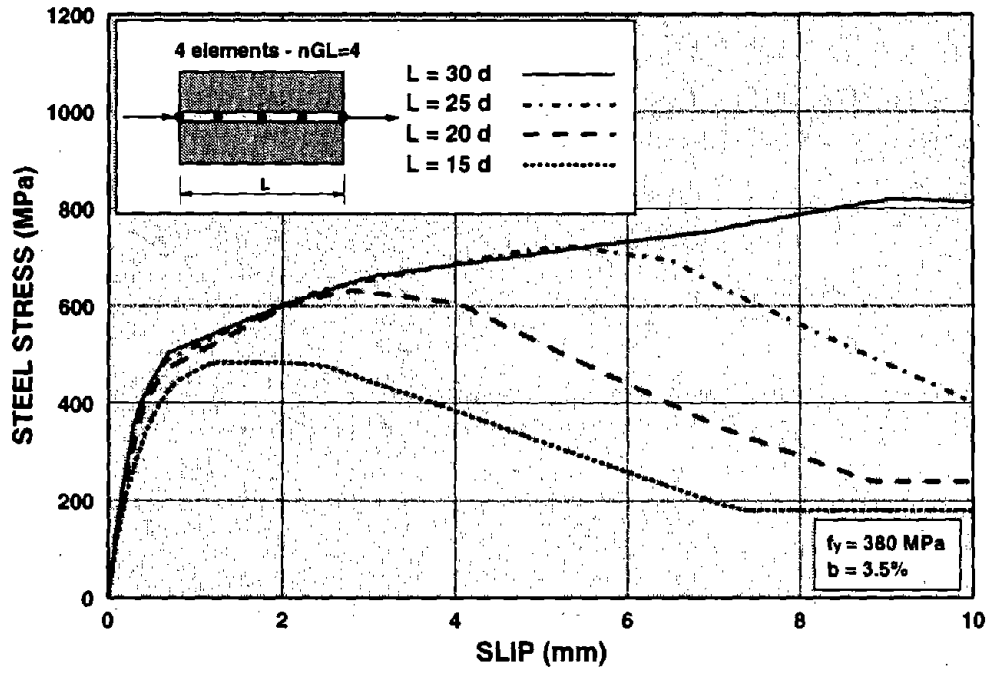


A: STEEL YIELD STRESS = 380 MPa

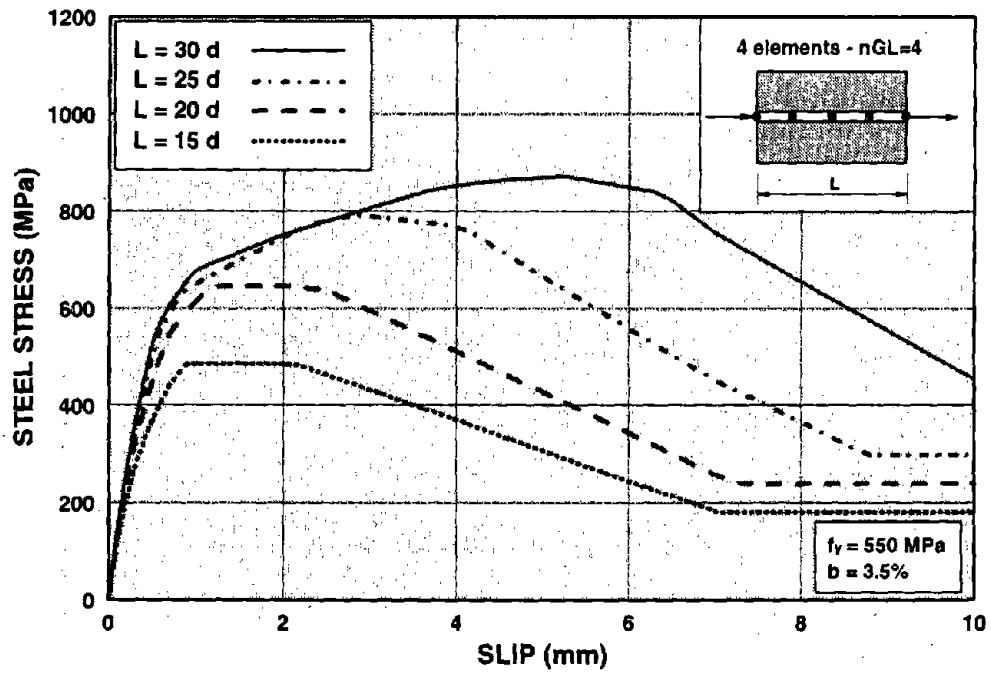


B: STEEL YIELD STRESS = 550 MPa

FIGURE 3.12 EFFECT OF YIELD STRENGTH ON ANCHORED BAR WITH 1.4% HARDENING

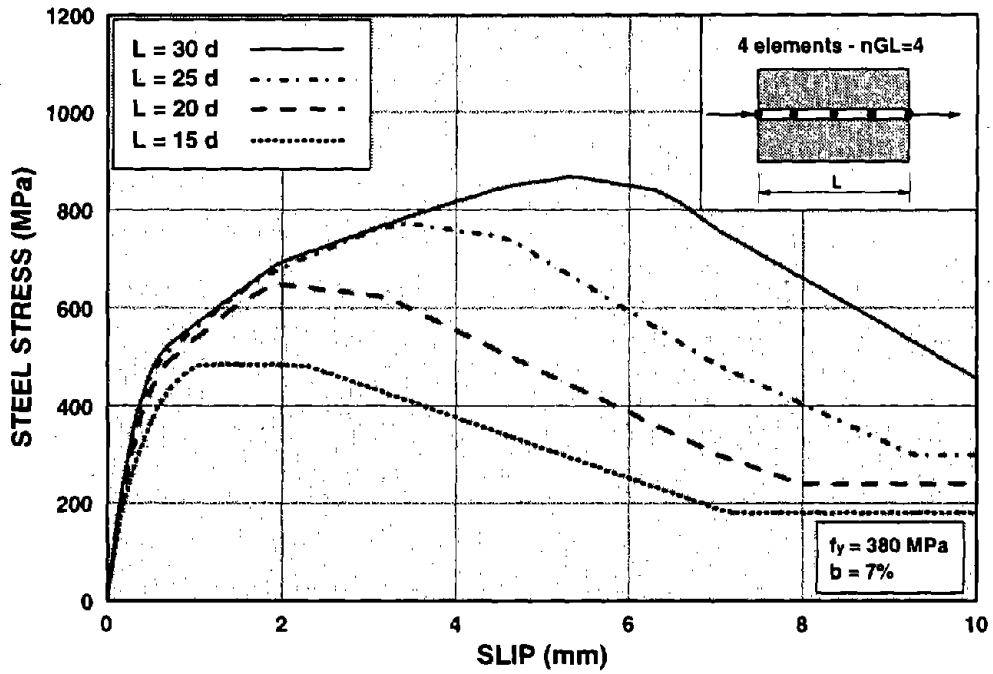


A: STEEL YIELD STRESS = 380 MPa

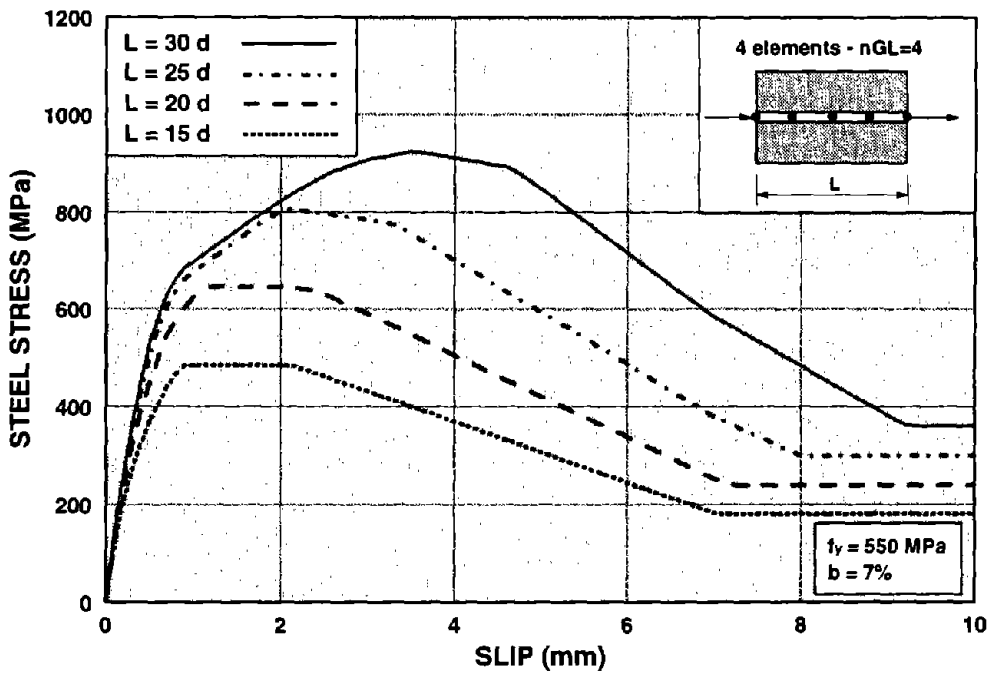


B: STEEL YIELD STRESS = 550 MPa

FIGURE 3.13 EFFECT OF YIELD STRENGTH ON ANCHORED BAR WITH 3.5% HARDENING



A: STEEL YIELD STRESS = 380 MPa



B: STEEL YIELD STRESS = 550 MPa

FIGURE 3.14 EFFECT OF YIELD STRENGTH ON ANCHORED BAR WITH 7% HARDENING

In the push-pull case an anchorage length of 30 bar diameters is not sufficient to prevent the pull-out of the bar with a 3.5% strain hardening ratio and a yield strength of 550 MPa and the same is true for both yield strength values, if the strain hardening ratio is equal to 7.0%. The reinforcing bar with anchorage lengths of 15 and 20 bar diameters slips through the anchorage block under small pull-out values.

The parametric studies in this chapter illustrate the capability of the proposed reinforcing bar model to simulate the behavior of anchorages under conditions of significant bond damage and strength loss due to pull-out. It can thus be a very valuable tool in the establishment of design guidelines for anchorage lengths under extreme loading conditions and in the simulation of the behavior of anchored bars in analytical studies of entire structures.

CHAPTER 4

ANALYTICAL STUDIES UNDER CYCLIC LOADING

4.1 General

A number of analytical studies are presented in this chapter with the objective of establishing the ability of the proposed model to simulate the response of an anchored reinforcing bar under cyclic displacement histories.

In the first part of the chapter two correlation studies between experimental and analytical results are conducted on reinforcing bars anchored, in the first case, in an exterior joint and, in the second case, in an interior beam-column joint. Some attention is devoted in these studies to the sensitivity of the response to the modeling of the anchored bar and to the selected bond stress-slip relation for simulating different confinement conditions along the bar anchorage. For the anchored bar in the exterior joint plots of the stress-slip response at the loaded end of the bar are presented along with stress, slip and bond distributions at different loading stages. For the straight reinforcing bar that simulates conditions in an interior beam-column joint plots of the stress-slip response at the bar ends are presented for cycles before and after the onset of yielding of the reinforcing steel.

In the second part of the chapter parametric push-pull studies are conducted with the objective of assessing the effect of anchorage length, yield strength and hardening ratio on the hysteretic response of the anchored reinforcing bar. These studies are conducted with the same parameter values as those of Chapter 3 and, thus, complement the conclusions about the monotonic behavior of anchored reinforcing bars. The studies in this chapter also address the importance of including the effect of progressive damage in the bond-slip relation. The evolution of progressive damage along the anchored bar is studied in some detail and conclusions are derived about the design of anchorages under cyclic loading conditions.

4.2 Correlation Studies

This section presents the correlation studies between analytical and experimental results for two reinforcing bars. The first bar is anchored in an exterior beam-column joint

with a standard 90° hook, while the second bar is straight, thus simulating conditions in an interior beam-column joint. These correlation studies are used to verify the ability of the proposed finite element model to represent the hysteretic behavior of anchored reinforcing bars under severe cyclic loading.

4.2.1 Bar Specimen B85 of Lin and Hawkins (1982)

The experimental results from an exterior anchored bar specimen called B85 and tested by Lin and Hawkins (1982) are compared with the results obtained with the proposed finite element model. The specimen consists of a #8 (bar diameter=24.5 mm) reinforcing bar anchored in an exterior beam-column joint with a standard 90° hook, as shown in Fig. 4.1. The dimensions of the concrete anchorage block are 1620 mm by 590 mm by 200 mm. The finite element model is shown in the lower part of Fig. 4.1. Following the recommendation of Eligehausen et al. (1982) the hook is represented by an equivalent straight portion with modified bond stress-slip relation. The extent of the equivalent straight portion is equal to four (4) bar diameters (Fig. 4.1).

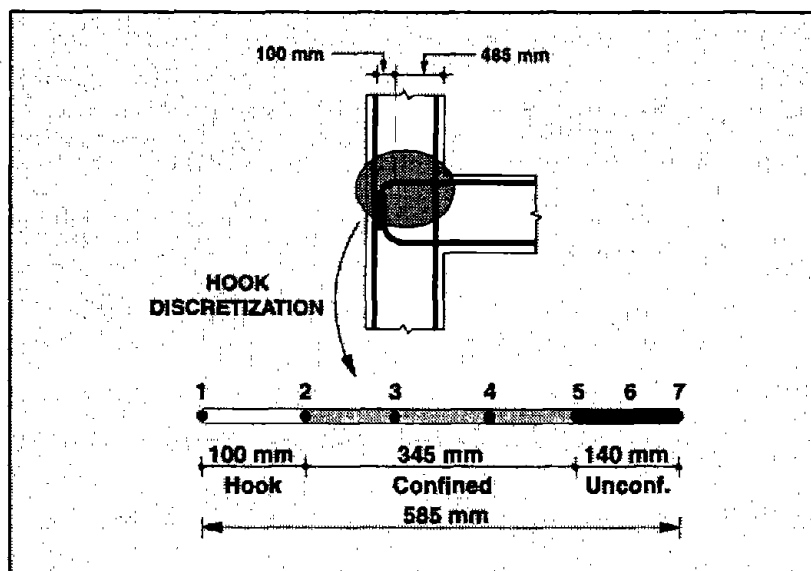


FIGURE 4.1 SPECIMEN B85 OF LIN, HAWKINS (1982): GEOMETRY AND FINITE ELEMENT MODEL

A cyclic pulling or pushing force is applied at the end of the bar with the load history of Fig. 4.2, which is expressed in terms of displacement ductility, i.e. the ratio of pull-out or push-in slip to pull-out displacement at the onset of yielding of the reinforcing bar. The applied force and the resulting relative slip were measured at the loaded end of the bar.

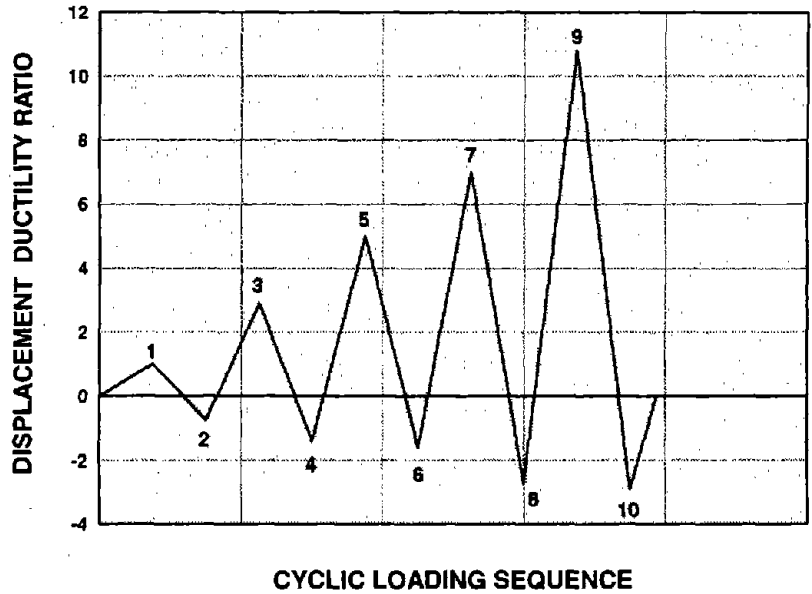


FIGURE 4.2 CYCLIC LOADING HISTORY FOR SPECIMEN B85 OF LIN AND HAWKINS (1982)

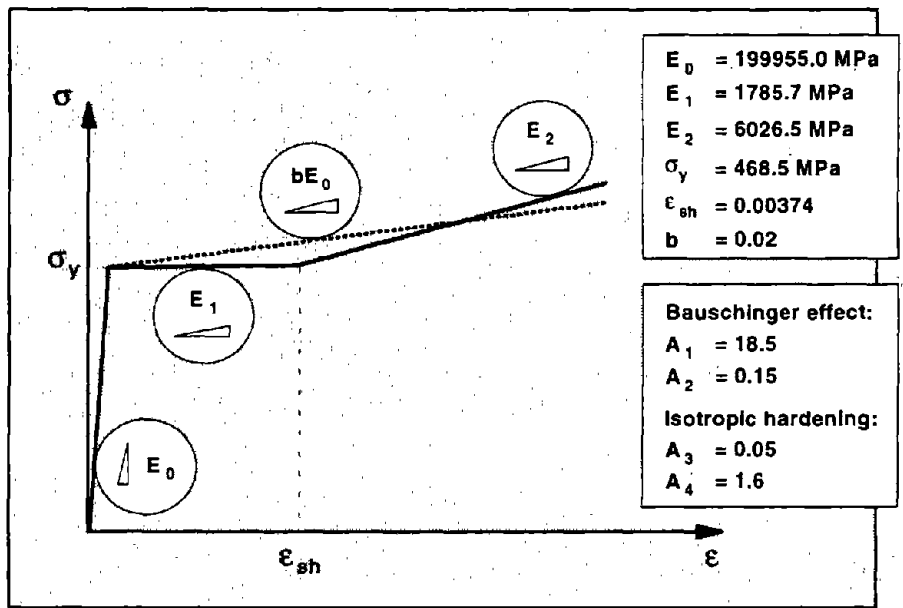


FIGURE 4.3 STEEL STRESS-STRAIN RELATION: MONOTONIC ENVELOPE

In the correlation study the exterior bar is subjected to the slip values measured at the loaded end of the anchored bar and shown Fig. 4.2. The finite element model of the anchored bar is subdivided into six (6) elements in Fig. 4.1 with four (4) Gauss-Lobatto integration points in each element. The first element represents the hook portion of the bar, the three middle elements the confined part and the last two the unconfined section of the bar. The length of the unconfined region (140 mm) is determined by adding the clear cover of 63.5

mm to half the spacing of the column ties in the joint, which amounts to 76 mm.

The monotonic envelope of the steel stress-strain relation is presented in Fig. 4.3. The mechanical properties of the reinforcing bar are derived from experimental data of steel coupon specimens under cyclic loading conditions and the selected values are listed in Fig. 4.3. The monotonic envelopes of the nonlinear bond stress-slip relation for the hook equivalent portion and the confined and unconfined bar straight portions are shown in Fig. 4.4. The material properties for #8 bars embedded in confined concrete and for the standard 90° hook are those used by Zulfiquar and Filippou (1990) and summarized in Fig 4.4.

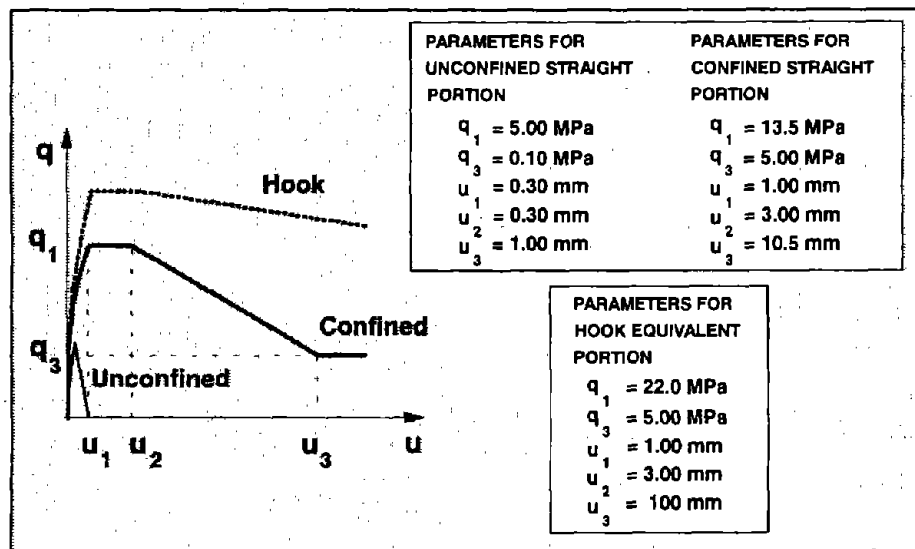


FIGURE 4.4 BOND FORCE-SLIP MODEL: MONOTONIC ENVELOPES

Fig. 4.5 shows the comparison between experimental and analytical results in terms of steel stress versus end slip displacement of the anchored bar. The analytical simulations show excellent agreement with experimental results both in terms of strength and stiffness of the anchored bar. Some differences are observed in the unloading and reloading phases. They can be probably attributed to the unloading slope of the proposed bond stress-slip model, which might be too steep and, thus, does not account for the elastic deformation of the concrete zone around the deformed bar. It is interesting to note that this discrepancy increases under increasing bar pull-out, reflecting the state of damage in the concrete zone surrounding the deformed bar. It should be noted, however, that experimental results are error prone during the sensitive unloading phase of the specimen, when load increments are typically large. It is important to note that the good agreement of the simulated with the observed strength of the specimen under, both, pull-out and push-in loading conditions in Fig. 4.5.

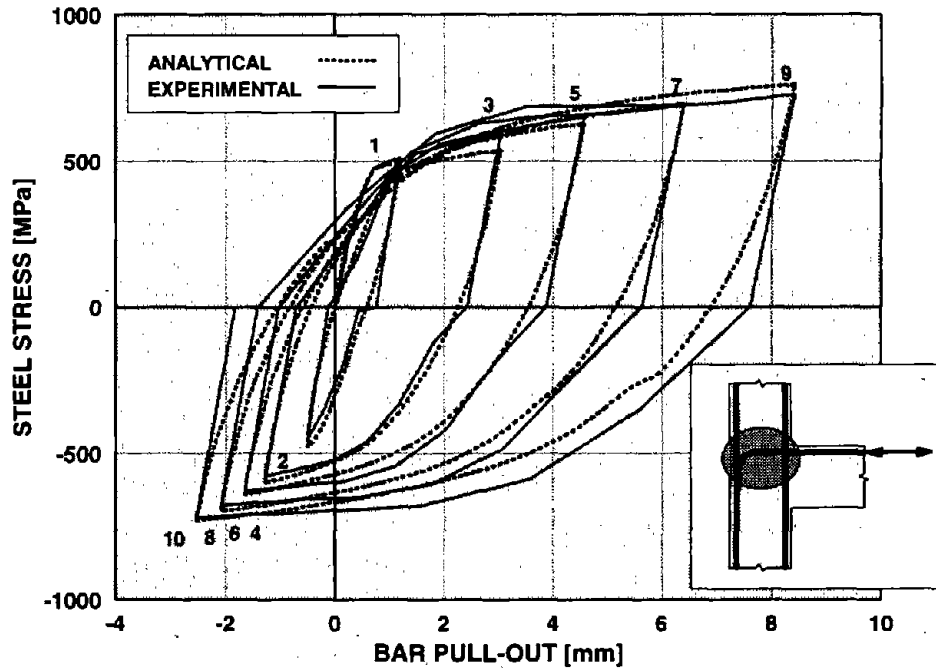


FIGURE 4.5 COMPARISON BETWEEN EXPERIMENTAL AND ANALYTICAL RESULTS:
STEEL STRESS- BAR PULL OUT RELATION

The distributions of steel stress, relative slip between steel and concrete and bond stress along the anchored reinforcing bar are shown in Figs. 4.6 through 4.8, both, under conditions of pull-out and push-in at the loaded end of the bar. The distributions are identified by the loading cycle number that corresponds to the loading cycle number in Figs. 4.2 and 4.5. The steel stress distributions in Fig. 4.6 highlight the progressive spread of yielding into the anchorage zone as the magnitude of pull-out increases. It is interesting to observe that a large portion of the reinforcing bar remains elastic during the entire loading history. The bond stress distributions in Fig. 4.8 permit the observation that the bond in the unconfined outer portion of the bar is completely destroyed after the first two loading cycles. This reflects the gradual formation of a pull-out cone at the loaded end of the bar, as has been observed in several experiments. When the loaded end of the bar is pushed-in, the cone is pushed back in contact and some bond stress transfer is possible for a few following cycles, as shown on the right of Fig. 4.8. The discontinuities in the bond stress distributions in Fig. 4.8 stem from the different bond stress-slip relations that are assigned to the bar segments to the left and right of nodes 2 and 5. At node 2 the transition from the hook to the straight confined portion necessitates a change in the bond stress-slip relation, while at node 5 the same is true for the transition from the confined to the unconfined portion of the anchored reinforcing bar. This is also evident in Fig. 4.9 which depicts the bond stress-slip history at

the nodes of the finite element model.

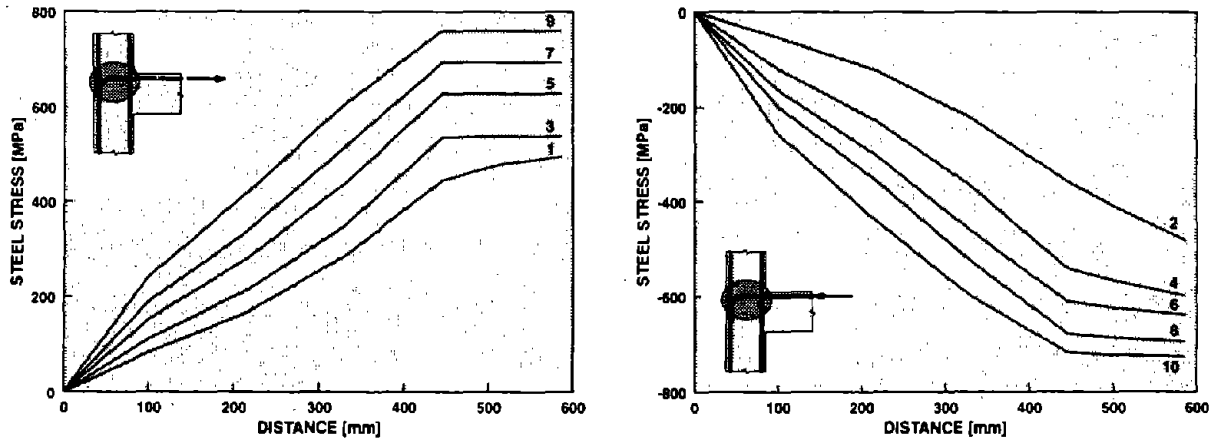


FIGURE 4.6 STEEL STRESS DISTRIBUTION ALONG REINFORCING BAR UNDER PULL-OUT (LEFT) AND PUSH-IN (RIGHT) CONDITIONS

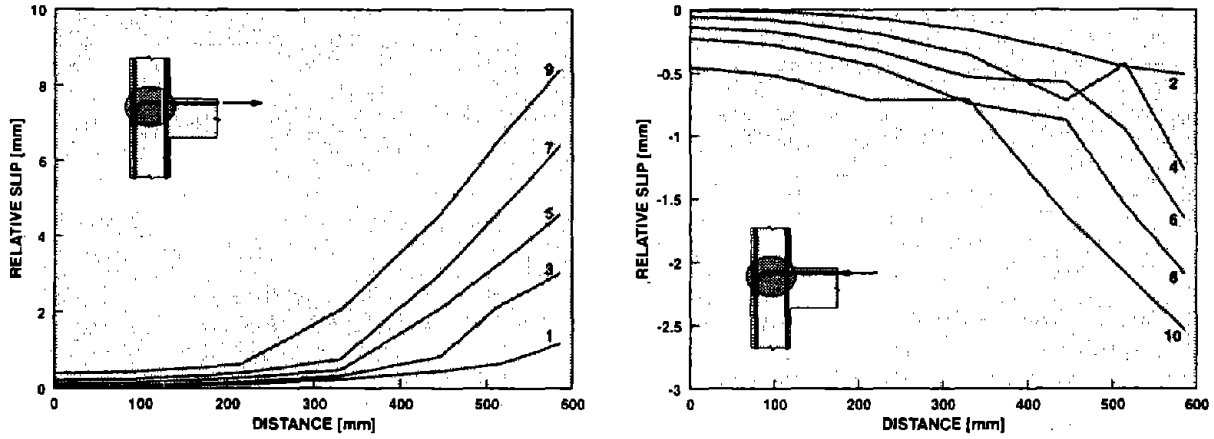


FIGURE 4.7 RELATIVE SLIP DISTRIBUTION ALONG REINFORCING BAR UNDER PULL-OUT (LEFT) AND PUSH-IN (RIGHT) CONDITIONS

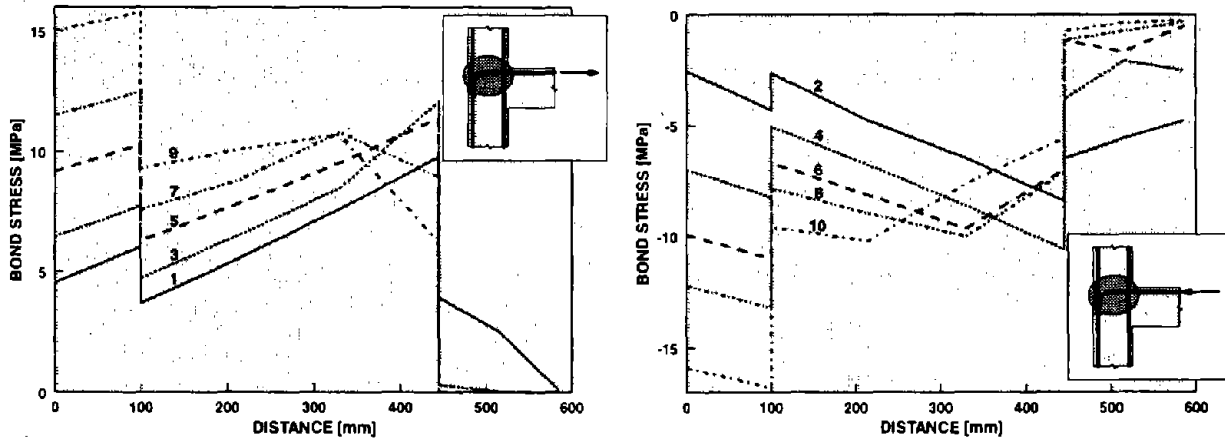


FIGURE 4.8 BOND STRESS DISTRIBUTION ALONG REINFORCING BAR UNDER PULL-OUT (LEFT) AND PUSH-IN (RIGHT) CONDITIONS

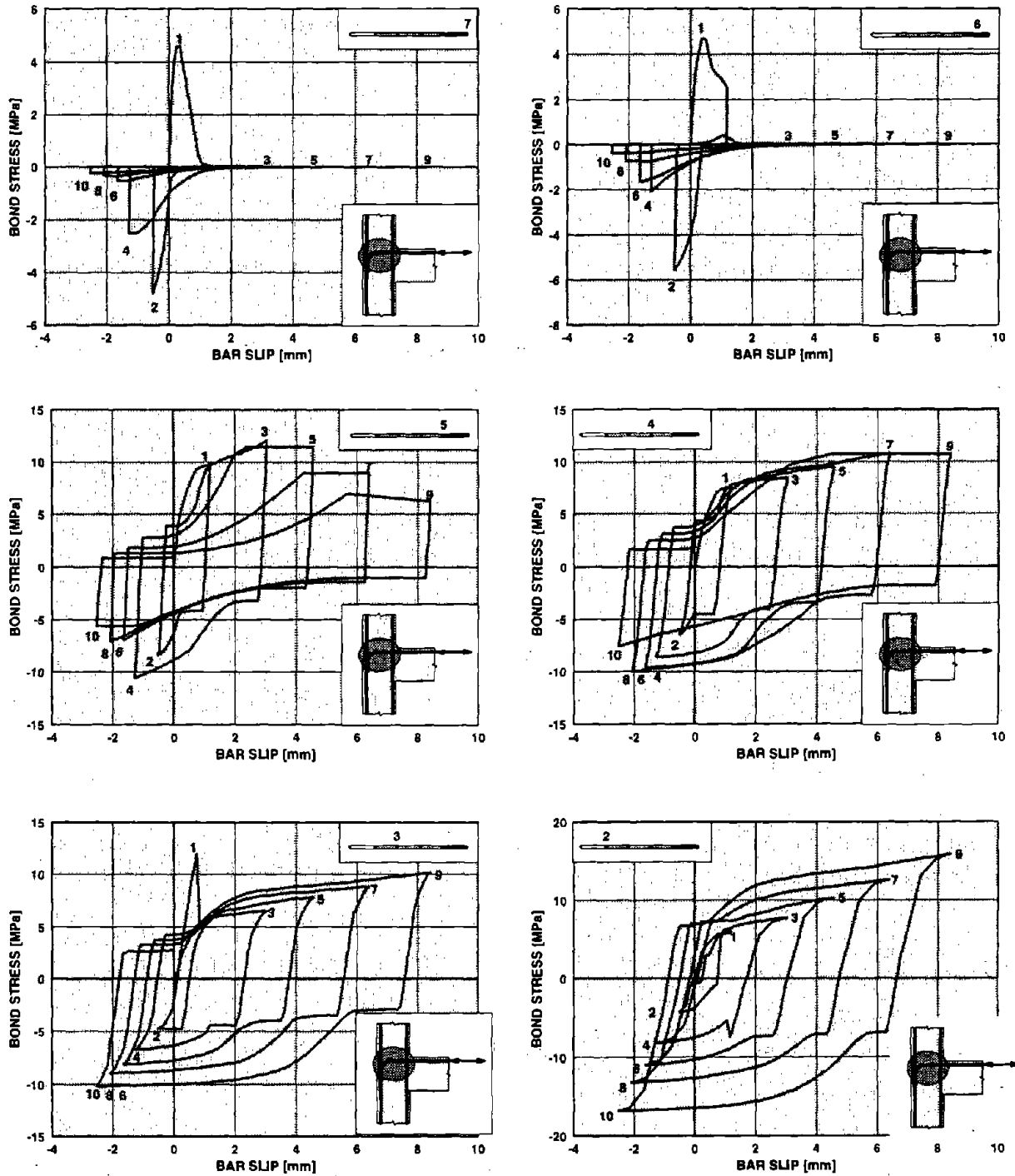


FIGURE 4.9 BOND STRESS- BAR PULL OUT RELATION AT NODES 2 THROUGH 7

It is important to note that the extreme irregularity of the bond-slip relation in the unconfined portion of the anchored bar does not affect the numerical convergence of the finite element model, which by virtue of its flexibility-based formulation is extremely robust in the presence of strength loss and softening.

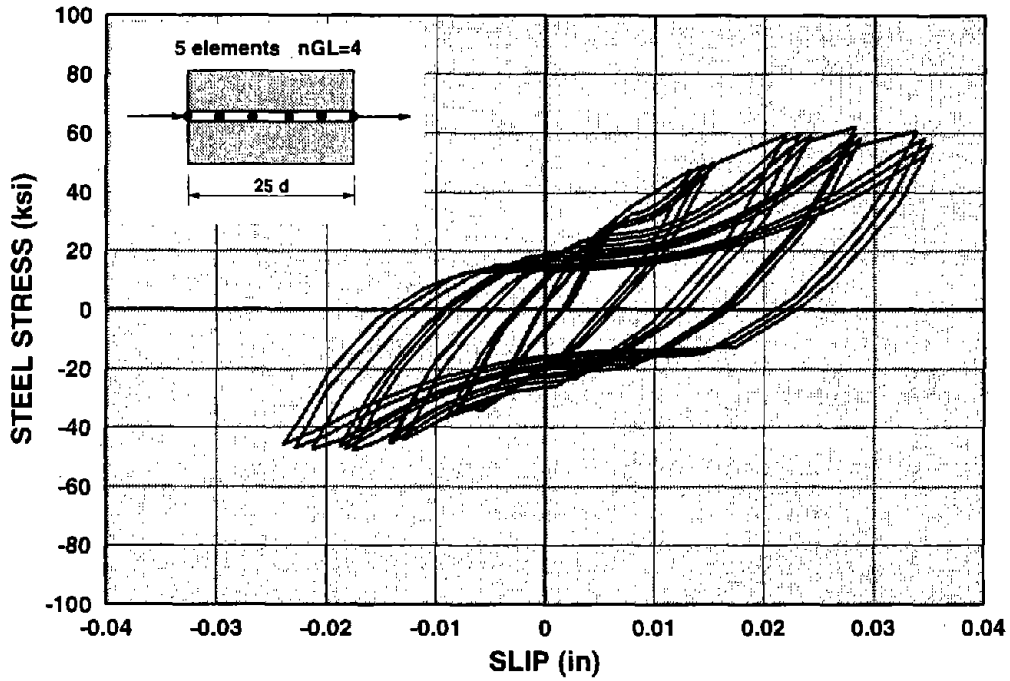
4.2.2 Straight Anchored Bar of Viwathanatepa et al. (1979)

Viwathanatepa, Popov and Bertero (1979) tested several anchored reinforcing bars simulating anchorage and loading conditions in interior beam-column joints and moment resisting frames under the combined action of gravity and high lateral loads.

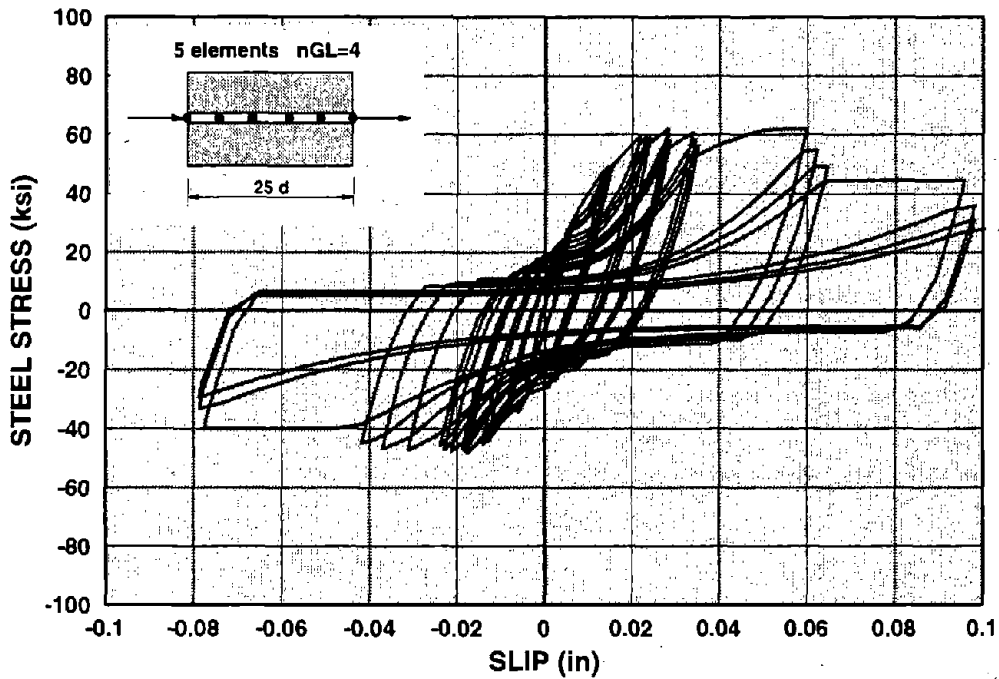
One of these specimens is selected for comparison with the proposed finite element model of a reinforcing bar with bond-slip. The specimen is a #8 reinforcing bar anchored in a well confined block of 25 inches width corresponding to an anchorage length of 25 bar diameters. It was subjected to a cyclic push-pull loading history with cycles of gradually increasing end displacement. The finite element model of the anchored bar is discretized into five elements with four Gauss-Lobatto integration points in each element.

The experimental and analytical results are shown in Figs. 4.10 and 4.11. In order to facilitate the direct comparison with the experimental data in Viwathanatepa, Popov and Bertero (1979) the analytical results are reported in the American System of Units, rather than the SI units that are used in the rest of the chapter.

Fig. 4.10 shows the end stress-slip relation of the reinforcing bar under cyclic push-pull loading. Fig. 4.10a shows the cycles before yielding of the reinforcement and Fig. 4.10b shows the entire response. The corresponding experimental responses are shown in Figs. 4.11a and b. The results of the proposed model show very good agreement with experimental data under large end displacement values, as reflected in the latter cycles of Figs 4.10b and 4.11b. It is noteworthy that the model is capable to simulate the gradual damage of bond and the resulting loss of strength and stiffness of the anchored reinforcing bar. The discrepancy between analytical and experimental results is, however, pronounced in the cycles before yielding of the reinforcing steel in Figs 4.10a and 4.11a. The major cause of this discrepancy is the assumed friction strength of the bond stress-slip relation. The analytical results are obtained with a friction strength of 5 Mpa, as supported by experimental evidence from reinforcing bars with short anchorage lengths in the studies by Eligehausen et al. (1982). The experimental results show a complete loss of frictional bond resistance during the reloading phase of the specimen even for end slip values smaller than 0.01 in. This is a very surprising result and casts some doubt on the accuracy and reliability of the measurements in the very sensitive reloading phase of the specimen.

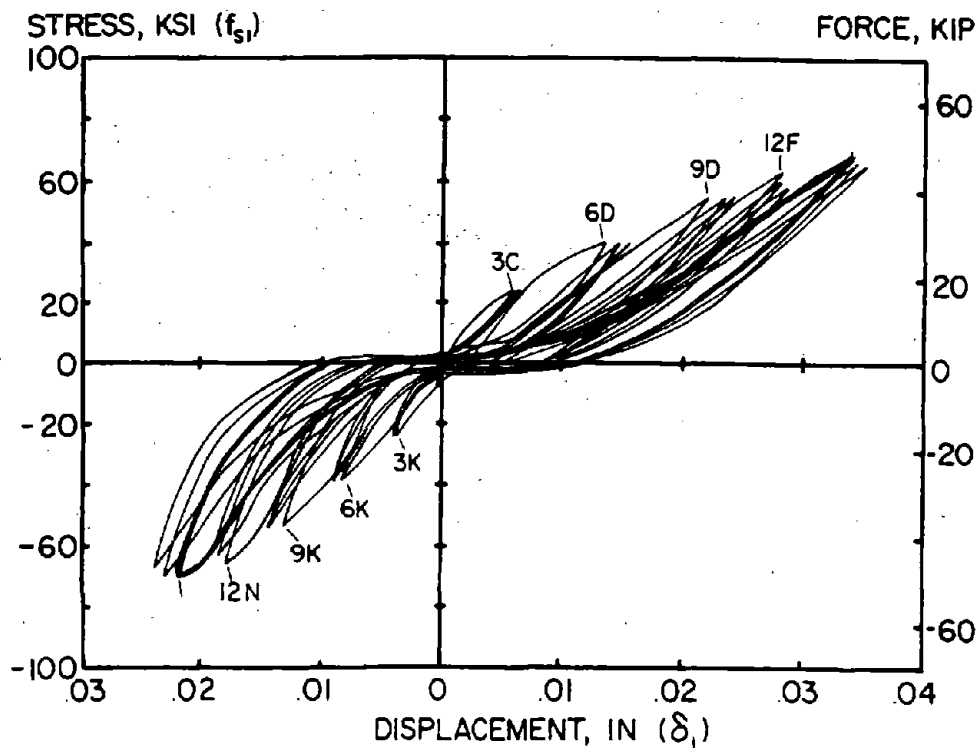


A: LOAD CYCLES BEFORE YIELDING OF REINFORCING STEEL

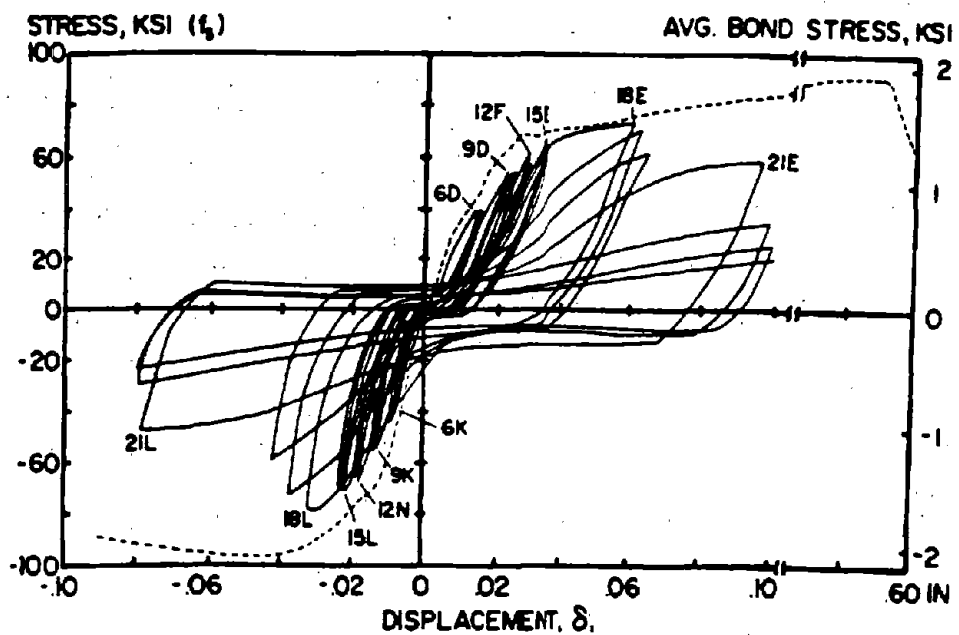


B: LOAD CYCLES AFTER YIELDING OF REINFORCING STEEL

FIGURE 4.10 STRESS-SLIP RESPONSE OF ANCHORED REINFORCING BAR UNDER CYCLIC PUSH-PULL: ANALYTICAL RESULTS



A: LOAD CYCLES BEFORE YIELDING OF REINFORCING STEEL



B: LOAD CYCLES AFTER YIELDING OF REINFORCING STEEL

FIGURE 4.11 STRESS-SLIP RESPONSE OF ANCHORED REINFORCING BAR UNDER CYCLIC PUSH-PULL: EXPERIMENTAL RESULTS

4.3 Parameter Studies under Cyclic Push-Pull Loading Conditions

A series of parameter studies on the hysteretic behavior of an anchored reinforcing bar under cyclic push-pull loading conditions are presented in this section. The anchored bar simulates the geometry and loading conditions typical of reinforcing bars in interior beam-column joints under the combination of gravity and lateral loads. The bar has a diameter of 24 mm and is embedded in a well confined block. The properties of the bond stress-slip relation are the same as those used in Section 3.2.1, i.e. : $u_1 = 0.7$ mm, $u_2 = 2.0$ mm, $u_3 = 10u_1$, $q_1 = 16.2$ MPa, $q_3 = 6.0$ MPa and $q_f = 3.0$ MPa. Young's modulus of reinforcing steel is equal to 205000 MPa, while the yield strength and strain hardening ratio are subject to parameter variation. The objective of the parameter studies is to investigate the sensitivity of the hysteretic behavior of the anchored bar relative to the following three parameters: 1) anchorage length, 2) yield strength of reinforcing steel, and 3) steel strain hardening ratio. Table 4.1 summarizes the range of selected values for these parameters. These values are the same as those used in the parameter studies of Chapter 3 are monotonic loading conditions.

Anchorage Length	Steel Yield Strength	Steel Strain Hardening Ratio
15 bar diameters	380 MPa	1.4%
25 bar diameters	470 MPa	3.5%
35 bar diameters	550 MPa	

TABLE 4.1 SELECTED PARAMETER VALUES

Each analysis with a given set of parameter values is performed twice: first with a bond stress-slip relation that does not include damage, so that the original envelope values of the bond stress-slip relation remain unaltered during the loading history, and, secondly with a bond slip-relation that includes damage, so that the original envelope values change as a function of the maximum previous slip and the total energy dissipation following the damage law proposed by Eligehausen et al. (1982) and Ciampi et al. (1982).

The finite element model of the anchored reinforcing bar consists of four elements with four Gauss-Lobatto integration points in each element. The following parameter studies evaluate the hysteretic response in terms of the hysteretic stress-slip relation at the end of the anchored bar and the damage distribution along the anchorage length.

4.3.1 Reinforcing Bar with Anchorage Length of 15 Bar Diameters

The parameter studies for this case are limited to one case only, namely a reinforcing bar with a yield strength of 380 MPa and strain hardening ratio of 1.4% in Fig. 4.12. Since the anchorage length is insufficient to transfer the imposed stresses at the ends of the anchored bar, the bar slips through the anchorage block before yielding of the reinforcement. Consequently, the change in the material parameters of reinforcing steel does not affect the hysteretic behavior of the anchored bar in Fig. 4.12. This behavior is, thus, dominated by the adopted bond stress-slip relation and the results in Fig. 4.12 are a vivid illustration of the effect of damage on the hysteretic bond-slip law.

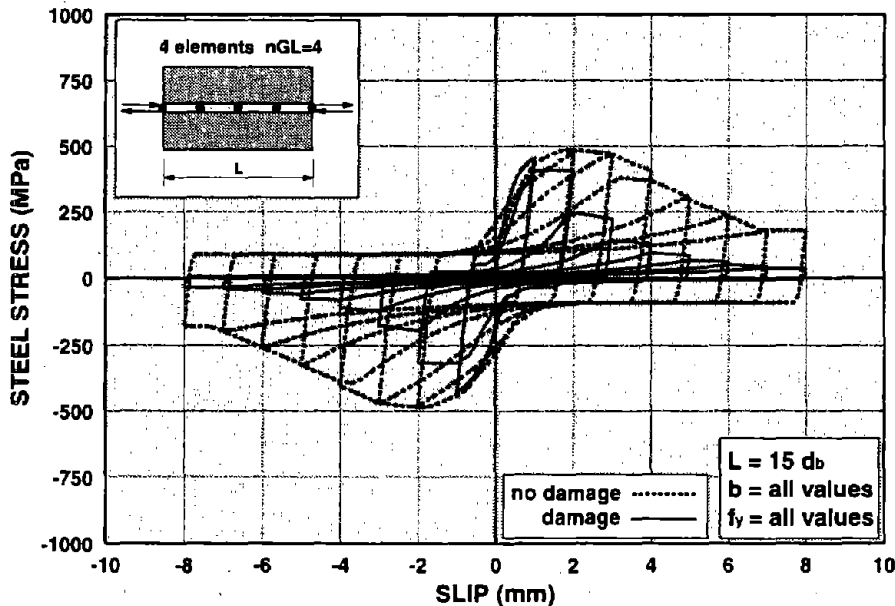


FIGURE 4.12 CYCLIC PUSH-PULL ON BAR WITH ANCHORAGE LENGTH OF 15 BAR DIAMETERS

4.3.2 Reinforcing Bar with Anchorage Length of 25 Bar Diameters

Figs. 4.13 and 4.14 present the effect of yield strength and strain hardening ratio of reinforcing steel on the hysteretic behavior of an anchored reinforcing bar with an anchorage length of 25 bar diameters. The results show the significant influence of the damage law on the hysteretic behavior of the anchored bar. The absence of any damage in the bond stress-slip relation might lead to the erroneous conclusion that an anchorage length of $25 d_b$ is sufficient for all but the highest yield strength case. By contrast, the experimentally observed damage of the hysteretic bond stress-slip relation leads to very unsatisfactory behavior of the anchored bar, even for the lowest yield strength and strain hardening ratio for this extreme loading case of imposed displacements of equal magnitude at the ends of the anchored bar.

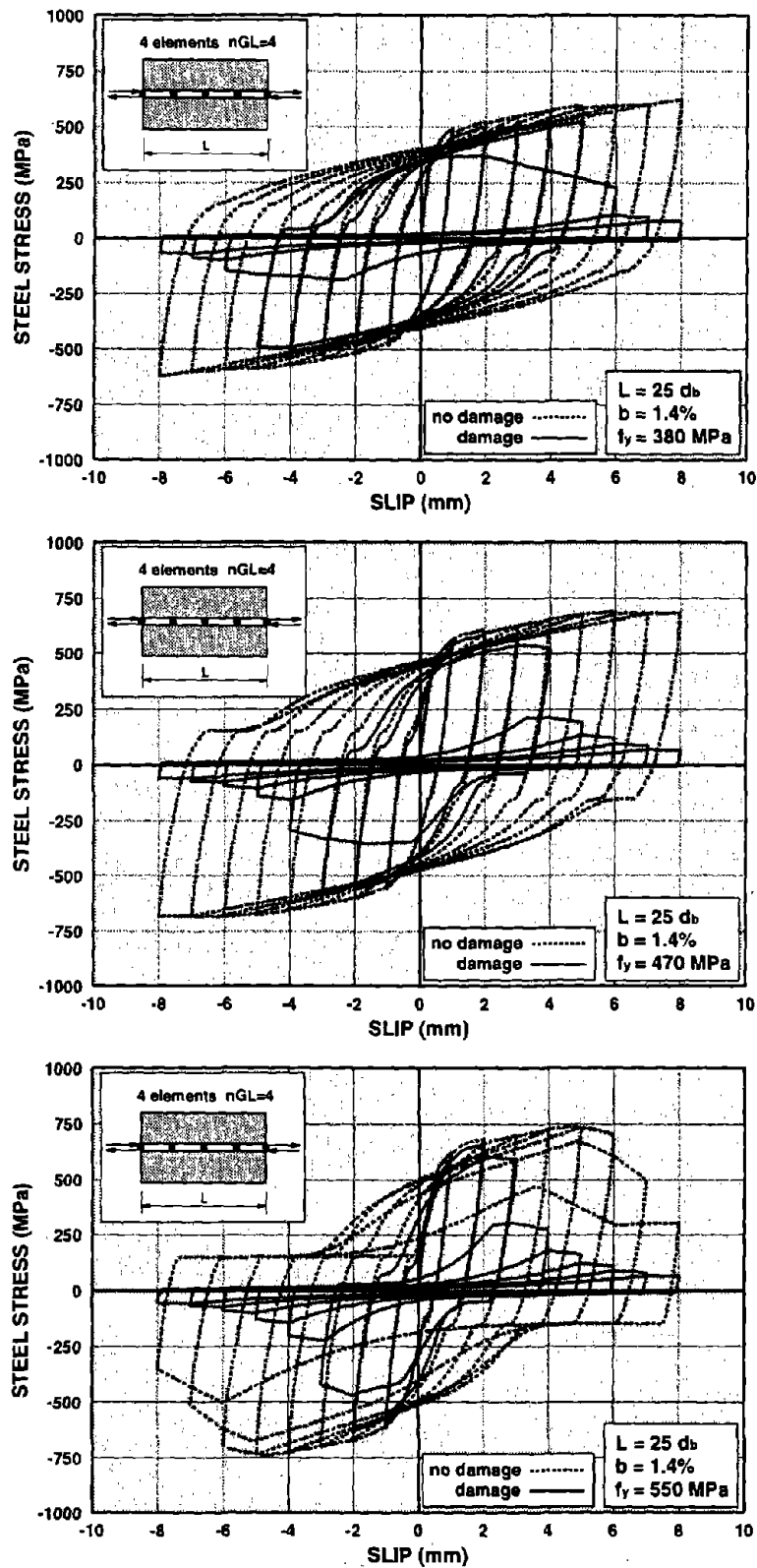


FIGURE 4.13 EFFECT OF YIELD STRENGTH ON CYCLIC PUSH-PULL OF ANCHORED BAR.
ANCHORAGE LENGTH = $25 d_b$; STRAIN HARDENING RATIO = 1.4%

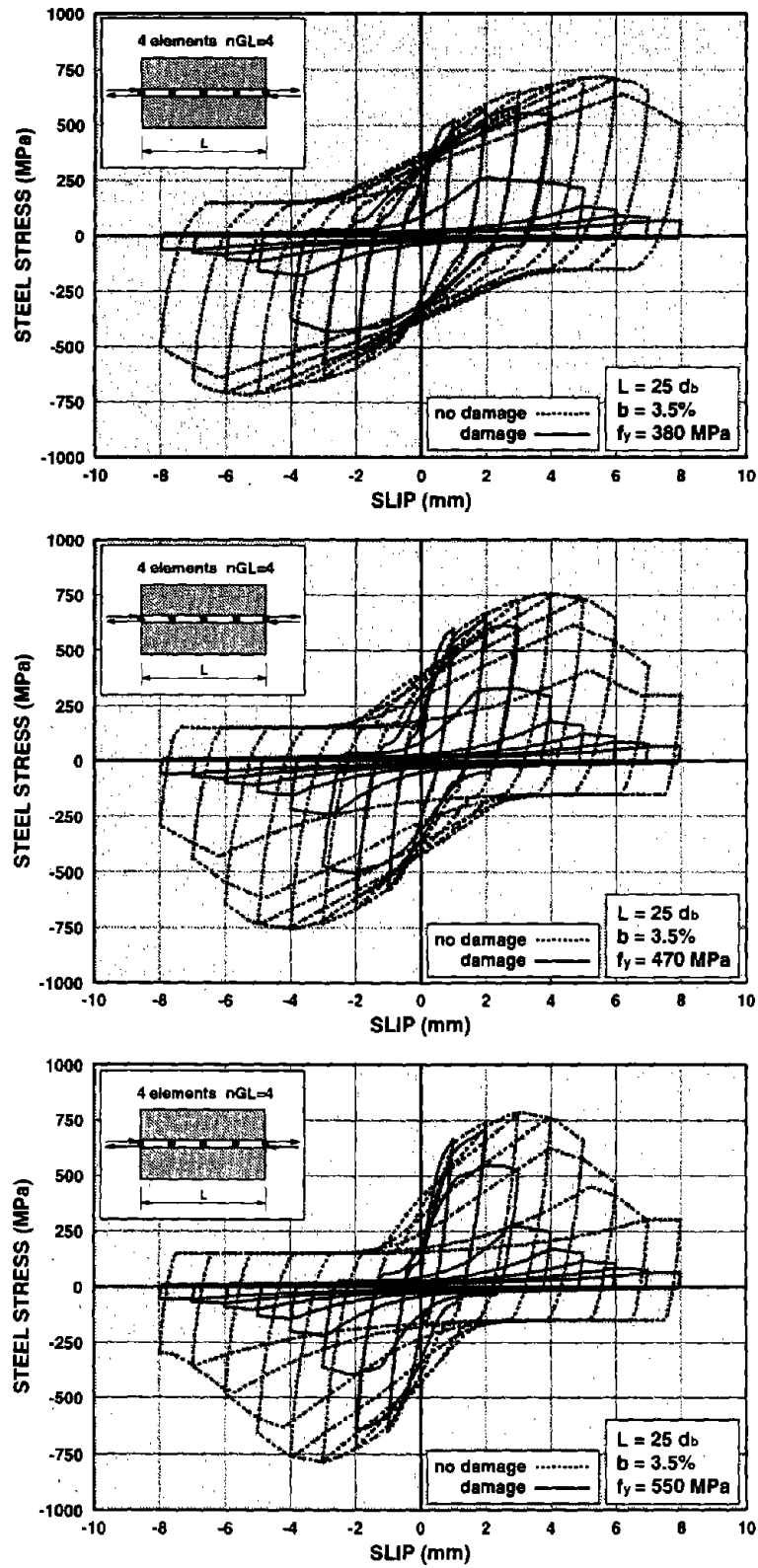


FIGURE 4.14 EFFECT OF YIELD STRENGTH ON CYCLIC PUSH-PULL OF ANCHORED BAR.
ANCHORAGE LENGTH = $25 d_b$; STRAIN HARDENING RATIO = 3.5%

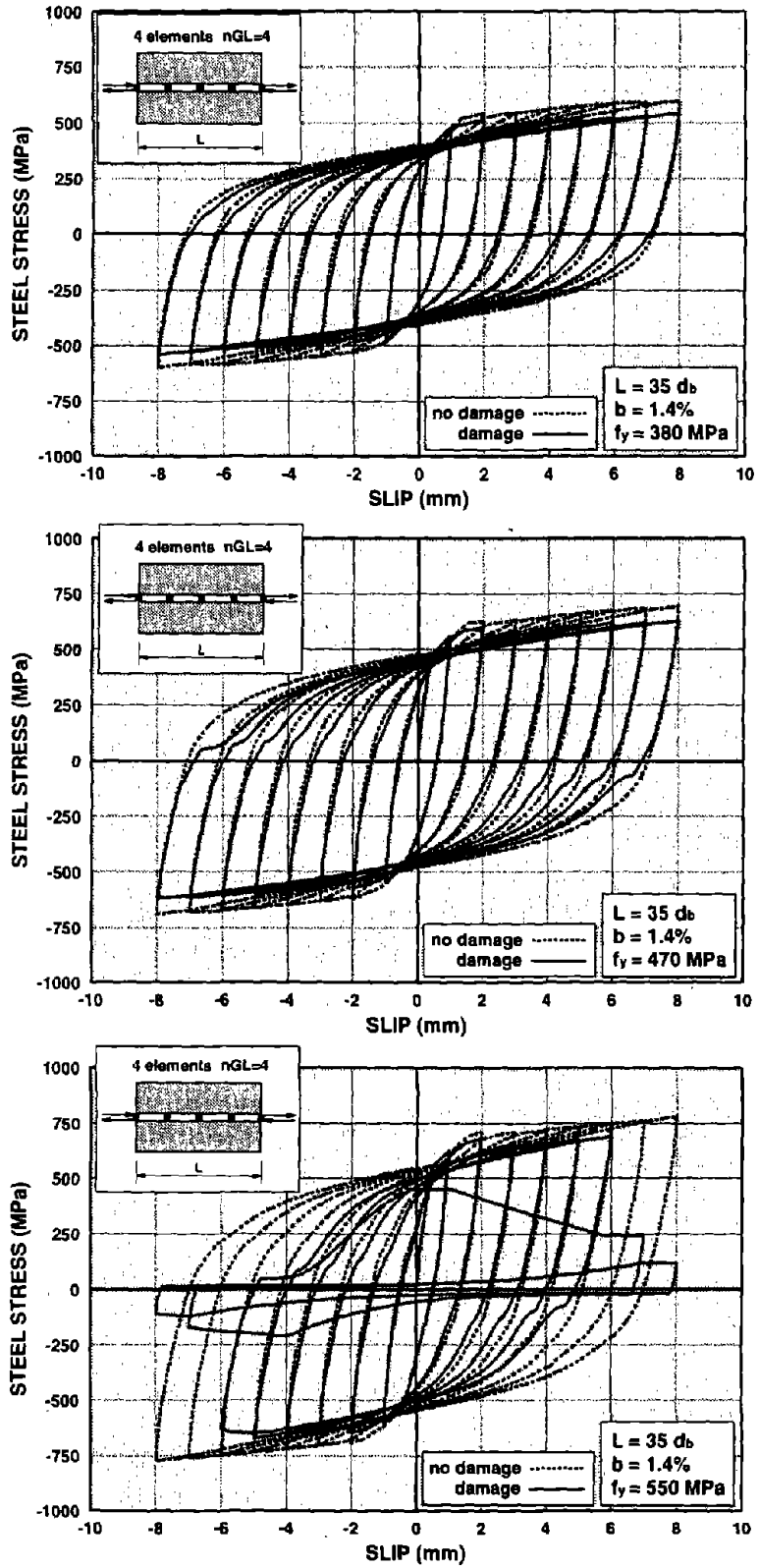


FIGURE 4.15 EFFECT OF YIELD STRENGTH ON CYCLIC PUSH-PULL OF ANCHORED BAR.
 ANCHORAGE LENGTH = $35 d_b$; STRAIN HARDENING RATIO = 1.4%

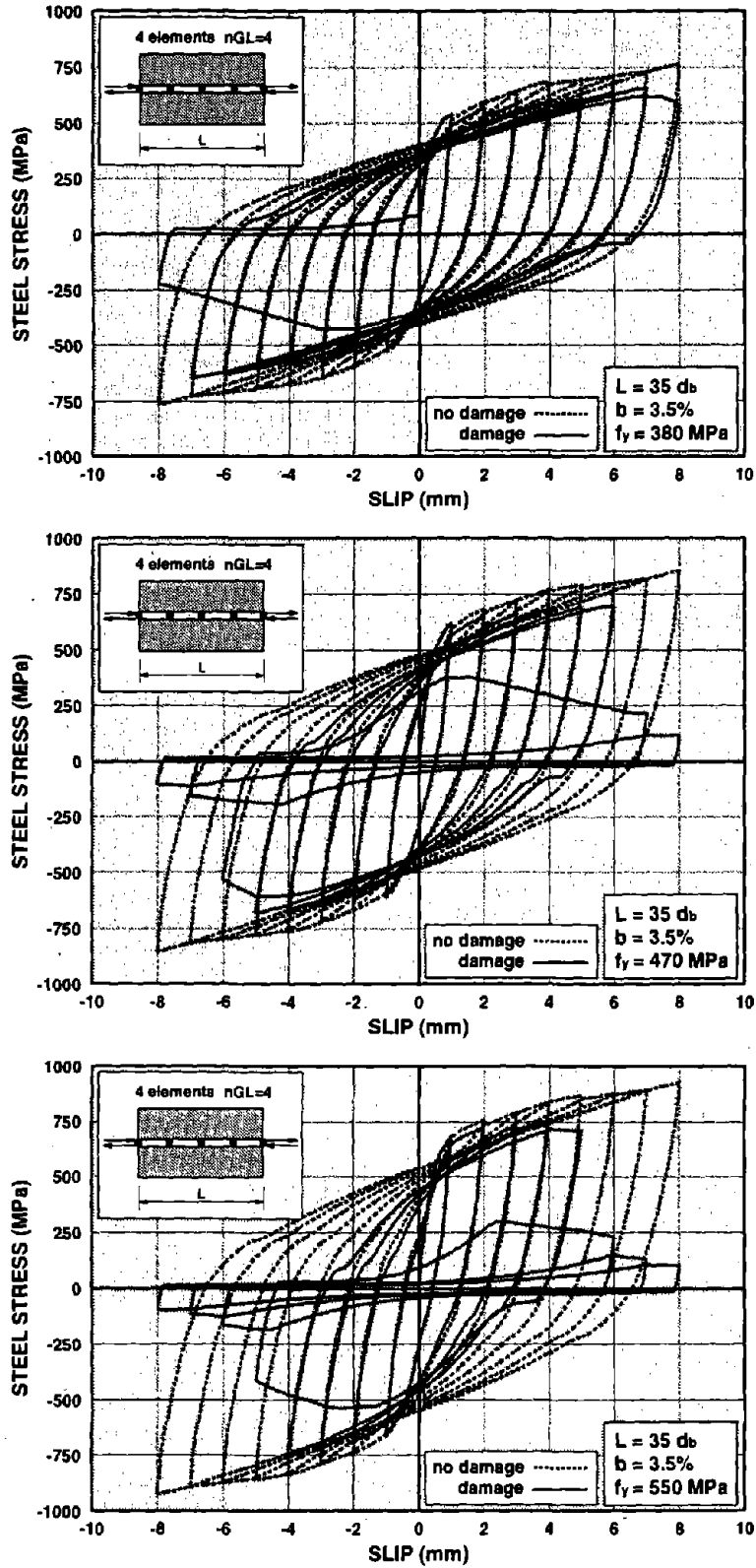


FIGURE 4.16 EFFECT OF YIELD STRENGTH ON CYCLIC PUSH-PULL OF ANCHORED BAR.
ANCHORAGE LENGTH = $35 d_b$; STRAIN HARDENING RATIO = 3.5%

It is evident from the results in Figs. 4.13 and 4.14 that the strength deterioration of the anchored reinforcing bar is more rapid for higher values of yield strength and hardening ratio. It is also clear from these results that the mechanical properties of reinforcing steel play a very important role in the determination of the anchorage length of reinforcing bars under cyclic loading conditions. While current codes address the effect of the yield strength of reinforcing steel, no attention is paid to the effect of strain hardening ratio which is important. A comparison of the response of the anchored reinforcing bar with a yield strength of 470 MPa in Figs. 4.13 and 4.14 demonstrates clearly the effect of strain hardening ratio, which is more pronounced in the case of no damage.

4.3.3 Reinforcing Bar with Anchorage Length of 35 Bar Diameters

Figs. 4.15 and 4.16 present the effect of yield strength and strain hardening ratio of reinforcing steel on the hysteretic behavior of an anchored reinforcing bar with an anchorage length of 35 bar diameters. The results show the significant influence of the damage law on the hysteretic behavior of the anchored bar. The models of the anchored reinforcing bar that do not include the effect of damage on the bond stress-slip relation show stable hysteretic behavior for all values of yield strength and strain hardening ratio of reinforcing steel. The inclusion of damage in the bond stress-slip relation changes the hysteretic behavior dramatically. Fig. 4.15 indicates that for a strain hardening ratio of 1.4% the reinforcing bars with yield strengths of 380 and 470 MPa do not show signs of pull-out. The reinforcing bar with yield strength of 550 MPa experiences a sudden drop in strength and stiffness after the loading cycle with an end slip value of 6 mm. For the reinforcing bar with a strain hardening ratio of 3.5% in Fig. 4.16 only the bar with yield strength of 380 MPa shows stable behavior after several cycles, while the bars with yield strength of 470 and 550 MPa exhibit abrupt loss of strength and pull-out after only a few cycles. These results further corroborate the previous finding about the importance of strain hardening ratio in the evaluation of anchorage lengths under monotonic and cyclic load conditions.

4.3.4 Bond Damage Distribution Along Anchorage

Figs. 4.18 and 4.18 show the distribution of bond damage along the bar anchorage for the parameter studies of Section 4.3. Bond damage is represented by the scalar value d of the bond stress-slip model of Eligehausen et al. (1982) and is shown at the instant of load reversal. A summary of the salient features of the model and of relevant equations is provided in Appendix A. The bond damage index d shown in Figs. 4.7 and 4.8 at the five nodes of the finite element model is defined in Eq. (A.7).

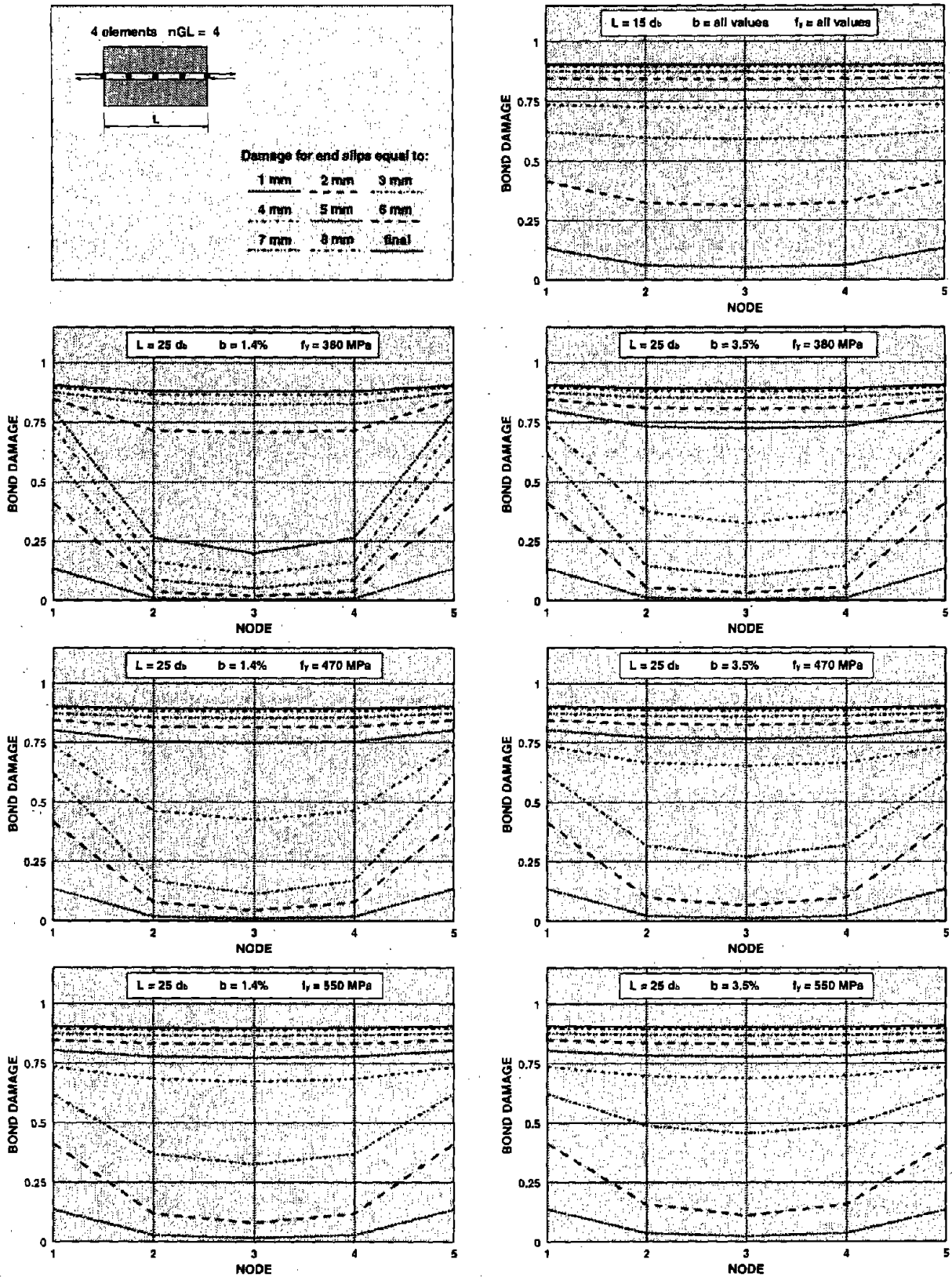


FIGURE 4.17 BOND DAMAGE DISTRIBUTION FOR REINFORCING BARS WITH ANCHORAGE LENGTH OF 15 AND 25 BAR DIAMETERS

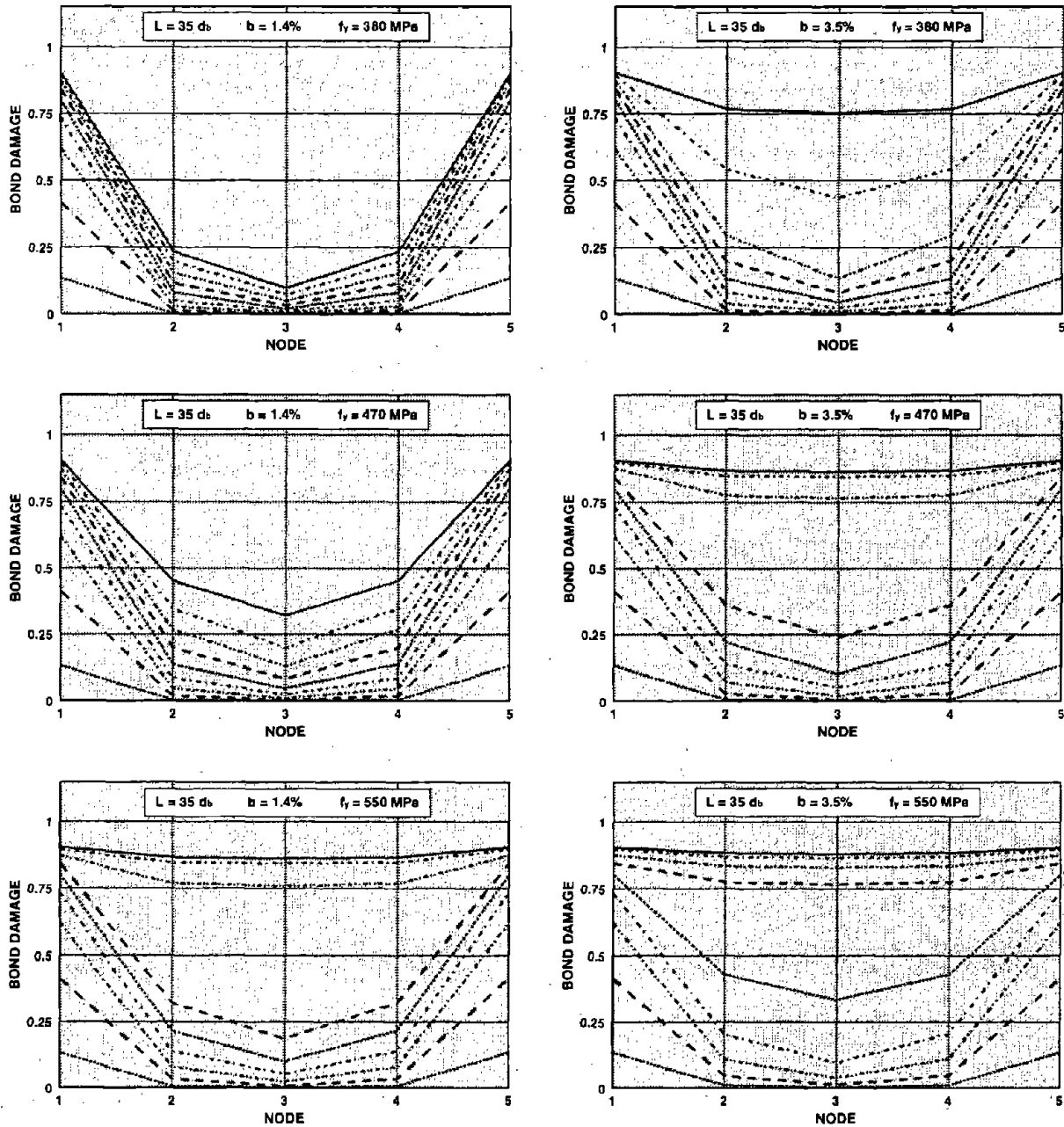


FIGURE 4.18 BOND DAMAGE DISTRIBUTION FOR REINFORCING BARS WITH ANCHORAGE LENGTH OF 35 BAR DIAMETERS

The nature of Eq. (A.7) indicates that the bond damage index d approaches the value of 1 only asymptotically. Thus, Figs. 4.17 and 4.18 suggest that a damage index value of 0.90 essentially implies complete damage, while a damage index value of value of zero signifies no damage.

A study of the distribution of bond damage in Figs. 4.17 and 4.18 underlines the

previous conclusions on the importance of yield strength, strain hardening ratio and, most importantly anchorage length on the hysteretic behavior of anchored reinforcing bars. It is particularly interesting to compare the bond damage of cases that only differ by the value of the steel strain hardening ratio and are plotted side by side. Two such cases are shown in Fig. 4.18 for a bar with yield strengths of 380 MPa and 470 MPa. In these cases the effect of the steel strain hardening ratio on the spread of bond damage into the anchorage length of the bar is clearly evident.

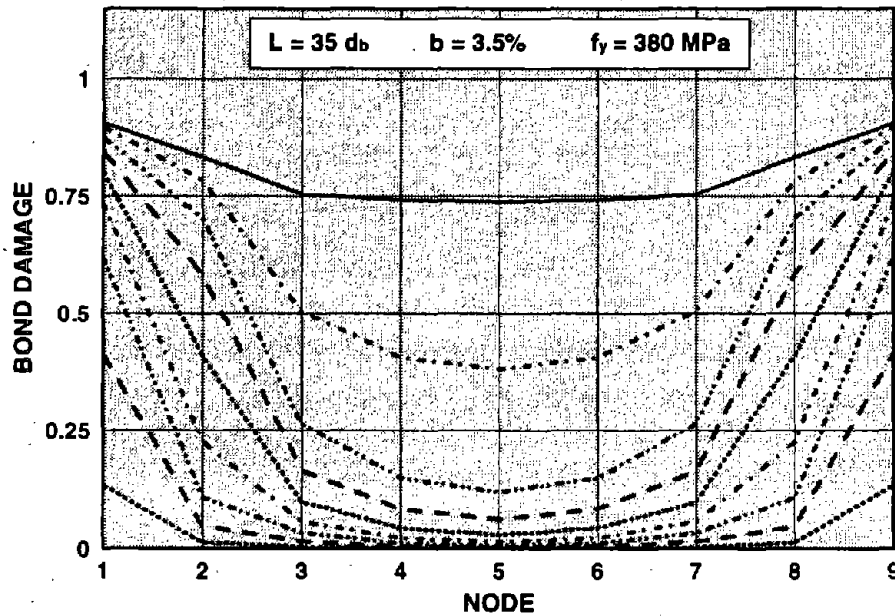


FIGURE 4.19 BOND DAMAGE DISTRIBUTION FOR A BAR MODEL WITH 8 ELEMENTS

It is important to point out that the distributions of bond damage in Figs. 4.17 and 4.18 are mesh independent. The damage index value at each node depends on the total energy dissipation in previous load cycles, and, thus, depends on the value of relative slip and bond stress at the corresponding node. Consequently, the damage index depends on the solution accuracy at each node and, since this does not improve appreciably in models with more than four elements, as already illustrated in Section 3.3.2, the damage distribution is not affected much by refining the anchored bar model beyond four elements. In order to verify the independence of the bond damage distribution from the size of the finite element mesh the reinforcing bar with an anchorage length of 35 bar diameters, a yield strength of 380 MPa and a strain hardening ratio of 1.4% is reanalyzed with a model that consists of eight (8) instead of four (4) elements. The damage distribution in Fig. 4.19 shows slight differences with respect to the corresponding distribution in Fig. 4.18 near the ends of the anchored bar, because of the presence of additional nodes. The damage index values at the common nodes of the two mesh configurations are, however, essentially identical.

CHAPTER 5

CONCLUSIONS

This study presents the development and the numerical implementation of a finite element for anchored reinforcing bars. The objective of the study is the development of a robust and efficient model within the framework of classical finite element methodology, so that the model can be later implemented in the analysis of reinforced concrete members, such as beam-column joints, where the interaction between reinforcing steel and concrete through bond plays an essential role in the characterization of the hysteretic behavior.

The development of the proposed model is based on the flexibility method of analysis. In this case force interpolation functions are used to approximate the force fields in the governing differential equations of the problem. For the problem of stress transfer between reinforcing steel and concrete through bond the force fields are the steel stress in the reinforcement and the bond stress acting on the circumference of the anchored bar. Since these two fields are, however, related by the equilibrium equation of the problem, only one can be selected independently. The development of the flexibility based model is motivated by the fact that anchored reinforcing bars that are subjected to large deformation reversals exhibit a smooth distribution of steel stress, while the strain and relative displacement between reinforcing steel and surrounding concrete are characterized by steep gradients in the inelastic portion of the anchored bar. In agreement with this physical observation only few elements suffice to approximate the steel stress distribution along the anchored bar and no provisions are necessary for refining the mesh of the model in the inelastic portion of the bar. For the same reason the model exhibits great numerical stability and convergence characteristics, even in the presence of strength loss and pull-out of the anchored reinforcing bar. This sets it apart from displacement based models that are known to be plagued by numerical instability and spurious unloading problems in the face of strength loss and softening.

The implementation of the flexibility based model in a standard finite element analysis program is, however, a challenging problem. This is accomplished in the proposed study by adapting a general method that has been proposed earlier by Ciampi and Carlesimo (1986)

and, subsequently, refined by Taucer et al. (1991). With this method the proposed element is incorporated in the well known general purpose finite element analysis program FEAP by R. L. Taylor.

The study concludes with correlations of analytical with a few experimental results from anchored reinforcing bars under severe cyclic excitations in order to illustrate the ability of the model to simulate the complex hysteretic behavior. The hysteretic material model that is used to describe the bond stress-slip relation includes the effect of damage and is, thus, able to simulate the cyclic bond deterioration along the anchored bar, which causes strength and stiffness loss of the bar.

Finally, a series of parameter studies under monotonic and cyclic loads illustrate the potential of the model as a tool for the assessment of the hysteretic behavior of reinforcing bar anchorages. In this respect it is interesting to conclude that material properties that are not accounted for in present design guidelines, such as the strain hardening ratio of reinforcing steel, play an important role in the hysteretic behavior of anchored reinforcing bars.

The potential of the model to serve as a building block of models for reinforced concrete members where the interaction between reinforcing steel and concrete through bond plays an essential role in the characterization of the hysteretic behavior is great by virtue of its efficiency, its numerical stability and its implementation in a general purpose finite element analysis program. This issue will be the subject of future studies.

REFERENCES

- Bertero, V.V. and Popov, E.P. (1977). "Seismic Behavior of Ductile Moment-Resisting Reinforced Concrete Frames", *Reinforced Concrete Structures in Seismic Zones*, ACI special publication SP-53, Detroit.
- Ciampi, V., Eligehausen, R., Bertero V.V. and Popov, E.P. (1982). "Analytical Model for Concrete Anchorages of Reinforcing Bars under Generalized Excitations." *Report EERC 82-23*, Earthquake Engineering Research Center, University of California, Berkeley.
- Ciampi, V. and Carlesimo, L. (1986). A Nonlinear Beam Element for Seismic Analysis of Structures. Proceedings 8th European Conference on Earthquake Engineering, Lisbon.
- deGroot, A.K., Kusters, G.M.A. and Monnier, T. (1981). "Numerical Modeling of Bond-Slip Behavior." *Heron, Concrete Mechanics*, Vol. 26, No.1B.
- Eligehausen, R., Popov, E.P., and Bertero, V.V. (1982). "Hysteretic Behaviour of Reinforcing Deformed Hooked Bars in Reinforced Concrete Joints," *Proceedings, 7th European Conference on Earthquake Engineering*, Athens, Vol. 4, pp. 171-178.
- Eligehausen, R., Popov, E.P. and Bertero V.V. (1983). "Local Bond Stress-Slip Relationships of Deformed Bars under Generalized Excitations." *Report EERC 83-23*, Earthquake Engineering Research Center, University of California, Berkeley.
- Filippou, F.C., Popov, E.P. and Bertero, V.V. (1983). "Effects of Bond Deterioration on Hysteretic Behavior of Reinforced Concrete Joints". *Report EERC 83-19*, Earthquake Engineering Research Center, University of California, Berkeley.
- Filippou, F.C. (1986). "A Simple Model for Reinforcing Bar Anchorages Under Cyclic Excitations". *Journal of Structural Engineering*, ASCE, 112(ST7), pp.1639-1659.
- Kwak, H.G. and Filippou, F.C. (1990). "Finite Element Analysis of Reinforced Concrete Structures Under Monotonic Loading", Report No. UCB/SEMM-90/14, Structural Engineering, Mechanics and Materials, Department of Civil Engineering, University of California, Berkeley.
- Keuser, M. and Mehlhorn, G. (1987). "Finite Elements Models for Bond Problems". *Journal of Structural Engineering*, ASCE, 113(ST10), pp. 2160-2173.
- Menegotto, M. and Pinto, P.E. (1973). "Method of Analysis for Cyclically Loaded Reinforced Concrete Plane Frames Including Changes in Geometry and Non-Elastic Behavior of Elements Under Combined Normal Force and Bending." *Proceedings, IABSE Symposium on "Resistance and Ultimate Deformability of Structures Acted on by Well Defined Repeated Loads"*, Lisbon.
- Ngo, D. and Scordelis, A.C. (1967). "Finite Element Analysis of Reinforced Concrete Beams." *Journal of ACI*, Vol. 64, No. 3, pp. 152-163.
- Nilson, A.H. (1971). "Internal Measurement of Bond-Slip". *Journal of ACI*, Vol. 69, No. 7, pp. 439-441.
- Reddy, J.N. (1993). *An Introduction to the Finite Element Method*. Second edition. McGraw Hill Book Company, New York.
- Stroud, A. H. and Secrest, D. (1966). *Gaussian Quadrature Formulas*, Prentice Hall, New Jersey.
- Taucer, F., Spacone, E. and Filippou, F.C. (1991). "A Fiber Beam-Column Element for Seismic Response Analysis of Reinforced Concrete Structures." *Report EERC 91-17*, Earthquake Engineering Research Center, University of California, Berkeley.

- Viathanatepa, S., Popov, E.P. and Bertero, V.V. (1979). "Effects of Generalized Loadings on Bond of Reinforcing Bars Embedded in Confined Concrete Blocks" *EERC 79-22*, Earthquake Engineering Research Center, University of California, Berkeley.
- Yankelevsky, D.Z. (1985). "New Finite Element for Bond-Slip Analysis". *Journal of Structural Engineering*, ASCE, 111(ST7), pp. 1533-1542.
- Zienkiewicz, O.C. and Taylor, R.L. (1989). *The Finite Element Method*. Volume 1. Basic Formulation and Linear Problems. Fourth edition. McGraw Hill, London.
- Zienkiewicz, O.C. and Taylor, R.L. (1991). *The Finite Element Method*. Volume 2. Solid and Fluid Mechanics, Dynamics and Non-Linearity. Fourth edition. McGraw Hill, London.
- Zulfiqar, N. and Filippou, F.C. (1990). "Model of Critical Regions in Reinforced concrete Frames under Earthquake Excitations." *Report EERC 90-06*, Earthquake Engineering Research Center, University of California, Berkeley.
-

APPENDIX A
MATERIAL MODELS

A.1 Steel Stress-Strain Relation

The reinforcing steel stress-strain behavior is described by the nonlinear model of Menegotto and Pinto (1973), as modified by Filippou et al. (1983) to include isotropic strain hardening (Fig. A.1). The model is computationally efficient and agrees very well with experimental results from cyclic tests on reinforcing steel bars.

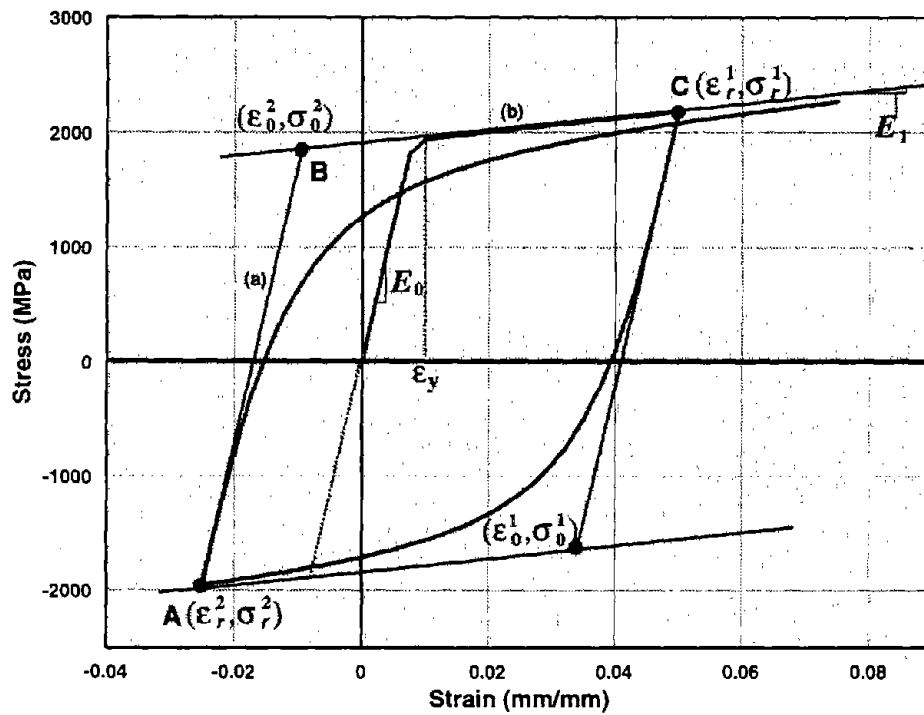


FIGURE A.1 MENEGOTTO-PINTO REINFORCING STEEL MODEL

The model, as presented in Menegotto and Pinto (1973) takes on the form

$$\sigma^* = b \cdot \varepsilon^* + \frac{(1-b) \cdot \varepsilon^*}{(1 + \varepsilon^{*R})^{1/R}} \quad (\text{A.1})$$

where

$$\varepsilon^* = \frac{\varepsilon - \varepsilon_r}{\varepsilon_0 - \varepsilon_r} \quad (\text{A.2})$$

and

$$\sigma^* = \frac{\sigma - \sigma_r}{\sigma_0 - \sigma_r} \quad (\text{A.3})$$

Eq. (A.1) represents a curved transition from a straight line asymptote with slope E_0 to another asymptote with slope E_1 (lines (a) and (b), respectively, in Fig. A.1). σ_0 and ε_0 are the stress and strain at the point where the two asymptotes of the branch under consideration meet (point B in Fig. A.1); similarly, σ_r and ε_r are the stress and strain at the point where the last strain reversal took place (point A in Fig. A.1); b is the strain hardening ratio, that is the ratio between slope E_1 and E_0 and R is a parameter that influences the shape of the transition curve and allows a good representation of the Bauschinger effect. As indicated in Fig. A.1, $(\varepsilon_0, \sigma_0)$ and $(\varepsilon_r, \sigma_r)$ are updated after each strain reversal.

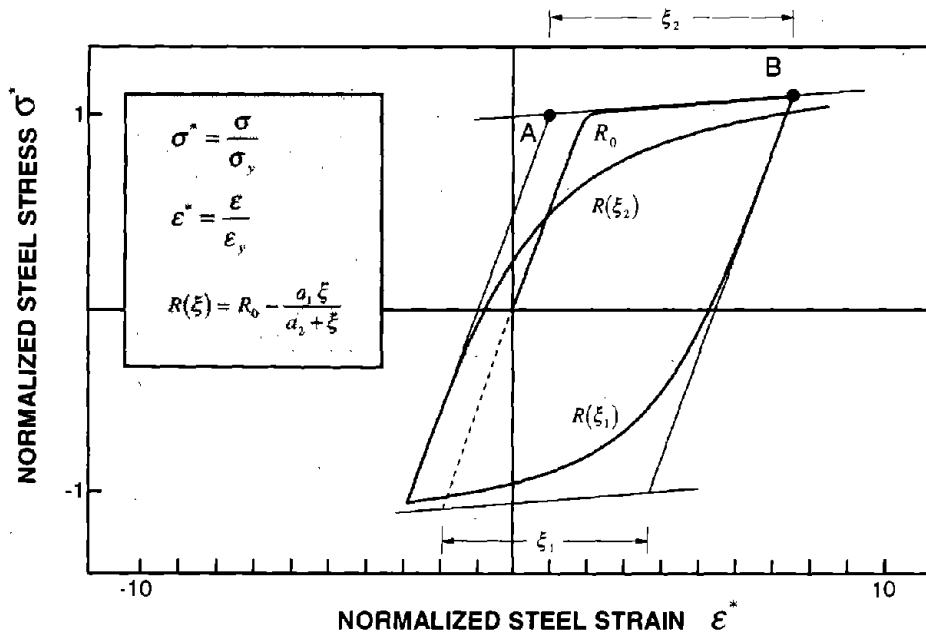


FIGURE A.2 DEFINITION OF CURVATURE PARAMETER R IN MENEGOTTO-PINTO STEEL MODEL

R is considered dependent on the strain difference between the current asymptote intersection point (point A in Fig. A.2) and the previous load reversal point with maximum or minimum strain depending on whether the corresponding steel stress is positive or negative (point B in Fig. A.2). The expression for R takes the form suggested in Menegotto and Pinto (1973)

$$R = R_0 - \frac{a_1 \cdot \xi}{a_2 + \xi} \quad (\text{A.4})$$

where ξ is updated following a strain reversal. R_0 is the value of the parameter R during first loading and a_1 , a_2 are experimentally determined parameters to be defined together with R_0 . The definition of ξ remains valid in case that reloading occurs after partial unloading.

Some clarification is needed in connection with the set of rules for unloading and reloading which complement Eqs. (A.2) and (A.3), allowing for a generalized load history. If the analytical model had a memory extending over all previous branches of the stress-strain history, it would follow the previous reloading branch, as soon as the new reloading curve reached it. This would require that the model store all necessary information to retrace all previous reloading curves which were left incomplete. This is clearly impractical from a computational standpoint. Memory of the past stress-strain history is, therefore, limited to a predefined number of controlling curves, which in the present model include,

1. the monotonic envelope,
2. the ascending upper branch curve originating at the reversal point with smallest ϵ value,
3. the descending lower branch curve originating at the reversal point with largest ϵ value,
4. the current curve originating at the most recent reversal point.

Due to the above restrictions reloading after partial unloading does not rejoin the original reloading curve after reaching the point from which unloading started, but, instead, continues on the new reloading curve until reaching the envelope. However, the discrepancy between the analytical model and the actual behavior is typically very small, as discussed in detail by Filippou et al. (1983).

The above implementation of the model corresponds to its simplest form, as proposed in Menegotto and Pinto (1973): elastic and yield asymptotes are assumed to be straight lines, the position of the limiting asymptotes corresponding to the yield surface is assumed to be fixed at all times and the slope E_0 remains constant (Fig. A.1).

In spite of the simplicity in formulation, the model is capable of reproducing well experimental results. Its major drawback stems from its failure to allow for isotropic hardening. To account for this effect Filippou et al. (1983) proposed a stress shift in the linear yield asymptote as a function of the maximum plastic strain as follows:

$$\frac{\sigma_{st}}{\sigma_y} = a_3 \cdot \left(\frac{\epsilon_{max}}{\epsilon_y} - a_4 \right) \quad (A.5)$$

where ϵ_{max} is the absolute maximum strain at the instant of strain reversal, ϵ_y , σ_y are, respectively, the strain and stress at yield, and a_3 and a_4 are experimentally determined parameters. The model used in this study was implemented without the isotropic strain hardening option. For this case the parameter values are: $R_0 = 20$, $a_1 = 18.5$, $a_2 = 0.15$, $a_3 = 0.$, $a_4 = 0$. With the exception of the last two parameters the values used are those in the original model of Menegotto and Pinto (1973).

A.2 Bond Stress-Slip Model

An accurate formulation of the bond stress-slip relation between reinforcing bars and surrounding concrete under random cyclic excitations is of great importance to analytical models of the hysteretic behavior of critical regions in reinforced concrete frames.

Extensive experimental and analytical studies of the bond-slip behavior of reinforcing bars under monotonic loading have been conducted to date (Goto 1971, Nilson 1971, Mirza and Houde 1976, Viwathanatepa et al. 1979, Somayaji and Shah 1981). A few more studies under repeated loads with a peak bond stress well below the bond strength have been conducted (Bresler and Bertero 1968, Rehm and Eligehausen 1979, Harajli 1988). The first model of the local bond stress-slip relation under *cyclic* loading was proposed by Morita and Kaku (1973). The model exhibits good agreement with experimental observations during the early load cycles. The observed deterioration of bond resistance under large slip values and the deterioration of frictional bond resistance with increasing number of cycles is, however, not taken into account. The model of Viwathanatepa et. al. (1979) takes into account several features of the experimentally observed behavior and is valid for cycling between arbitrary slip values. In spite of its complexity, this model is not general, since it depends on many parameters which must be derived from experimental data.

In 1983 Elgehausen et al. (1983) conducted an extensive experimental investigation of the local bond stress-slip relation of reinforcing bars under large slip reversals. 125 reinforcing bar specimens anchored in confined concrete with a short embedment length of five bar diameters were tested. The specimens simulated the confinement and loading conditions in interior and exterior joints of moment resisting frames. The influence of a number of parameters, such as bar diameter, concrete strength and transverse confining pressure on the local bond stress-slip relation was investigated. Based on these experimental results a general analytical model was proposed. This model is valid for a wide range of slip values which are of interest in seismic response analysis of RC structures. The key aspects of the model will be summarized below.

A.2.1 General Model Description

The model of the local bond stress-slip relation between reinforcing bars and surrounding concrete consists of the following parts:

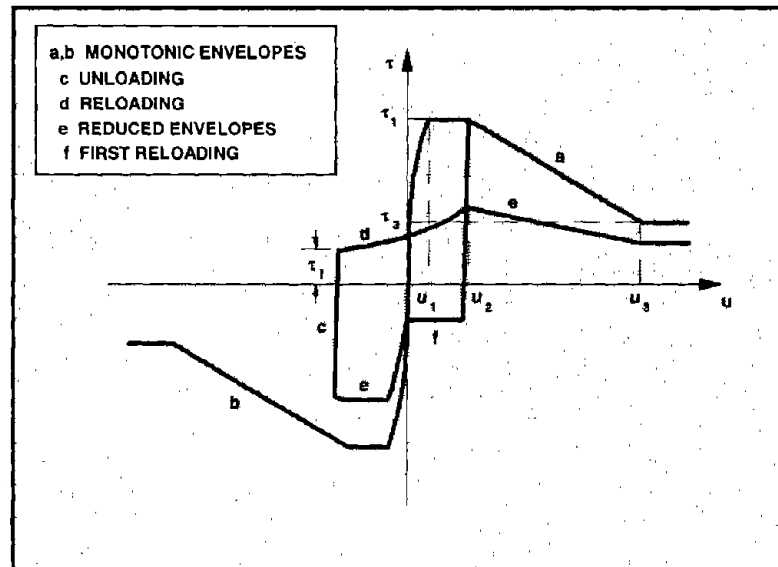


FIGURE A.3 BOND STRESS-SLIP RELATION

- (1) Two monotonic envelopes, one in tension and one in compression, which are updated at each slip reversal to reflect incurred damage (curves (a) and (b) in Fig. A.3).

- (2) A typical unloading-reloading path described by the unloading curve (c), the current frictional bond resistance q_f and a reloading curve (d), along with a set of rules for unloading and reloading for incomplete cycles (Fig. A.3).
- (3) A set of relations for updating the monotonic envelope values and the frictional bond resistance as a function of incurred damage.

The parts of the model are described in more detail below.

Monotonic Bond Stress-Slip Envelope.- The monotonic envelope consists of an initial nonlinear relation $q = q_1 \cdot (u/u_1)^\alpha$, valid for $u \leq u_1$, followed by a plateau $q = q_1$ for $u_1 \leq u \leq u_2$. For $u \geq u_2$, q decreases linearly to the value of ultimate frictional bond resistance q_3 at a slip value of u_3 which is assumed to be equal to the clear distance between the lugs of deformed bars.

Behavior during Unloading.- When the load is reversed at some slip value, unloading takes place along a steep straight line until the frictional bond resistance q_f is reached (curve c Fig. A.3).

Behavior during Reloading.- The reloading curve is described by a fourth degree polynomial (curve d in Fig. A.3) starting from the frictional bond resistance value and leading to the intersection between reduced envelope and previous unloading curve. In case that no slip has been previously imposed in the same loading direction, reloading takes place along a horizontal line until reaching the reduced envelope (curve f in Fig. A.3). The use of a fourth degree polynomial for the reloading curve was first introduced by Filippou et al. (1983) to better account for the experimentally observed bond stress-slip behavior.

Reduced Bond Stress-Slip Envelope.- During each half cycle following the first unloading, the monotonic envelopes are updated (curve e Fig. A.3) by reducing the characteristic bond stress values q_1 and q_3 by a factor, which is function of the 'damage parameter' d . The reduction in stress is given by (Eligehausen et al. 1983)

$$q_1(N) = q_1 \cdot (1 - d) \quad (\text{A.6})$$

where q_1 is the characteristic value of the virgin envelope curve and $q_1(N)$ is the corresponding value after N cycles. The damage parameter depends on the total energy dissipated by the bond-slip process and is given by

$$d = 1 - e^{-1.2(E/E_0)^{1.1}} \quad (\text{A.7})$$

where E is the total dissipated energy. E_0 is the energy absorbed under monotonically increasing slip up to the value u_3 and is used as a normalization parameter.

Analogously, the friction stress value q_f is reduced by a factor which is function of a 'damage parameter' d_f . The reduction in stress is given by (Eligehausen et al. 1983)

$$q_f(N) = q_f \cdot (1 - d_f) \quad (\text{A.8})$$

where q_1 is the characteristic value of the virgin envelope curve and $q_1(N)$ is the corresponding value after N cycles. The damage parameter depends on the frictional energy dissipated by the bond-slip process and is given by

$$d_f = 1 - e^{-1.2(E_f/E_{0f})^{0.67}} \quad (\text{A.9})$$

where E_f is the frictional energy, that is the energy dissipated on the reloading branches when $\Delta u \cdot u < 0$, where Δu is the current slip increment and u is the current slip value. $E_{0f} = q_f \cdot u_3$ is the frictional energy absorbed under monotonically increasing slip up to the value u_3 and is used as a normalization parameter.

Frictional Bond Resistance.- The frictional bond resistance q_f depends on the maximum value of previous slip u_{\max} in either direction of loading and the ultimate bond resistance $q_3(N)$ of the corresponding reduced envelope curve. If cyclic reversals are performed under fixed values of slip, q_f is further reduced by multiplying its initial value with a factor which depends on the energy dissipated by friction alone. Explicit expressions for these relations are given by Eligehausen et al. (1983).

In the nonlinear bond stress-slip model all expressions are cast in dimensionless form except for the characteristic values of the monotonic envelope curve. The model can thus be readily extended to describe the local bond stress-slip relation of reinforcing bars under different bond and loading conditions by only changing the characteristic values of the monotonic envelope curve. These characteristic values depend on several parameters such as bar diameter, concrete strength, bar deformation pattern, clear spacing between bars and transverse pressure due to loading or confinement. Ideally, the characteristic values should be derived from experiments which simulate the actual geometric and loading conditions of the structure under investigation. In the absence of experimental data the characteristic values of the envelope curve can be based on the recommendations given below for different conditions of bond and loading.

	u_1 [mm]	u_2 [mm]	u_3 [mm]	q_1 [MPa]	q_3 [MPa]	α
Tension	1.00	3.00	10.50	13.50	5.00	0.40
Compression	1.00	3.00	10.50	13.50	5.00	0.40

TABLE A.1 CHARACTERISTIC VALUES OF MONOTONIC ENVELOPE OF BOND STRESS-SLIP RELATION FOR DEFORMED STRAIGHT BARS EMBEDDED IN CONFINED CONCRETE

A.2.2 Bond Stress-Slip Relation in Confined Concrete

The recommendations for the characteristic values of the monotonic envelope curve for bars embedded in well confined concrete are based on the experiments conducted by Eligehausen et al. (1983). Identical envelopes of the bond stress-slip relation are observed in tension and compression, i.e. in case the bar is pulled or pushed. Table A.1 lists the characteristic monotonic envelope values for average bond conditions of #8 reinforcing bars. The compressive strength of the concrete surrounding the bars is and no external transverse pressure is applied. The clear spacing between bars is four times the bar diameter.

Due to inevitable scatter of experimental results the values of q_1 , q_3 and α may well vary by up to $\pm 15\%$.

These values need to be modified to account for differences in bar diameter, concrete strength, clear spacing between bars, deformation pattern and external pressure. The modifications follow the recommendations of Eligehausen et al. (1983) and are summarized here for the sake of completeness.

- (1) q_1 should be increased by 10%, if #6 bars are used, and q_1 should be reduced by 10%, if #10 bars are used instead of #8 bars.
- (2) The influence of concrete strength can be taken into account by multiplying q_1 and q_3 with $\sqrt{f'_c/30}$ where f'_c is the concrete compressive strength in MPa. Similarly, the value of u_1 should be modified in direct proportion to $\sqrt{30/f'_c}$.
- (3) If the clear spacing between bars is smaller than $4d_b$, where d_b is the bar diameter, q_1 and q_3 should be reduced using the information in Fig. 4.15 of the report by

- Eligehausen et al. (1983). For $3d_b$ the reduction is approximately 2%, for $2d_b$ 7% and for $1d_b$ 17%.
- (4) The values of u_1 , u_2 and u_3 should be multiplied by $c_1/10.5$, where c_1 is the clear spacing between lugs in mm, but this modification should not be greater than $\pm 30\%$.
 - (5) If the value of the relative rib area α_{SR} differs from 0.065, its influence should be taken into account by modifying u_1 , q_1 and α according to the information in Fig. 2.14 of the report by Eligehausen et al. (1983).
 - (6) The influence of external transverse pressure p such as axial compressive column forces can be taken into account by increasing q_1 and q_3 according to Fig. 4.17 of the report by Eligehausen et al. (1983). For $p = 5$ MPa the increase is approximately 18%, for $p = 10$ MPa about 22% and for $p = 15$ MPa about 25%.
 - (7) The unloading slope is equal to 180 N/mm^3 for #8 bars. It should be modified in the same way as q_1 for different conditions.

A.2.3 Bond Stress-Slip Relation in Hook Anchorages

Experiments were conducted by Eligehausen et al. (1982) to study the bond stress-slip relation of deformed hooked bars embedded in well confined concrete and subjected to monotonic and cyclic loadings. Based on these experimental results it was concluded that the model proposed by Eligehausen et al. (1983) can be readily extended to describe the bond stress-slip behavior of the hook by idealizing the hook as a straight bar with an equivalent length of five bar diameters and proposing new characteristic values for the monotonic envelope in tension and compression. The proposed characteristic values for #8 bars which are anchored in concrete of compressive strength are listed in Table A.2 (Eligehausen et al. 1982).

Identical envelopes apply in tension and compression. The bond stress-slip behavior under cyclic load reversals is defined by the same damage parameter, which is used for straight bars in confined concrete.

	u_1 [mm]	u_2 [mm]	u_3 [mm]	q_1 [MPa]	q_3 [MPa]	α
Hooks bent against direction of casting	1.00	3.00	100.00	22.00	4.00	0.20
Hooks bent in direction of casting	2.00	3.00	100.00	22.00	4.00	0.20

**TABLE A.2 CHARACTERISTIC VALUES OF MONOTONIC ENVELOPE OF BOND STRESS-SLIP
RELATION FOR HOOKED BARS EMBEDDED IN CONFINED CONCRETE**

EARTHQUAKE ENGINEERING RESEARCH CENTER REPORT SERIES

EERC reports are available from the National Information Service for Earthquake Engineering (NISEE) and from the National Technical Information Service (NTIS). Numbers in parentheses are Accession Numbers assigned by the National Technical Information Service; these are followed by a price code. Contact NTIS, 5285 Port Royal Road, Springfield Virginia, 22161 for more information. Reports without Accession Numbers were not available from NTIS at the time of printing. For a current complete list of EERC reports (from EERC 67-1) and availability information, please contact University of California, EERC, NISEE, 1301 South 46th Street, Richmond, California 94804-4698.

- UCB/EERC-84/01 "Pseudodynamic Test Method for Seismic Performance Evaluation: Theory and Implementation," by Shing, P.-S.B. and Mahin, S.A., January 1984, (PB84 190 644)A08.
- UCB/EERC-84/02 "Dynamic Response Behavior of Kiang Hong Dian Dam," by Clough, R.W., Chang, K.-T., Chen, H.-Q. and Stephen, R.M., April 1984, (PB84 209 402)A08.
- UCB/EERC-84/03 "Refined Modelling of Reinforced Concrete Columns for Seismic Analysis," by Kaba, S.A. and Mahin, S.A., April 1984, (PB84 234 384)A06.
- UCB/EERC-84/04 "A New Floor Response Spectrum Method for Seismic Analysis of Multiply Supported Secondary Systems," by Asfura, A. and Der Kiureghian, A., June 1984, (PB84 239 417)A06.
- UCB/EERC-84/05 "Earthquake Simulation Tests and Associated Studies of a 1/5th-scale Model of a 7-Story R/C Frame-Wall Test Structure," by Bertero, V.V., Aktan, A.E., Charney, F.A. and Sause, R., June 1984, (PB84 239 409)A09.
- UCB/EERC-84/06 "Unassigned," by Unassigned, 1984.
- UCB/EERC-84/07 "Behavior of Interior and Exterior Flat-Plate Connections Subjected to Inelastic Load Reversals," by Zee, H.L. and Moehle, J.P., August 1984, (PB86 117 629/AS)A07.
- UCB/EERC-84/08 "Experimental Study of the Seismic Behavior of a Two-Story Flat-Plate Structure," by Moehle, J.P. and Diebold, J.W., August 1984, (PB86 122 553/AS)A12.
- UCB/EERC-84/09 "Phenomenological Modeling of Steel Braces under Cyclic Loading," by Ikeda, K., Mahin, S.A. and Dermitzakis, S.N., May 1984, (PB86 132 198/AS)A08.
- UCB/EERC-84/10 "Earthquake Analysis and Response of Concrete Gravity Dams," by Fenves, G.L. and Chopra, A.K., August 1984, (PB85 193 902/AS)A11.
- UCB/EERC-84/11 "EAGD-84: A Computer Program for Earthquake Analysis of Concrete Gravity Dams," by Fenves, G.L. and Chopra, A.K., August 1984, (PB85 193 613/AS)A05.
- UCB/EERC-84/12 "A Refined Physical Theory Model for Predicting the Seismic Behavior of Braced Steel Frames," by Ikeda, K. and Mahin, S.A., July 1984, (PB85 191 450/AS)A09.
- UCB/EERC-84/13 "Earthquake Engineering Research at Berkeley - 1984," by EERC, August 1984, (PB85 197 341/AS)A10.
- UCB/EERC-84/14 "Moduli and Damping Factors for Dynamic Analyses of Cohesionless Soils," by Seed, H.B., Wong, R.T., Idriss, I.M. and Tokimatsu, K., September 1984, (PB85 191 468/AS)A04.
- UCB/EERC-84/15 "The Influence of SPT Procedures in Soil Liquefaction Resistance Evaluations," by Seed, H.B., Tokimatsu, K., Harder, L.F. and Chung, R.M., October 1984, (PB85 191 732/AS)A04.
- UCB/EERC-84/16 "Simplified Procedures for the Evaluation of Settlements in Sands Due to Earthquake Shaking," by Tokimatsu, K. and Seed, H.B., October 1984, (PB85 197 887/AS)A03.
- UCB/EERC-84/17 "Evaluation of Energy Absorption Characteristics of Highway Bridges Under Seismic Conditions - Volume I (PB90 262 627)A16 and Volume II (Appendices) (PB90 262 635)A13," by Imbsen, R.A. and Penzien, J., September 1986.
- UCB/EERC-84/18 "Structure-Foundation Interactions under Dynamic Loads," by Liu, W.D. and Penzien, J., November 1984, (PB87 124 889/AS)A11.
- UCB/EERC-84/19 "Seismic Modelling of Deep Foundations," by Chen, C.-H. and Penzien, J., November 1984, (PB87 124 798/AS)A07.
- UCB/EERC-84/20 "Dynamic Response Behavior of Quan Shui Dam," by Clough, R.W., Chang, K.-T., Chen, H.-Q., Stephen, R.M., Ghanaat, Y. and Qi, J.-H., November 1984, (PB86 115177/AS)A07.
- UCB/EERC-85/01 "Simplified Methods of Analysis for Earthquake Resistant Design of Buildings," by Cruz, E.F. and Chopra, A.K., February 1985, (PB86 112299/AS)A12.
- UCB/EERC-85/02 "Estimation of Seismic Wave Coherency and Rupture Velocity using the SMART 1 Strong-Motion Array Recordings," by Abrahamson, N.A., March 1985, (PB86 214 343)A07.
- UCB/EERC-85/03 "Dynamic Properties of a Thirty Story Condominium Tower Building," by Stephen, R.M., Wilson, E.L. and Stander, N., April 1985, (PB86 118965/AS)A06.
- UCB/EERC-85/04 "Development of Substructuring Techniques for On-Line Computer Controlled Seismic Performance Testing," by Dermitzakis, S. and Mahin, S., February 1985, (PB86 132941/AS)A08.
- UCB/EERC-85/05 "A Simple Model for Reinforcing Bar Anchorages under Cyclic Excitations," by Filippou, F.C., March 1985, (PB86 112 919/AS)A05.
- UCB/EERC-85/06 "Racking Behavior of Wood-framed Gypsum Panels under Dynamic Load," by Oliva, M.G., June 1985, (PB90 262 643)A04.

- UCB/EERC-85/07 "Earthquake Analysis and Response of Concrete Arch Dams," by Fok, K.-L. and Chopra, A.K., June 1985, (PB86 139672/AS)A10.
- UCB/EERC-85/08 "Effect of Inelastic Behavior on the Analysis and Design of Earthquake Resistant Structures," by Lin, J.P. and Mahin, S.A., June 1985, (PB86 135340/AS)A08.
- UCB/EERC-85/09 "Earthquake Simulator Testing of a Base-Isolated Bridge Deck," by Kelly, J.M., Buckle, I.G. and Tsai, H.-C., January 1986, (PB87 124 152/AS)A06.
- UCB/EERC-85/10 "Simplified Analysis for Earthquake Resistant Design of Concrete Gravity Dams," by Fenves, G.L. and Chopra, A.K., June 1986, (PB87 124 160/AS)A08.
- UCB/EERC-85/11 "Dynamic Interaction Effects in Arch Dams," by Clough, R.W., Chang, K.-T., Chen, H.-Q. and Ghanaat, Y., October 1985, (PB86 135027/AS)A05.
- UCB/EERC-85/12 "Dynamic Response of Long Valley Dam in the Mammoth Lake Earthquake Series of May 25-27, 1980," by Lai, S. and Seed, H.B., November 1985, (PB86 142304/AS)A05.
- UCB/EERC-85/13 "A Methodology for Computer-Aided Design of Earthquake-Resistant Steel Structures," by Austin, M.A., Pister, K.S. and Mahin, S.A., December 1985, (PB86 159480/AS)A10.
- UCB/EERC-85/14 "Response of Tension-Leg Platforms to Vertical Seismic Excitations," by Liou, G.-S., Penzien, J. and Yeung, R.W., December 1985, (PB87 124 871/AS)A08.
- UCB/EERC-85/15 "Cyclic Loading Tests of Masonry Single Piers: Volume 4 - Additional Tests with Height to Width Ratio of 1," by Sveinsson, B., McNiven, H.D. and Sucuoglu, H., December 1985, (PB87 165031/AS)A08.
- UCB/EERC-85/16 "An Experimental Program for Studying the Dynamic Response of a Steel Frame with a Variety of Infill Partitions," by Yancev, B. and McNiven, H.D., December 1985, (PB90 262 676)A05.
- UCB/EERC-86/01 "A Study of Seismically Resistant Eccentrically Braced Steel Frame Systems," by Kasai, K. and Popov, E.P., January 1986, (PB87 124 178/AS)A14.
- UCB/EERC-86/02 "Design Problems in Soil Liquefaction," by Seed, H.B., February 1986, (PB87 124 186/AS)A03.
- UCB/EERC-86/03 "Implications of Recent Earthquakes and Research on Earthquake-Resistant Design and Construction of Buildings," by Bertero, V.V., March 1986, (PB87 124 194/AS)A05.
- UCB/EERC-86/04 "The Use of Load Dependent Vectors for Dynamic and Earthquake Analyses," by Leger, P., Wilson, E.L. and Clough, R.W., March 1986, (PB87 124 202/AS)A12.
- UCB/EERC-86/05 "Two Beam-To-Column Web Connections," by Tsai, K.-C. and Popov, E.P., April 1986, (PB87 124 301/AS)A04.
- UCB/EERC-86/06 "Determination of Penetration Resistance for Coarse-Grained Soils using the Becker Hammer Drill," by Harder, L.F. and Seed, H.B., May 1986, (PB87 124 210/AS)A07.
- UCB/EERC-86/07 "A Mathematical Model for Predicting the Nonlinear Response of Unreinforced Masonry Walls to In-Plane Earthquake Excitations," by Mengi, Y. and McNiven, H.D., May 1986, (PB87 124 780/AS)A06.
- UCB/EERC-86/08 "The 19 September 1985 Mexico Earthquake: Building Behavior," by Bertero, V.V., July 1986.
- UCB/EERC-86/09 "EACD-3D: A Computer Program for Three-Dimensional Earthquake Analysis of Concrete Dams," by Fok, K.-L., Hall, J.F. and Chopra, A.K., July 1986, (PB87 124 228/AS)A08.
- UCB/EERC-86/10 "Earthquake Simulation Tests and Associated Studies of a 0.3-Scale Model of a Six-Story Concentrically Braced Steel Structure," by Uang, C.-M. and Bertero, V.V., December 1986, (PB87 163 564/AS)A17.
- UCB/EERC-86/11 "Mechanical Characteristics of Base Isolation Bearings for a Bridge Deck Model Test," by Kelly, J.M., Buckle, I.G. and Koh, C.-G., November 1987, (PB90 262 668)A04.
- UCB/EERC-86/12 "Effects of Axial Load on Elastomeric Isolation Bearings," by Koh, C.-G. and Kelly, J.M., November 1987.
- UCB/EERC-87/01 "The FPS Earthquake Resisting System: Experimental Report," by Zayas, V.A., Low, S.S. and Mahin, S.A., June 1987, (PB88 170 287)A06.
- UCB/EERC-87/02 "Earthquake Simulator Tests and Associated Studies of a 0.3-Scale Model of a Six-Story Eccentrically Braced Steel Structure," by Whittaker, A., Uang, C.-M. and Bertero, V.V., July 1987, (PB88 166 707/AS)A18.
- UCB/EERC-87/03 "A Displacement Control and Uplift Restraint Device for Base-Isolated Structures," by Kelly, J.M., Griffith, M.C. and Aiken, I.D., April 1987, (PB88 169 933)A04.
- UCB/EERC-87/04 "Earthquake Simulator Testing of a Combined Sliding Bearing and Rubber Bearing Isolation System," by Kelly, J.M. and Chalhoub, M.S., December 1990.
- UCB/EERC-87/05 "Three-Dimensional Inelastic Analysis of Reinforced Concrete Frame-Wall Structures," by Moazzami, S. and Bertero, V.V., May 1987, (PB88 169 586/AS)A08.
- UCB/EERC-87/06 "Experiments on Eccentrically Braced Frames with Composite Floors," by Ricles, J. and Popov, E., June 1987, (PB88 173 067/AS)A14.
- UCB/EERC-87/07 "Dynamic Analysis of Seismically Resistant Eccentrically Braced Frames," by Ricles, J. and Popov, E., June 1987, (PB88 173 075/AS)A16.
- UCB/EERC-87/08 "Undrained Cyclic Triaxial Testing of Gravels-The Effect of Membrane Compliance," by Evans, M.D. and Seed, H.B., July 1987, (PB88 173 257)A19.

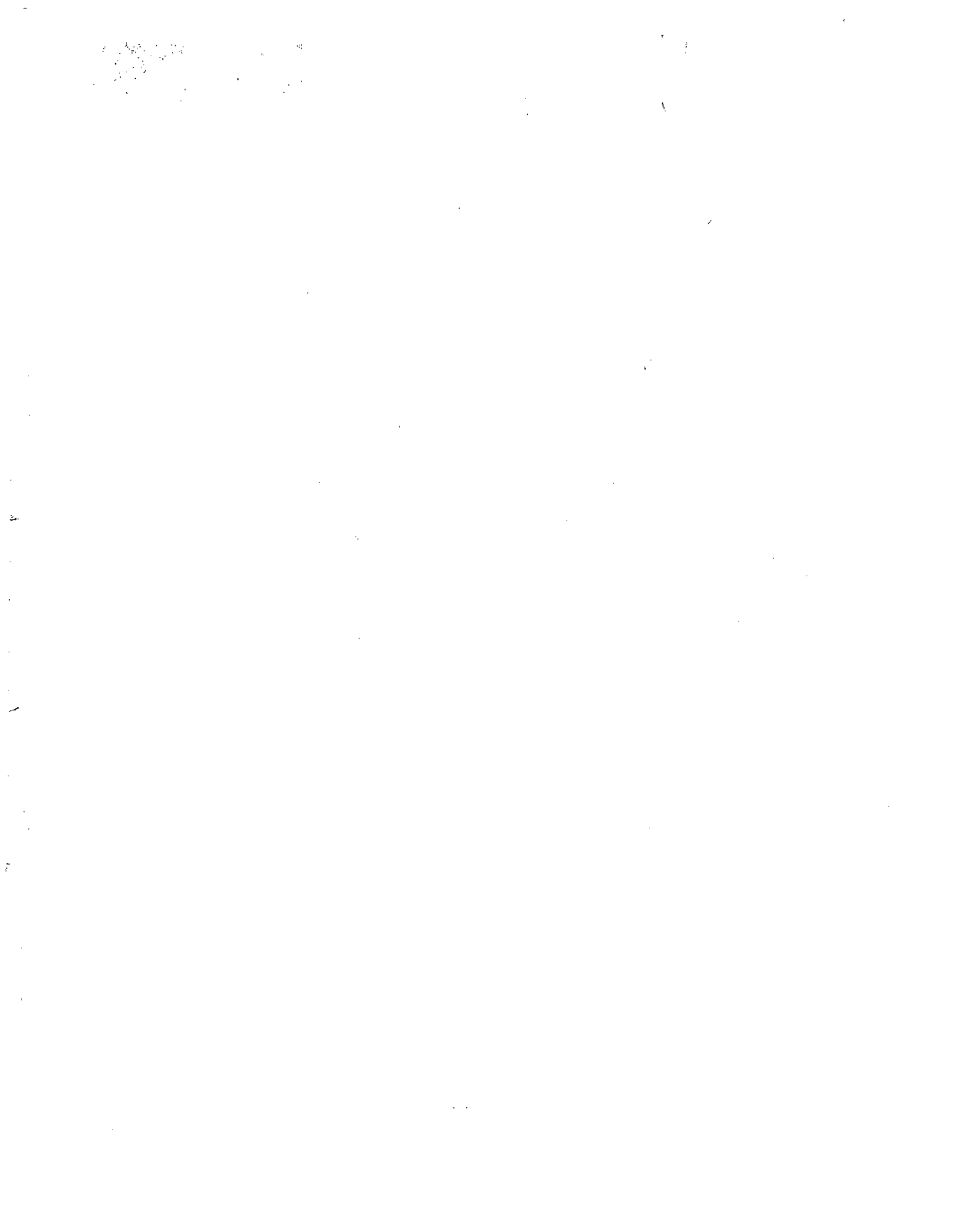
- UCB/EERC-87/09 "Hybrid Solution Techniques for Generalized Pseudo-Dynamic Testing," by Thewalt, C. and Mahin, S.A., July 1987, (PB 88 179 007)A07.
- UCB/EERC-87/10 "Ultimate Behavior of Butt Welded Splices in Heavy Rolled Steel Sections," by Bruneau, M., Mahin, S.A. and Popov, E.P., September 1987, (PB90 254 285)A07.
- UCB/EERC-87/11 "Residual Strength of Sand from Dam Failures in the Chilean Earthquake of March 3, 1985," by De Alba, P., Seed, H.B., Retamal, E. and Seed, R.B., September 1987, (PB88 174 321/AS)A03.
- UCB/EERC-87/12 "Inelastic Seismic Response of Structures with Mass or Stiffness Eccentricities in Plan," by Bruneau, M. and Mahin, S.A., September 1987, (PB90 262 650/AS)A14.
- UCB/EERC-87/13 "CSTRUCT: An Interactive Computer Environment for the Design and Analysis of Earthquake Resistant Steel Structures," by Austin, M.A., Mahin, S.A. and Pister, K.S., September 1987, (PB88 173 339/AS)A06.
- UCB/EERC-87/14 "Experimental Study of Reinforced Concrete Columns Subjected to Multi-Axial Loading," by Low, S.S. and Moehle, J.P., September 1987, (PB88 174 347/AS)A07.
- UCB/EERC-87/15 "Relationships between Soil Conditions and Earthquake Ground Motions in Mexico City in the Earthquake of Sept. 19, 1985," by Seed, H.B., Romo, M.P., Sun, J., Jaime, A. and Lysmer, J., October 1987, (PB88 178 991)A06.
- UCB/EERC-87/16 "Experimental Study of Seismic Response of R. C. Setback Buildings," by Shahrooz, B.M. and Moehle, J.P., October 1987, (PB88 176 359)A16
- UCB/EERC-87/17 "The Effect of Slabs on the Flexural Behavior of Beams," by Pantazopoulou, S.J. and Moehle, J.P., October 1987, (PB90 262 700)A07.
- UCB/EERC-87/18 "Design Procedure for R-FBI Bearings," by Mostaghel, N. and Kelly, J.M., November 1987, (PB90 262 718)A04.
- UCB/EERC-87/19 "Analytical Models for Predicting the Lateral Response of R C Shear Walls: Evaluation of their Reliability," by Vulcano, A. and Bertero, V.V., November 1987, (PB88 178 983)A05.
- UCB/EERC-87/20 "Earthquake Response of Torsionally-Coupled Buildings," by Hejal, R. and Chopra, A.K., December 1987.
- UCB/EERC-87/21 "Dynamic Reservoir Interaction with Monticello Dam," by Clough, R.W., Ghanaat, Y. and Qiu, X-F., December 1987, (PB88 179 023)A07.
- UCB/EERC-87/22 "Strength Evaluation of Coarse-Grained Soils," by Siddiqi, F.H., Seed, R.B., Chan, C.K., Seed, H.B. and Pyke, R.M., December 1987, (PB88 179 031)A04.
- UCB/EERC-88/01 "Seismic Behavior of Concentrically Braced Steel Frames," by Khatib, I., Mahin, S.A. and Pister, K.S., January 1988, (PB91 210 898/AS)A11.
- UCB/EERC-88/02 "Experimental Evaluation of Seismic Isolation of Medium-Rise Structures Subject to Uplift," by Griffith, M.C., Kelly, J.M., Coveney, V.A. and Koh, C.G., January 1988, (PB91 217 950/AS)A09.
- UCB/EERC-88/03 "Cyclic Behavior of Steel Double Angle Connections," by Astaneh-Asl, A. and Nader, M.N., January 1988, (PB91 210 872)A05.
- UCB/EERC-88/04 "Re-evaluation of the Slide in the Lower San Fernando Dam in the Earthquake of Feb. 9, 1971," by Seed, H.B., Seed, R.B., Harder, L.F. and Jong, H.-L., April 1988, (PB91 212 456/AS)A07.
- UCB/EERC-88/05 "Experimental Evaluation of Seismic Isolation of a Nine-Story Braced Steel Frame Subject to Uplift," by Griffith, M.C., Kelly, J.M. and Aiken, I.D., May 1988, (PB91 217 968/AS)A07.
- UCB/EERC-88/06 "DRAIN-2DX User Guide.," by Allahabadi, R. and Powell, G.H., March 1988, (PB91 212 530)A12.
- UCB/EERC-88/07 "Theoretical and Experimental Studies of Cylindrical Water Tanks in Base-Isolated Structures," by Chalhoub, M.S. and Kelly, J.M., April 1988, (PB91 217 976/AS)A05.
- UCB/EERC-88/08 "Analysis of Near-Source Waves: Separation of Wave Types Using Strong Motion Array Recording," by Darragh, R.B., June 1988, (PB91 212 621)A08.
- UCB/EERC-88/09 "Alternatives to Standard Mode Superposition for Analysis of Non-Classically Damped Systems," by Kusainov, A.A. and Clough, R.W., June 1988, (PB91 217 992/AS)A04.
- UCB/EERC-88/10 "The Landslide at the Port of Nice on October 16, 1979," by Seed, H.B., Seed, R.B., Schlosser, F., Blondeau, F. and Juran, I., June 1988, (PB91 210 914)A05.
- UCB/EERC-88/11 "Liquefaction Potential of Sand Deposits Under Low Levels of Excitation," by Carter, D.P. and Seed, H.B., August 1988, (PB91 210 880)A15.
- UCB/EERC-88/12 "Nonlinear Analysis of Reinforced Concrete Frames Under Cyclic Load Reversals," by Filippou, F.C. and Issa, A., September 1988, (PB91 212 589)A07.
- UCB/EERC-88/13 "Implications of Recorded Earthquake Ground Motions on Seismic Design of Building Structures," by Uang, C.-M. and Bertero, V.V., November 1988, (PB91 212 548)A06.
- UCB/EERC-88/14 "An Experimental Study of the Behavior of Dual Steel Systems," by Whittaker, A.S., Uang, C.-M. and Bertero, V.V., September 1988, (PB91 212 712)A16.
- UCB/EERC-88/15 "Dynamic Moduli and Damping Ratios for Cohesive Soils," by Sun, J.I., Golesorkhi, R. and Seed, H.B., August 1988, (PB91 210 922)A04.
- UCB/EERC-88/16 "Reinforced Concrete Flat Plates Under Lateral Load: An Experimental Study Including Biaxial Effects," by Pan, A. and Moehle, J.P., October 1988, (PB91 210 856)A13.

- UCB/EERC-88/17 "Earthquake Engineering Research at Berkeley - 1988," by EERC, November 1988, (PB91 210 864)A10.
- UCB/EERC-88/18 "Use of Energy as a Design Criterion in Earthquake-Resistant Design," by Uang, C.-M. and Bertero, V.V., November 1988, (PB91 210 906/AS)A04.
- UCB/EERC-88/19 "Steel Beam-Column Joints in Seismic Moment Resisting Frames," by Tsai, K.-C. and Popov, E.P., November 1988, (PB91 217 984/AS)A20.
- UCB/EERC-88/20 "Base Isolation in Japan, 1988," by Kelly, J.M., December 1988, (PB91 212 449)A05.
- UCB/EERC-89/01 "Behavior of Long Links in Eccentrically Braced Frames," by Engelhardt, M.D. and Popov, E.P., January 1989, (PB92 143 056)A18.
- UCB/EERC-89/02 "Earthquake Simulator Testing of Steel Plate Added Damping and Stiffness Elements," by Whittaker, A., Bertero, V.V., Alonso, J. and Thompson, C., January 1989, (PB91 229 252/AS)A10.
- UCB/EERC-89/03 "Implications of Site Effects in the Mexico City Earthquake of Sept. 19, 1985 for Earthquake-Resistant Design Criteria in the San Francisco Bay Area of California," by Seed, H.B. and Sun, J.I., March 1989, (PB91 229 369/AS)A07.
- UCB/EERC-89/04 "Earthquake Analysis and Response of Intake-Outlet Towers," by Goyal, A. and Chopra, A.K., July 1989, (PB91 229 286/AS)A19.
- UCB/EERC-89/05 "The 1985 Chile Earthquake: An Evaluation of Structural Requirements for Bearing Wall Buildings," by Wallace, J.W. and Moehle, J.P., July 1989, (PB91 218 008/AS)A13.
- UCB/EERC-89/06 "Effects of Spatial Variation of Ground Motions on Large Multiply-Supported Structures," by Hao, H., July 1989, (PB91 229 161/AS)A08.
- UCB/EERC-89/07 "EADAP - Enhanced Arch Dam Analysis Program: Users's Manual," by Ghanaat, Y. and Clough, R.W., August 1989, (PB91 212 522)A06.
- UCB/EERC-89/08 "Seismic Performance of Steel Moment Frames Plastically Designed by Least Squares Stress Fields," by Ohi, K. and Mahin, S.A., August 1989, (PB91 212 597)A05.
- UCB/EERC-89/09 "Feasibility and Performance Studies on Improving the Earthquake Resistance of New and Existing Buildings Using the Friction Pendulum System," by Zayas, V., Low, S., Mahin, S.A. and Bozzo, L., July 1989, (PB92 143 064)A14.
- UCB/EERC-89/10 "Measurement and Elimination of Membrane Compliance Effects in Undrained Triaxial Testing," by Nicholson, P.G., Seed, R.B. and Anwar, H., September 1989, (PB92 139 641/AS)A13.
- UCB/EERC-89/11 "Static Tilt Behavior of Unanchored Cylindrical Tanks," by Lau, D.T. and Clough, R.W., September 1989, (PB92 143 049)A10.
- UCB/EERC-89/12 "ADAP-88: A Computer Program for Nonlinear Earthquake Analysis of Concrete Arch Dams," by Fenves, G.L., Mojtahedi, S. and Reimer, R.B., September 1989, (PB92 139 674/AS)A07.
- UCB/EERC-89/13 "Mechanics of Low Shape Factor Elastomeric Seismic Isolation Bearings," by Aiken, I.D., Kelly, J.M. and Tajirian, F.F., November 1989, (PB92 139 732/AS)A09.
- UCB/EERC-89/14 "Preliminary Report on the Seismological and Engineering Aspects of the October 17, 1989 Santa Cruz (Loma Prieta) Earthquake," by EERC, October 1989, (PB92 139 682/AS)A04.
- UCB/EERC-89/15 "Experimental Studies of a Single Story Steel Structure Tested with Fixed, Semi-Rigid and Flexible Connections," by Nader, M.N. and Astaneh-Asl, A., August 1989, (PB91 229 211/AS)A10.
- UCB/EERC-89/16 "Collapse of the Cypress Street Viaduct as a Result of the Loma Prieta Earthquake," by Nims, D.K., Miranda, E., Aiken, I.D., Whittaker, A.S. and Bertero, V.V., November 1989, (PB91 217 935/AS)A05.
- UCB/EERC-90/01 "Mechanics of High-Shape Factor Elastomeric Seismic Isolation Bearings," by Kelly, J.M., Aiken, I.D. and Tajirian, F.F., March 1990.
- UCB/EERC-90/02 "Javid's Paradox: The Influence of Preform on the Modes of Vibrating Beams," by Kelly, J.M., Sackman, J.L. and Javid, A., May 1990, (PB91 217 943/AS)A03.
- UCB/EERC-90/03 "Earthquake Simulator Testing and Analytical Studies of Two Energy-Absorbing Systems for Multistory Structures," by Aiken, I.D. and Kelly, J.M., October 1990, (PB92 192 988)A13.
- UCB/EERC-90/04 "Unassigned," by Unassigned, 1990.
- UCB/EERC-90/05 "Preliminary Report on the Principal Geotechnical Aspects of the October 17, 1989 Loma Prieta Earthquake," by Seed, R.B., Dickenson, S.E., Riemer, M.F., Bray, J.D., Sitar, N., Mitchell, J.K., Idriss, I.M., Kayen, R.E., Kropp, A., Harder, L.F., Jr. and Power, M.S., April 1990, (PB 192 970)A08.
- UCB/EERC-90/06 "Models of Critical Regions in Reinforced Concrete Frames Under Seismic Excitations," by Zulfqar, N. and Filippou, F.C., May 1990.
- UCB/EERC-90/07 "A Unified Earthquake-Resistant Design Method for Steel Frames Using ARMA Models," by Takewaki, I., Conte, J.P., Mahin, S.A. and Pister, K.S., June 1990.
- UCB/EERC-90/08 "Soil Conditions and Earthquake Hazard Mitigation in the Marina District of San Francisco," by Mitchell, J.K., Masood, T., Kayen, R.E. and Seed, R.B., May 1990, (PB 193 267/AS)A04.
- UCB/EERC-90/09 "Influence of the Earthquake Ground Motion Process and Structural Properties on Response Characteristics of Simple Structures," by Conte, J.P., Pister, K.S. and Mahin, S.A., July 1990, (PB92 143 064)A15.

- UCB/EERC-90/10 "Experimental Testing of the Resilient-Friction Base Isolation System." by Clark, P.W. and Kelly, J.M., July 1990, (PB92 143 072)A08.
- UCB/EERC-90/11 "Seismic Hazard Analysis: Improved Models, Uncertainties and Sensitivities," by Araya, R. and Der Kiureghian, A., March 1988.
- UCB/EERC-90/12 "Effects of Torsion on the Linear and Nonlinear Seismic Response of Structures," by Sedarat, H. and Bertero, V.V., September 1989, (PB92 193 002/AS)A15.
- UCB/EERC-90/13 "The Effects of Tectonic Movements on Stresses and Deformations in Earth Embankments," by Bray, J. D., Seed, R. B. and Seed, H. B., September 1989.
- UCB/EERC-90/14 "Inelastic Seismic Response of One-Story, Asymmetric-Plan Systems," by Goel, R.K. and Chopra, A.K., October 1990, (PB93 114 767)A11.
- UCB/EERC-90/15 "Dynamic Crack Propagation: A Model for Near-Field Ground Motion.," by Seyyedian, H. and Kelly, J.M., 1990.
- UCB/EERC-90/16 "Sensitivity of Long-Period Response Spectra to System Initial Conditions," by Blasquez, R., Ventura, C. and Kelly, J.M., 1990.
- UCB/EERC-90/17 "Behavior of Peak Values and Spectral Ordinates of Near-Source Strong Ground-Motion over a Dense Array," by Niazi, M., June 1990, (PB93 114 833)A07.
- UCB/EERC-90/18 "Material Characterization of Elastomers used in Earthquake Base Isolation," by Papoulia, K.D. and Kelly, J.M., 1990, PB94-190063.
- UCB/EERC-90/19 "Cyclic Behavior of Steel Top-and-Bottom Plate Moment Connections," by Harriott, J.D. and Astaneh-Asl, A., August 1990, (PB91 229 260/AS)A05.
- UCB/EERC-90/20 "Seismic Response Evaluation of an Instrumented Six Story Steel Building," by Shen, J.-H. and Astaneh-Asl, A., December 1990, (PB91 229 294/AS)A04.
- UCB/EERC-90/21 "Observations and Implications of Tests on the Cypress Street Viaduct Test Structure," by Bollo, M., Mahin, S.A., Moehle, J.P., Stephen, R.M. and Qi, X., December 1990, (PB93 114 775)A13.
- UCB/EERC-91/01 "Experimental Evaluation of Nitinol for Energy Dissipation in Structures," by Nims, D.K., Sasaki, K.K. and Kelly, J.M., 1991.
- UCB/EERC-91/02 "Displacement Design Approach for Reinforced Concrete Structures Subjected to Earthquakes," by Qi, X. and Moehle, J.P., January 1991, (PB93 114 569/AS)A09.
- UCB/EERC-91/03 "A Long-Period Isolation System Using Low-Modulus High-Damping Isolators for Nuclear Facilities at Soft-Soil Sites," by Kelly, J.M., March 1991, (PB93 114 577/AS)A10.
- UCB/EERC-91/04 "Dynamic and Failure Characteristics of Bridgestone Isolation Bearings," by Kelly, J.M., April 1991, (PB93 114 528)A05.
- UCB/EERC-91/05 "Base Sliding Response of Concrete Gravity Dams to Earthquakes," by Chopra, A.K. and Zhang, L., May 1991, (PB93 114 544/AS)A05.
- UCB/EERC-91/06 "Computation of Spatially Varying Ground Motion and Foundation-Rock Impedance Matrices for Seismic Analysis of Arch Dams," by Zhang, L. and Chopra, A.K., May 1991, (PB93 114 825)A07.
- UCB/EERC-91/07 "Estimation of Seismic Source Processes Using Strong Motion Array Data," by Chiou, S.-J., July 1991, (PB93 114 551/AS)A08.
- UCB/EERC-91/08 "A Response Spectrum Method for Multiple-Support Seismic Excitations," by Der Kiureghian, A. and Neuenhofer, A., August 1991, (PB93 114 536)A04.
- UCB/EERC-91/09 "A Preliminary Study on Energy Dissipating Cladding-to-Frame Connection," by Cohen, J.M. and Powell, G.H., September 1991, (PB93 114 510)A05.
- UCB/EERC-91/10 "Evaluation of Seismic Performance of a Ten-Story RC Building During the Whittier Narrows Earthquake," by Miranda, E. and Bertero, V.V., October 1991, (PB93 114 783)A06.
- UCB/EERC-91/11 "Seismic Performance of an Instrumented Six-Story Steel Building," by Anderson, J.C. and Bertero, V.V., November 1991, (PB93 114 809)A07.
- UCB/EERC-91/12 "Performance of Improved Ground During the Loma Prieta Earthquake," by Mitchell, J.K. and Wentz, Jr., F.J., October 1991, (PB93 114 791)A06.
- UCB/EERC-91/13 "Shaking Table - Structure Interaction," by Rinawi, A.M. and Clough, R.W., October 1991, (PB93 114 917)A13.
- UCB/EERC-91/14 "Cyclic Response of RC Beam-Column Knee Joints: Test and Retrofit," by Mazzoni, S., Moehle, J.P. and Thewalt, C.R., October 1991, (PB93 120 277)A03.
- UCB/EERC-91/15 "Design Guidelines for Ductility and Drift Limits: Review of State-of-the-Practice and State-of-the-Art in Ductility and Drift-Based Earthquake-Resistant Design of Buildings," by Bertero, V.V., Anderson, J.C., Krawinkler, H., Miranda, E. and The CUREe and The Kajima Research Teams, July 1991. (PB93 120 269)A08.
- UCB/EERC-91/16 "Evaluation of the Seismic Performance of a Thirty-Story RC Building," by Anderson, J.C., Miranda, E., Bertero, V.V. and The Kajima Project Research Team, July 1991, (PB93 114 841)A12.
- UCB/EERC-91/17 "A Fiber Beam-Column Element for Seismic Response Analysis of Reinforced Concrete Structures," by Taucer, F., Spacone, E. and Filippou, F.C., December 1991, (PB94 117 629AS)A07.

- UCB/EERC-91/18 "Investigation of the Seismic Response of a Lightly-Damped Torsionally-Coupled Building," by Boroschek, R. and Mahin, S.A., December 1991, (PB93 120 335)A13.
- UCB/EERC-92/01 "Studies of a 49-Story Instrumented Steel Structure Shaken During the Loma Prieta Earthquake," by Chen, C.-C., Bonowitz, D. and Astaneh-Asl, A., February 1992, (PB93 221 778)A08.
- UCB/EERC-92/02 "Response of the Dumbarton Bridge in the Loma Prieta Earthquake," by Fenves, G.L., Filippou, F.C. and Sze, D.T., January 1992, (PB93 120 319)A09.
- UCB/EERC-92/03 "Models for Nonlinear Earthquake Analysis of Brick Masonry Buildings," by Mengi, Y., McNiven, H.D. and Tanrikulu, A.K., March 1992, (PB93 120 293)A08.
- UCB/EERC-92/04 "Shear Strength and Deformability of RC Bridge Columns Subjected to Inelastic Cyclic Displacements," by Aschheim, M. and Moehle, J.P., March 1992, (PB93 120 327)A06.
- UCB/EERC-92/05 "Parameter Study of Joint Opening Effects on Earthquake Response of Arch Dams," by Fenves, G.L., Mojtahedi, S. and Reimer, R.B., April 1992, (PB93 120 301)A04.
- UCB/EERC-92/06 "Seismic Behavior and Design of Semi-Rigid Steel Frames," by Nader, M.N. and Astaneh-Asl, A., May 1992.
- UCB/EERC-92/07 "A Beam Element for Seismic Damage Analysis," by Spacone, E., Ciampi, V. and Filippou, F.C., August 1992.
- UCB/EERC-92/08 "Nonlinear Static and Dynamic Analysis of Reinforced Concrete Subassemblages," by Filippou, F.C., D'Ambrisi, A. and Issa, A., August 1992.
- UCB/EERC-92/09 "Evaluation of Code Accidental-Torsion Provisions Using Earthquake Records from Three Nominally Symmetric-Plan Buildings," by De la Llera, J.C. and Chopra, A.K., September 1992, (PB94 117 611)A08.
- UCB/EERC-92/10 "Slotted Bolted Connection Energy Dissipators," by Grigorian, C.E., Yang, T.-S. and Popov, E.P., July 1992, (PB92 120 285)A03.
- UCB/EERC-92/11 "Mechanical Characteristics of Neoprene Isolation Bearings," by Kelly, J.M. and Quiroz, E., August 1992, (PB93 221 729)A07.
- UCB/EERC-92/12 "Application of a Mass Damping System to Bridge Structures," by Hasegawa, K. and Kelly, J.M., August 1992, (PB93 221 786)A06.
- UCB/EERC-92/13 "Earthquake Engineering Research at Berkeley - 1992," by EERC, October 1992.
- UCB/EERC-92/14 "Earthquake Risk and Insurance," by Brillinger, D.R., October 1992, (PB93 223 352)A03.
- UCB/EERC-92/15 "A Friction Mass Damper for Vibration Control," by Inaudi, J.A. and Kelly, J.M., October 1992, (PB93 221 745)A04.
- UCB/EERC-92/16 "Tall Reinforced Concrete Buildings: Conceptual Earthquake-Resistant Design Methodology," by Bertero, R.D. and Bertero, V.V., December 1992, (PB93 221 695)A12.
- UCB/EERC-92/17 "Performance of Tall Buildings During the 1985 Mexico Earthquakes," by Terán-Gilmore, A. and Bertero, V.V., December 1992, (PB93 221 737)A11.
- UCB/EERC-92/18 "Dynamic Analysis of Nonlinear Structures using State-Space Formulation and Partitioned Integration Schemes," by Inaudi, J.A. and De la Llera, J.C., December 1992, (PB94 117 702/AS/A05).
- UCB/EERC-93/01 "Seismic Performance of an Instrumented Six-Story Reinforced-Concrete Building," by Anderson, J.C. and Bertero, V.V., 1993.
- UCB/EERC-93/02 "Evaluation of an Active Variable-Damping-Structure," by Polak, E., Meeker, G., Yamada, K. and Kurata, N., 1993, (PB93 221 711)A05.
- UCB/EERC-93/03 "An Experimental Study of Flat-Plate Structures under Vertical and Lateral Loads," by Hwang, S.-H. and Moehle, J.P., February 1993, (PB94 157 690/AS)A13.
- UCB/EERC-93/04 "Seismic Performance of a 30-Story Building Located on Soft Soil and Designed According to UBC 1991," by Terán-Gilmore, A. and Bertero, V.V., 1993, (PB93 221 703)A17.
- UCB/EERC-93/05 "Multiple-Support Response Spectrum Analysis of the Golden Gate Bridge," by Nakamura, Y., Der Kiureghian, A. and Liu, D., May 1993, (PB93 221 752)A05.
- UCB/EERC-93/06 "On the Analysis of Structures with Viscoelastic Dampers," by Inaudi, J.A., Zambrano, A. and Kelly, J.M., August 1993, PB94-165867.
- UCB/EERC-93/07 "Earthquake Analysis and Response of Concrete Gravity Dams Including Base Sliding," by Chávez, J.W. and Fenves, G.L., December 1993, (PB94 157 658/AS)A10.
- UCB/EERC-93/08 "Model for Anchored Reinforcing Bars under Seismic Excitations," by Monti, G., Spacone, E. and Filippou, F.C., December 1993.

REPORT DOCUMENTATION PAGE		1. REPORT NO. NSF/ENG-94007		2.		 PB95-192183	
Title and Subtitle Model for Anchored Reinforcing Bars Under Seismic Excitations"				5. Report Date December 1993		6.	
Author(s) Lorgio Monti, Enrico Spacone, and Filip C. Filippou				8. Performing Organization Rept. No. UCB/EERC-93/08			
Performing Organization Name and Address Earthquake Engineering Research Center University of California, Berkeley 1301 So. 46th Street Richmond, Calif. 94804				10. Project/Task/Work Unit No.		11. Contract(C) or Grant(G) No. (C) (G) ECE-8657525	
Sponsoring Organization Name and Address National Science Foundation 1800 G Street, N.W. Washington, D.C. 20550				13. Type of Report & Period Covered		14.	
Supplementary Notes							
Abstract (Limit: 200 words) This study presents a finite element model for reinforcing bars anchored in concrete and subjected to severe cyclic excitations. The solution to the problem of stress transfer between reinforcing steel and concrete is based on the flexibility method. In this case, the governing differential equations are solved by force interpolation functions that strictly satisfy equilibrium along the anchored reinforcing bar. This solution method results in a very robust and stable nonlinear algorithm, particularly for systems that exhibit severe stiffness and strength deterioration, as is the case for anchored reinforcing bars. In the systematic derivation of the proposed solution method, the model is viewed as a simple mechanical system that is comprised of two components in parallel. The first component is the reinforcing bar and the second is the interface between reinforcing steel and surrounding concrete. The nonlinear hysteretic behavior of the model derives entirely from the nonlinear constitutive behavior of these two components. The hysteretic behavior of the reinforcing bar is described by a cyclic steel stress-strain relation, while the hysteretic behavior of the interface derives from a cyclic bond stress-slip relation that includes a damage parameter for representing the progressive deterioration of bond. The integration of the flexibility based finite element model in a conventional stiffness based finite element program faces several challenges that are addressed in this study with a new iterative algorithm. This algorithm is characterized by robust and stable numerical behavior even under conditions of significant strength and stiffness loss of the anchored reinforcing bar. The study concludes with correlation studies between analytical and experimental results and several parametric studies. The former are intended to establish the validity of the proposed model, while the latter serve the purpose of identifying the significance of key parameters on the local and global response of anchored reinforcing bars and for providing some guidance for their design in regions of high seismic risk.							
7. Document Analysis a. Descriptors							
b. Identifiers/Open-Ended Terms							
c. COSATI Field/Group							
Availability Statement: Release Unlimited				19. Security Class (This Report) unclassified		21. No. of Pages 99	
				20. Security Class (This Page) unclassified		22. Price \$15.00	



REPORT DOCUMENTATION PAGE		1. REPORT NO. NSF/ENG-94007	2.	 PB95-192183	
4. Title and Subtitle "Model for Anchored Reinforcing Bars Under Seismic Excitations"				5. Report Date December 1993	
7. Author(s) Giorgio Monti, Enrico Spacone, and Filip C. Filippou				6.	
9. Performing Organization Name and Address Earthquake Engineering Research Center University of California, Berkeley 1301 So. 46th Street Richmond, Calif. 94804				8. Performing Organization Rept. No. UCB/EERC-93/08	
12. Sponsoring Organization Name and Address National Science Foundation 1800 G Street, N.W. Washington, D.C. 20550				10. Project/Task/Work Unit No.	
				11. Contract(G) or Grant(G) No. (G) (G)ECE-8657525	
15. Supplementary Notes				13. Type of Report & Period Covered	
				14.	
16. Abstract (Limit: 200 words) This study presents a finite element model for reinforcing bars anchored in concrete and subjected to severe cyclic excitations. The solution to the problem of stress transfer between reinforcing steel and concrete is based on the flexibility method. In this case, the governing differential equations are solved by force interpolation functions that strictly satisfy equilibrium along the anchored reinforcing bar. This solution method results in a very robust and stable nonlinear algorithm, particularly for systems that exhibit severe stiffness and strength deterioration, as is the case for anchored reinforcing bars. In the systematic derivation of the proposed solution method, the model is viewed as a simple mechanical system that is comprised of two components in parallel. The first component is the reinforcing bar and the second is the interface between reinforcing steel and surrounding concrete. The nonlinear hysteretic behavior of the model derives entirely from the nonlinear constitutive behavior of these two components. The hysteretic behavior of the reinforcing bar is described by a cyclic steel stress-strain relation, while the hysteretic behavior of the interface derives from a cyclic bond stress-slip relation that includes a damage parameter for representing the progressive deterioration of bond. The integration of the flexibility based finite element model in a conventional stiffness based finite element program faces several challenges that are addressed in this study with a new iterative algorithm. This algorithm is characterized by robust and stable numerical behavior even under conditions of significant strength and stiffness loss of the anchored reinforcing bar. The study concludes with correlation studies between analytical and experimental results and several parametric studies. The former are intended to establish the validity of the proposed model, while the latter serve the purpose of identifying the significance of key parameters on the local and global response of anchored reinforcing bars and for providing some guidance for their design in regions of high seismic risk.					
17. Document Analysis a. Descriptors					
b. Identifiers/Open-Ended Terms					
c. COSATI Field/Group					
18. Availability Statement Release Unlimited			19. Security Class (This Report) unclassified		21. No. of Pages 99
			20. Security Class (This Page) unclassified		22. Price \$15.00

